

UNIVERSITY OF CALGARY

Behaviour of Unsaturated Soils under Direct Shear and Triaxial Compression

by

Martin C.H. Lun

A THESIS

SUBMITTED TO THE FACULTY OF GRADUATE STUDIES
IN PARTIAL FULFILMENT OF THE REQUIREMENTS FOR THE
DEGREE OF MASTER OF SCIENCE

DEPARTMENT OF CIVIL ENGINEERING

CALGARY, ALBERTA

APRIL, 2005

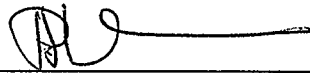
© Martin C.H. Lun 2005

UNIVERSITY OF CALGARY
FACULTY OF GRADUATE STUDIES

The undersigned certify that they have read, and recommend to the Faculty of Graduate Studies for acceptance, a thesis entitled "Behaviour of Unsaturated Soils under Direct Shear and Triaxial Compression" submitted by Martin C.H. Lun in partial fulfillment of the requirements for the degree of Master of Science.



Supervisor, Dr. R.C.K. Wong, Department of Civil Engineering



Dr. P. J. Hettiaratchi, Department of Civil Engineering



Dr. C. Valeo, Department of Geomatics Engineering

April 1, 2005

Date

ABSTRACT

The objective of the research reported herein is to investigate the behavior of slider block-basal and slider block-interslice springs proposed in Wong's landslide model. Studies of the characteristics of the two springs quantify equations for describing their stiffness and strength behaviors to be proposed. The test results show a significant drop in the stiffness and strength of the three soils studied with decreasing matric suction at low net confining stress ranging from 0 to 100 kPa. This response is confirmed by applying the proposed shear strength equation to a slope stability analysis in Sunnyside Hill, Calgary. The decrease of the factor of safety to 1.0 or below at this site associated with the decrease in the soil strength caused by a decrease of matric suction to 5 kPa or below recorded in the field measurements. The back analysis exercise suggests that the previous landslides in 1997 and 1998 might happen due to loss in matric suction.

ACKNOWLEDGEMENTS

I would like to express my sincere gratitude and appreciation to Dr. Ron Wong for his consistent guidance and advice throughout this study. The opportunity to work with him and witness his insight covering the field of geotechnical engineering was an invaluable experience.

I wish to thank Dr. Mahmoud Mahmoud of Golder Associates Ltd. for providing the opportunity to participate in the slope stability analysis in Sunnyside Hill and Ms. Karen Moffit of Golder Associates Ltd. for her assistance on the field work. I also wish to thank Mr. Ed Wilson for his valuable comments and proof reading this thesis.

I would also like to thank Thurber Engineering Ltd. and Almor Testing Ltd. for the knowledge and experience they gave me.

TABLE OF CONTENTS

Approval page	ii
Abstract	iii
Acknowledgements	iv
Table of Contents	v
List of Tables	viii
List of Figures	viii
CHAPTER 1: INTRODUCTION	1
1.1 Introduction	1
1.2 Objective of Thesis	3
1.3 Outline of Thesis	3
CHAPTER 2: LITERATURE REVIEW	7
2.1 Unsaturated Soil Mechanics	7
2.1.1 Phases of an unsaturated soil	7
2.1.2 Stress state variables	7
2.2 Matric Suction	9
2.3 Wong's Landslide Model	10
CHAPTER 3: DIRECT SHEAR BOX TESTS	15
3.1 Introduction	15
3.2 Description of Soil Samples	15
3.3 Tests and Testing Procedures	16
3.3.1 Sieve analysis, soil classification, and compaction curves	16
3.3.2 Direct shear box tests	16
3.3.3 Soil and matric suction measurements	18
3.4 Data Acquisition and Compilation	19
3.4.1 Soil-water characteristic curve	19

3.4.2 Shear stress (τ) versus horizontal displacement (δ_h)	20
3.4.3 Vertical displacement (δ_v) versus horizontal displacement (δ_h)	21
3.4.4 Shear stiffness (k_h) versus net confining stress ($\sigma - u_a$) and matric suction ($u_a - u_w$)	21
3.4.5 Shear strength (τ) versus net confining stress ($\sigma - u_a$) and matric suction ($u_a - u_w$)	24
3.5 Data Analysis and Discussion	25
3.6 Illustrative Examples	30
3.7 Conclusion	31
CHAPTER 4: TRIAXIAL COMPRESSION TESTS	54
4.1 Introduction	54
4.2 Description of Triaxial Compression Tests	54
4.3 Testing Procedures	55
4.4 Data Acquisition and Compilation	56
4.4.1 Deviator stress ($\sigma_1 - \sigma_3$) versus vertical displacement (δ_v)	56
4.4.2 Compressive stiffness (k_h) versus net confining stress ($\sigma - u_a$) and matric suction ($u_a - u_w$)	57
4.4.3 Compressive strength ($\sigma_1 - \sigma_3$) versus net confining stress ($\sigma - u_a$) and matric suction ($u_a - u_w$)	58
4.5 Data Analysis and Discussion	60
4.6 Illustrative Examples	64
4.7 Comparison of Strength Parameters from Direct Shear Box and Triaxial Compression Tests	65
4.8 Conclusion	67
CHAPTER 5: CASE STUDIES	89
5.1 Introduction	89
5.2 Description of the Site	90
5.2.1 Surface conditions	90

5.2.2 Subsurface conditions	90
5.3 Slope Instability	90
5.3.1 Instability history	90
5.3.2 Description of previous slope failures and remedial measures	91
5.4 Field Investigation	92
5.4.1 Boreholes drilling program	92
5.4.2 Soil suction measurement program	92
5.4.3 Field density tests	93
5.5 Laboratory Investigations	93
5.6 Field Data Analysis	93
5.7 Slope Stability Analyses	94
5.8 Discussion	96
5.9 Conclusion	97
CHAPTER 6: CONCLUSIONS AND RECOMMENDATION FOR FUTURE WORK	108
6.1 Conclusions	108
6.2 Recommendation for Future Work	109
REFERENCES	111
APPENDIX A: Soil compaction curves results	114
APPENDIX B: Raw data of direct shear box tests	117
APPENDIX C: Plots of shear stress versus horizontal displacement for three soil samples	119
APPENDIX D: Plots of vertical displacement versus horizontal displacement for the three soil samples	126
APPENDIX E: Raw data of triaxial compression tests	133
APPENDIX F: Plots of deviator stress versus vertical displacement of three soil samples	135
APPENDIX G: Field testing in Sunnyside Hill	142

LIST OF TABLES

Table 3-1	Soil classification of the three soil samples	33
Table 3-2	Summary of results of direct shear box tests of the three soil types	33
Table 3-3	Summary of the rate of dilation	34
Table 3-4	Coefficient of determination (R^2) for shear stiffness and strength equations	34
Table 4-1	Summary of results of triaxial tests of three different soil types	70
Table 4-2	Coefficient of multiple determination (R^2) for compressive stiffness and strength equations	71
Table 4-3	Parameters in strength equations from direct shear box test results	71
Table 4-4	Parameters in strength equations from triaxial compression test results	71
Table 4-5	Change of volumetric water contents from start to failure during direct shear box tests for initial matric suctions ranging from 10 to 50 kPa	72
Table 4-6	Change of volumetric water contents from start to failure during triaxial compression tests for initial matric suctions ranging from 10 to 50 kPa	72
Table 5-1	Factors of safety for the specific slope at Sunnyside Hill	99

LIST OF FIGURES

Figure 1-1	Landslide model – shallow slope (translational) failure surface	5
Figure 1-2	Basal and interslice spring-slider models	6
Figure 2-1	Free body diagram of each block	13
Figure 2-2	Plot of generalized direct shear box test results	14
Figure 2-3	Plot of generalized triaxial compression test results	14
Figure 3-1	Soil suction measurement and borehole locations	35
Figure 3-2	Direct shear box apparatus	36
Figure 3-3	Grain size distribution of the three examined soil samples	37

Figure 3-4	Soil-water characteristics curves of the three examined soil samples	37
Figure 3-5	Soil moisture probe	38
Figure 3-6	Plot of shear stress versus horizontal displacement (soil sample: Sunnyside Hill, normal stress: 100 kPa)	39
Figure 3-7	Plot of vertical displacement versus horizontal displacement (soil sample: Sunnyside Hill, normal stress: 100 kPa)	39
Figure 3-8	Plot of k_h versus σ (soil: Discovery Ridge, void ratio ≥ 0.456)	40
Figure 3-9	Plot of k_h versus σ (soil: Discovery Ridge, void ratio < 0.456)	40
Figure 3-10	Plot of k_h versus σ (soil: Sunnyside Hill, void ratio ≥ 0.480)	41
Figure 3-11	Plot of k_h versus σ (soil: Sunnyside Hill, void ratio < 0.480)	41
Figure 3-12	Plot of k_h versus σ (soil: UC Site, void ratio ≥ 0.460)	42
Figure 3-13	Plot of k_h versus σ (soil: UC Site, Void ratio < 0.460)	42
Figure 3-14	Plot of k_h versus u_s (soil: Discovery Ridge, void ratio ≥ 0.456)	43
Figure 3-15	Plot of k_h versus u_s (soil: Discovery Ridge, void ratio < 0.456)	43
Figure 3-16	Plot of k_h versus u_s (soil: Sunnyside Hill, void ratio ≥ 0.480)	44
Figure 3-17	Plot of k_h versus u_s (soil: Sunnyside Hill, void ratio < 0.480)	44
Figure 3-18	Plot of k_h versus u_s (soil: UC Site, void ratio ≥ 0.460)	45
Figure 3-19	Plot of k_h versus u_s (soil: UC Site, void ratio < 0.460)	45
Figure 3-20	Plot of τ versus σ (soil: Discovery Ridge, void ratio ≥ 0.456)	46
Figure 3-21	Plot of τ versus σ (soil: Discovery Ridge, void ratio < 0.456)	46
Figure 3-22	Plot of τ versus σ (soil: Sunnyside Hill, void ratio ≥ 0.480)	47
Figure 3-23	Plot of τ versus σ (soil: Sunnyside Hill, void ratio < 0.480)	47
Figure 3-24	Plot of τ versus σ (soil: UC Site, void ratio ≥ 0.460)	48
Figure 3-25	Plot of τ versus σ (soil: UC Site, void ratio < 0.460)	48
Figure 3-26	Plot of c versus u_s (soil: Discovery Ridge)	49
Figure 3-27	Plot of c versus u_s (soil: Sunnyside Hill)	49
Figure 3-28	Plot of c versus u_s (soil: UC Site)	50
Figure 3-29	Relationship among shear stiffness, net confining stress, and matric suction	51

Figure 3-30	Relationship among shear strength, net confining stress, and matric suction	52
Figure 3-31	Results from the proposed equation for Sunnyside Hill for $\sigma = 40$ kPa	53
Figure 4-1	Schematic diagram of a triaxial cell	73
Figure 4-2	Deviator stress versus vertical displacement (soil: Sunnyside Hill, net confining stress: 30 kPa)	74
Figure 4-3	Compressive stiffness versus net confining stress (soil: Discovery Ridge, void ratio ≥ 0.456)	74
Figure 4-4	Compressive stiffness versus net confining stress (soil: Discovery Ridge, void ratio < 0.456)	75
Figure 4-5	Compressive stiffness versus net confining stress (soil: Sunnyside Hill, void ratio ≥ 0.452)	75
Figure 4-6	Compressive stiffness versus net confining stress (soil: Sunnyside Hill, void ratio < 0.452)	76
Figure 4-7	Compressive stiffness versus net confining stress (soil: UC Site, void ratio ≥ 0.406)	76
Figure 4-8	Compressive stiffness versus net confining stress (soil: UC Site, void ratio < 0.406)	77
Figure 4-9	Compressive stiffness versus suction (soil: Discovery Ridge, void ratio ≥ 0.456)	77
Figure 4-10	Compressive stiffness versus suction (soil: Discovery Ridge, void ratio < 0.456)	78
Figure 4-11	Compressive stiffness versus suction (soil: Sunnyside Hill, void ratio ≥ 0.452)	78
Figure 4-12	Compressive stiffness versus suction (soil: Sunnyside Hill, void ratio < 0.452)	79
Figure 4-13	Compressive stiffness versus net confining stress (soil: UC Site, void ratio ≥ 0.406)	79
Figure 4-14	Compressive stiffness versus net confining stress (soil: UC Site, void ratio < 0.406)	80

Figure 4-15	Compressive strength versus net confining stress (soil: Discovery Ridge, void ratio ≥ 0.456)	80
Figure 4-16	Compressive strength versus net confining stress (soil: Discovery Ridge, void ratio < 0.456)	81
Figure 4-17	Compressive strength versus net confining stress (soil: Sunnyside Hill, void ratio ≥ 0.452)	81
Figure 4-18	Compressive strength versus net confining stress (soil: Sunnyside Hill, void ratio < 0.452)	82
Figure 4-19	Compressive strength versus net confining stress (soil: UC Site, void ratio ≥ 0.406)	82
Figure 4-20	Compressive strength versus net confining stress (soil: UC Site, void ratio < 0.406)	83
Figure 4-21	Cohesion versus suction (soil: Discovery Ridge)	83
Figure 4-22	Cohesion versus suction (soil: Sunnyside Hill)	84
Figure 4-23	Cohesion versus suction (soil: UC Site)	84
Figure 4-24	Relationship among compressive stiffness, net confining stress, and matric suction (triaxial compression tests)	85
Figure 4-25	Relationship among compressive strength, net confining stress, and matric suction (triaxial compression tests)	86
Figure 4-26	Results from the proposed equation for Sunnyside Hill for $\sigma = 40$ kPa for sample length = 115 mm, diameter = 110 mm	87
Figure 4-27	Internal friction angles at non-linear and linear stages	87
Figure 4-28	Angles relative to matric suction at non-linear and linear stages	88
Figure 5-1	Location of Sunnyside Hill	100
Figure 5-2	Cross-section of slides in Sunnyside Hill (modified from Golder Associates Ltd. report, 'Stability of Sunnyside Hill in Calgary, Alberta.')	100
Figure 5-3	Suction versus moisture content at 0.3 m from surface in Sunnyside Hill (May to August 2001)	101

Figure 5-4	Suction versus moisture content at 0.3 m from surface in Sunnyside Hill (September to November 2001)	101
Figure 5-5	Suction versus moisture content at 0.3 m from surface in Sunnyside Hill (May and June 2002)	102
Figure 5-6	Change of suction at 0.3 m from surface in Sunnyside Hill throughout the year (locations S1 to S5)	102
Figure 5-7	Change of suction at 0.3 m from surface in Sunnyside Hill throughout the year (locations S6 to S10)	103
Figure 5-8	Precipitation records at Calgary International Airport (1997 to 2002)	104
Figure 5-9	Comparison of laboratory and field suction readings in Sunnyside Hill	105
Figure 5-10	Suction versus moisture content in UC Site	105
Figure 5-11	Soil suction profile in UC Site	106
Figure 5-12	Comparison of laboratory and field suction readings in UC Site	106
Figure 5-13	Factors of safety with slope angle (ψ) ranging from 22-26°	107

CHAPTER 1: INTRODUCTION

1.1 Introduction

The success of the practice of soil mechanics has been fully recognized since Terzaghi (1936) developed the effective stress concept. The effective stress concept forms the fundamental basis for studying saturated soil mechanics. However, difficulty has been experienced in extending this classical concept to embrace unsaturated soils, despite the fact that researchers, including Biot (1941), Bishop (1959), and Aitchison (1961) have made numerous attempts to express effective stress in different forms to accept unsaturated soils.

Fredlund and Morgenstern (1977) also examined the effective stress concept in describing the behavior of unsaturated soils. They described the stress state of an unsaturated soil within the context of multiphase continuum mechanics. Equilibrium equations for each phase of an unsaturated soil were written in terms of measurable variables. The most satisfactory variables for use in engineering practice are the net confining stress ($\sigma - u_a$) and matric suction ($u_a - u_w$) combinations.

The lack of a fundamental concept to describe the mechanical behaviors of unsaturated soils has limited engineers in solving unsaturated soils related problems such as natural slope failures. A widely publicized case is the landslide at Po-Shan in Hong Kong, which claimed 67 lives. (Fredlund and Rahardjo 1993)

Slope stability problems arose frequently in history when the delicate balance of natural slopes was disrupted by either human beings or natural forces. Engineers use all sorts of methods to understand the problems and search for prevention. In the past decades, the increasing demand for engineered cut and fill slopes on construction projects further

emphasizes the importance and requirement for slope stability analysis to assist in the prediction of slope failure occurrences.

However, the commonly performed stability analysis is essentially static even after the dynamic variation of external conditions is incorporated, and it only assesses whether a slope might fail and provides no insight on the behavior of mass movement during the sliding process. This missing information is essential to the modeling of long-term slope evolution, since the distance of translation downslope controls the change of slope form. Additionally, it also helps an engineer to evaluate hazard and land use zoning.

Models of the threshold for cessation of motion have been developed for debris flow, in terms of flow thickness and slope gradient, but there is a lack of models for prediction of mass movement process. Thus, detailed mechanisms of slope failure constitute an important theme for slope stability research (Anderson and Richards 1987). Iverson (1986) developed models to predict the progress of failure. The models present a detailed analysis for a complex landslide undergoing progressive failure as the downslope translation on the lower slope removes support for the material upslope.

Chau and Wong (2003) proposed a landslide model to characterize the movement of soil mass in shallow slope slides during failure process and described the extension of the model to soils with strain-softening characteristics. Yam (2005) developed numerical solutions for soil movements subjected to external load, matric suction loss, and water level rise. The landslide model divides the entire sliding mass into numerous blocks as shown in Figure 1-1. In the landslide model, two spring-slider systems are proposed. One is located between the bottom of each block and the sliding surface (slider block-basal spring) and the other is located between the interfaces of each block (slide block-interslice spring) as shown in Figure 1-2. The detailed equilibrium equations are presented in the literature review section in Chapter 2.

The mechanical behaviors of the two spring-slider systems can be controlled by the two stress state variables, net confining stress ($\sigma - u_a$) and matric suction ($u_a - u_w$). The physical properties of unsaturated soils can be altered by their void ratios and clay contents. These four parameters are expected to impart influences on stiffness and strength of the spring-slider systems and will be examined by laboratory testing in this study.

1.2 Objective of Thesis

The objectives of the thesis are to examine the behaviors of the two spring-slider systems in Wong's model through laboratory testing. These can be achieved as follows:

- Simulate the slider block-basal spring by performing direct shear box tests on disturbed samples of three soils to determine the shear stiffness and strength parameters, net confining stress ($\sigma - u_a$) and matric suction ($u_a - u_w$)
- Simulate the slider block-interslice spring by performing triaxial compression tests on the same samples to determine the same compressive stiffness and strength parameters as direct shear box tests
- Correlate these stiffness and strength parameters with four measurable parameters, net confining stress ($\sigma - u_a$) and matric suction ($u_a - u_w$), void ratio, and clay content
- Conduct case study to illustrate the effectiveness of the correlation

1.3 Outline of Thesis

Chapter 1 provides the background information on this research investigation, introduces the objectives of this thesis, and outlines the contents of each chapter.

Chapter 2 presents literature review on soil mechanics for unsaturated soils, the definition of matric suction, and a detailed description of Wong's landslide model.

Chapter 3 describes a series of direct shear box tests, which determine the effects of different parameters on the behavior of slider block-basal spring. Shear stiffness and strength equations are developed in terms of matric suction and net confining stress based on the results of the tests.

Chapter 4 discusses the effects of the same parameters from direct shear box tests on the behavior of slider block-interslice spring. A series of triaxial tests were performed to develop equations in describing the compressive stiffness and strength in terms of matric suction and net confining stress.

Chapter 5 presents a case study of slope failure in Sunnyside Hill, Calgary. A geotechnical investigation was conducted on the slope, which consisted of field works including drilling test holes by Golder Associate Ltd. and monitoring soil suction for one year. One of the proposed equations in Chapters 2 was implemented to a slope stability analysis of the most recent slope slides at this site.

Chapter 6 concludes the findings of this thesis and recommends some future studies.

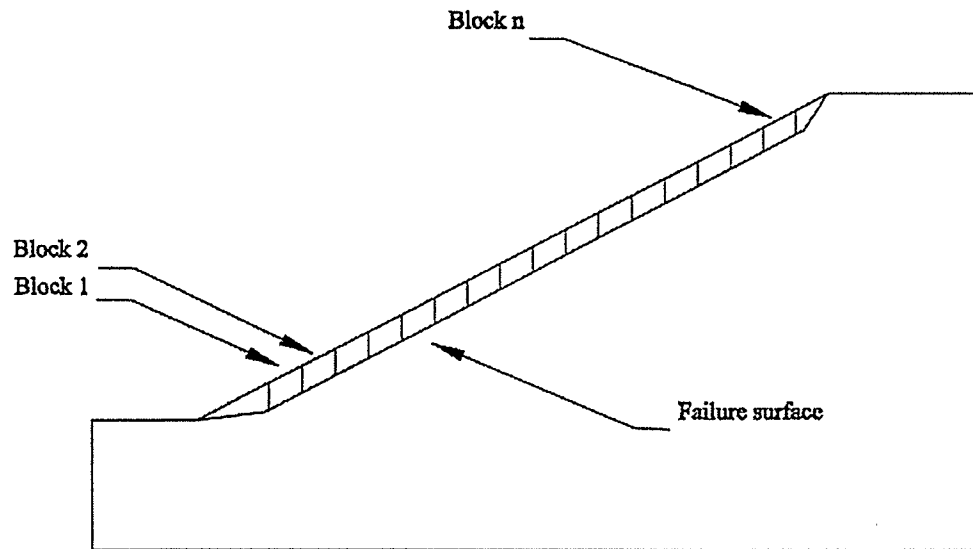


Figure 1-1: Landslide model – shallow slope (translational) failure surface

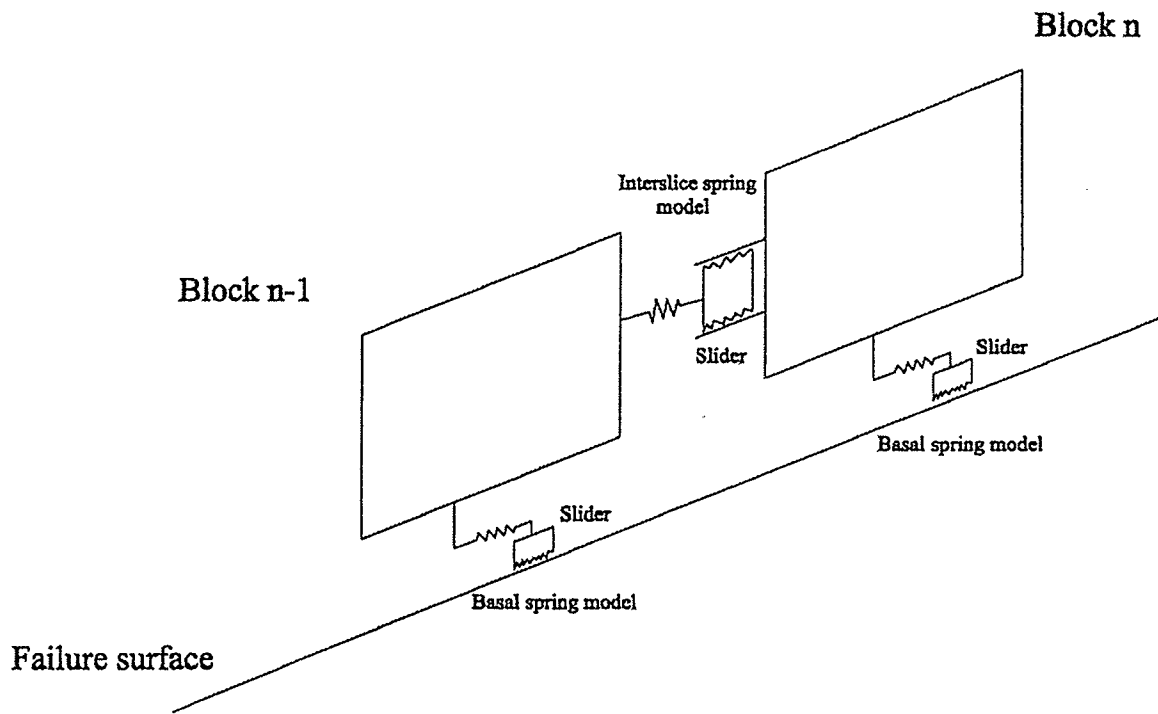


Figure 1-2: Basal and interslice spring-slider models

CHAPTER 2: LITERATURE REVIEW

2.1 Unsaturated Soil Mechanics

Soil mechanics is a combination of engineering mechanics and the properties of soils. This description is broad and can encompass a wide range of soil types. These soils could either be saturated or unsaturated. The classical concept of saturated soil mechanics has been successfully applied to various engineering problems; however, the differentiation between saturated and unsaturated soils becomes necessary due to basic differences in their nature and engineering behavior.

2.1.1 Phases of an unsaturated soil

An unsaturated soil is commonly referred to as a three-phase system, which consists of the air, water, and soil solid phases. The contractile skin (i.e., the air-water interface) has been introduced as a fourth and independent phase (Fredlund and Morgenstern 1977). The most distinctive property of the contractile skin is its ability to exert a tensile pull. It behaves like an elastic membrane under tension throughout the soil structure. The tensile pull generates surface tension on the contractile skin, and its magnitude is governed by the term, matric suction ($u_a - u_w$). The definition of matric suction is described in details in Section 2.2.

2.1.2 Stress state variables

The mechanical behavior of a soil can be described in terms of the state of stress in the soil. The state of stress in a soil consists of certain combinations of stress variables that can be referred to as stress state variables. The definition of stress state variables is the non-material variables required for the characterization of the stress condition (Fredlund and Rahardjo 1993).

The stress state variable for a saturated soil is effective stress ($\sigma - u_w$), which is defined as the difference of the total normal stress and pore water pressure. The effective stress concept forms the fundamental basis for studying saturated soil mechanics. All mechanical aspects of a saturated soil are governed by the effective stress. The effective stress has proven to be the only stress state variable controlling the behavior of a saturated soil.

Unsaturated soil behavior is more complex than saturated soil behavior because it changes from a two-phase system as a saturated soil to a four-phase system. As a result, the effective stress concept can not adequately describe the unsaturated soil behavior.

Fredlund and Morgenstern (1977) presented a theoretical stress analysis of an unsaturated soil on the basis of multi-phase continuum mechanics. In the four-phase system, the soil particles were assumed to be incompressible and the soil was treated as though it were chemically inert. These assumptions are consistent with those used in saturated soil mechanics. In their conclusions, any two of three possible normal stress variables can be used to describe the stress state of an unsaturated soil. The three possible combinations are (1) $(\sigma - u_a)$ and $(u_a - u_w)$, (2) $(\sigma - u_w)$ and $(u_a - u_w)$, and (3) $(\sigma - u_a)$ and $(\sigma - u_w)$.

The proposed stress state variables for unsaturated soils have been experimentally tested and the tests are called “null” tests. The idea of the ‘null’ tests is based on the criterion that a suitable set of independent stress state variables are those that produce no distortion or volume change of an element when the individual components of the stress state variables are modified, but the stress state variables themselves are kept constant. Thus the stress state variables for each phase should produce equilibrium in that phase when a stress point in space is considered (Fredlund and Morgenstern 1977). The results of the tests prove that all three possible combinations can be the stress state variables of an unsaturated soil.

In this study, the net confining stress ($\sigma - u_a$) and matric suction ($u_a - u_w$) combination is used because the effects of a change in total normal stress can be separated from the effects caused by a change in the pore water pressure.

2.2 Matric Suction

In soil physics, the soil suction theory was mainly developed in relation to the soil-water-plant system. Matric suction is a portion of soil suction and it is commonly referred to as the free energy state of soil water. The free energy of the soil water can be measured in terms of the partial vapor pressure of the soil water (Fredlund and Rahardjo 1993).

In geotechnical engineering, matric suction is often related to the difference of the pore air and pore water pressure acting on the contractile skin. The phenomenon of surface tension is the result of matric suction. A molecule in the interior of the water experiences equal forces in all directions, which means there is no unbalanced force. A water molecule within the contractile skin experiences an unbalanced force towards the interior of the water. This unbalanced force generates a tensile pull along the contractile skin and the tensile pull causes the phenomenon of surface tension on the contractile skin (Fredlund and Rahardjo 1993).

Matric suction is also associated with the capillary phenomenon. In the capillary model, the radius of curvature is inversely proportional to the capillary rise. The radius of curvature can be considered analogous to the pore radius in a soil. As a result, the smaller the pore radius of a soil, the higher the matric suction can be (Fredlund and Rahardjo 1993).

The surface tension associated with the contractile skin results in a reaction force on the wall of the capillary tube. The resultant of the force produces compressive stresses on the wall of the tube. Therefore, the contractile skin results in an increased compression of the soil structure. In other words, the presence of matric suction in an unsaturated soil

increases the shear strength of the soil. This also indicates that matric suction has the ability to control the mechanical behavior of an unsaturated soil and it is one of the stress state variables (Fredlund and Rahardjo 1993).

2.3 Wong's Landslide Model

In Wong's landslide model, free body diagrams of the blocks and their force components are presented in Figure 2-1. From the free body diagrams, dynamic equilibrium equations along x and y directions, parallel and perpendicular respectively, to the failure surface are derived as follows:

Block 1

$$\Sigma F_x = 0;$$

$$m_1 \frac{d^2 x_1}{dt^2} - F_1 + R_{12} \cos(\theta_{12} - \alpha) + W_1 \sin \alpha = 0 \quad (2.1)$$

$$\Sigma F_y = 0;$$

$$N_1' - W_1 \cos \alpha - R_{12} \sin(\theta_{12} - \alpha) = 0 \quad (2.2)$$

Block 2

$$\Sigma F_x = 0;$$

$$m_2 \frac{d^2 x_2}{dt^2} - F_2 - R_{12} \cos(\theta_{12} - \alpha) + R_{23} \cos(\theta_{23} - \alpha) + W_2 \sin \alpha = 0 \quad (2.3)$$

$$\Sigma F_y = 0;$$

$$N_2' - W_2 \cos \alpha + R_{12} \sin(\theta_{12} - \alpha) - R_{23} \sin(\theta_{23} - \alpha) = 0 \quad (2.4)$$

Block n

$$\Sigma F_x = 0;$$

$$m_n \frac{d^2 x_n}{dt^2} - F_n - R_{(n-1,n)} \cos(\theta_{n-1,n} - \alpha) + W_n \sin \alpha = 0 \quad (2.5)$$

$$\Sigma F_y = 0;$$

$$N_n' - W_n \cos \alpha + R_{(n-1,n)} \sin(\theta_{n-1,n} - \alpha) = 0 \quad (2.6)$$

where

m_1, m_2, m_n = masses of soil blocks for Blocks 1, 2, and n, respectively

F_1, F_2, F_n = basal friction forces for Blocks 1, 2, and n, respectively

$R_{12}, R_{23}, R_{(n-1,n)}$ = interslice reaction force for Blocks 1, 2, and n, respectively

N_1', N_2', N_n' = basal normal forces for Blocks 1, 2, and n, respectively

W_1, W_2, W_n = weight force of soil blocks for Blocks 1, 2, and n, respectively

x_1, x_2, x_n = distances of blocks traveled for Blocks 1, 2, and n, respectively

α = slope angle

Each of the front and end blocks (Blocks 1 and n) has five unknowns. The five unknowns of Block 1 are displacement (x_1), basal friction and normal forces (F_1, N_1'), interslice reaction forces (R_{12}), and the angle of the force component ($\theta - \alpha$). The five unknowns of Block n are $x_n, F_n, R_{(n-1,n)}, (\theta - \alpha), N_n'$. Each of the blocks, between Block 2 to Block (n-1), has six unknowns ($x_2, F_2, R_{12}, R_{23}, (\theta - \alpha), N_2'$). For shallow slides, angle, θ , is approximately equal to slope angle, α . x_1, x_2 and x_n represent the distances the blocks traveled, which are the output results of the slide model analysis. If the force components $R_{(n-1,n)}, R_{(n,n+1)}, F_n$, and N_n' can be solved, this leaves n unknowns with n equations and the slide model equations can also be solved.

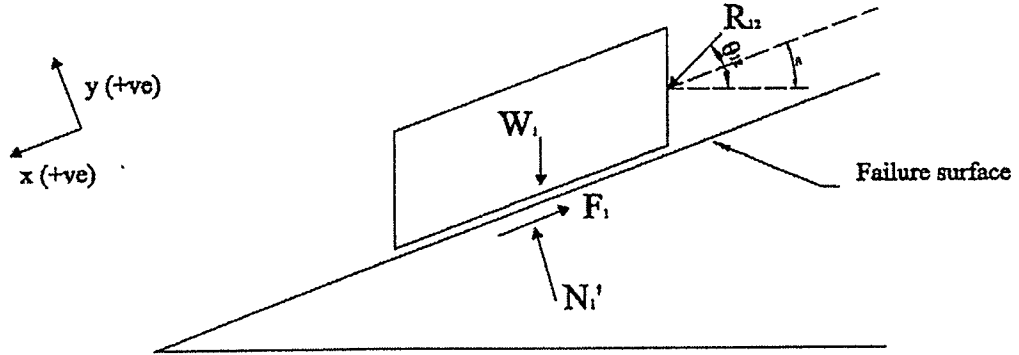
The interslice and basal forces are inter-related to the displacements in the soil spring-slider models of using the Mohr-Coulomb theory. The unknown force components can be determined by adding two spring-slider systems as shown in Figure 1-2.

The properties of slider block-basal spring can be obtained from direct shear box tests. In such a spring, elastic is followed by plastic. The results of these tests can be presented as

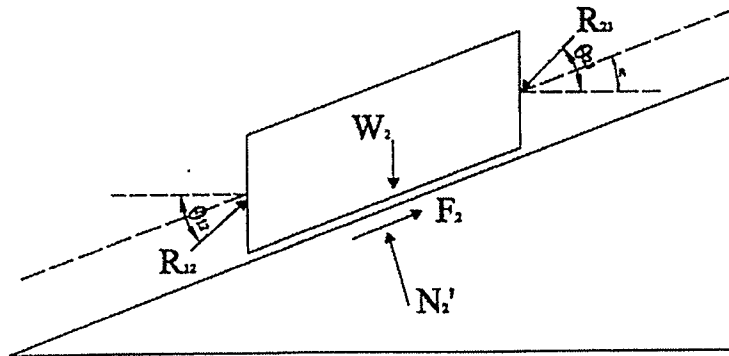
plots of F/N' (ratio of friction and normal forces) and δ_h (horizontal displacement) as shown in Figure 2-2. From this test data, the unknown, F and N' in equations (2.1) to (2.6), can be determined.

The properties of the slider block-interslice spring can be determined from triaxial compression tests. The plots of σ_a (axial stress) and ε_a (axial strain), presented in Figure 2-3, provide the required information to determine the relationship between the block relative displacements and interslice forces. From this test data, the unknown, R in equations (2.1) to (2.6), can also be determined.

Block 1



Block 2



Block n

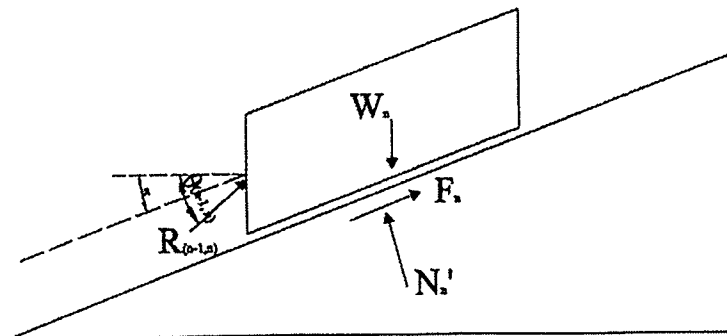


Figure 2-1: Free body diagram of each block

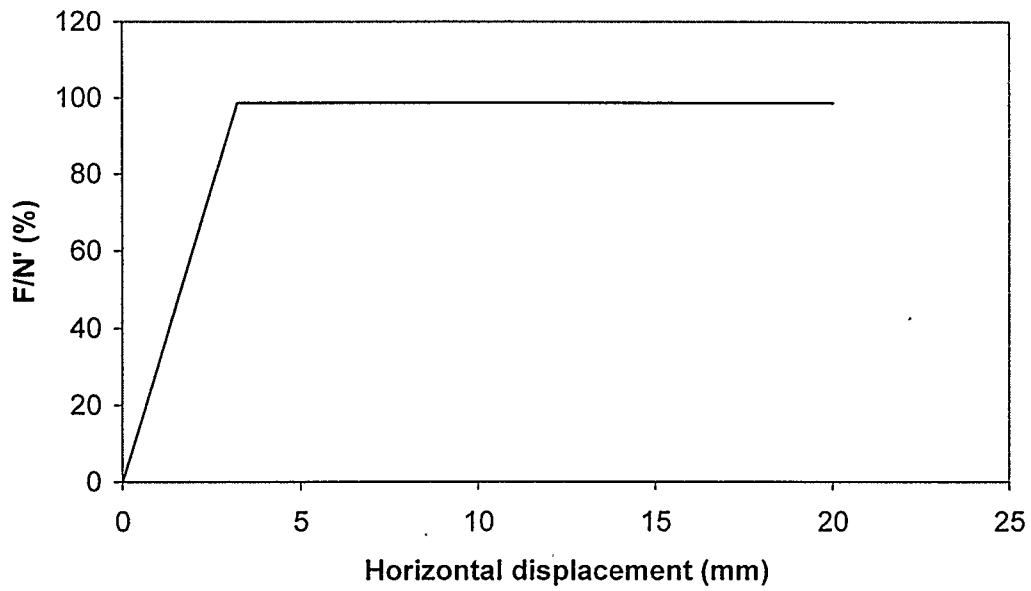


Figure 2-2: Plot of generalized direct shear box test results

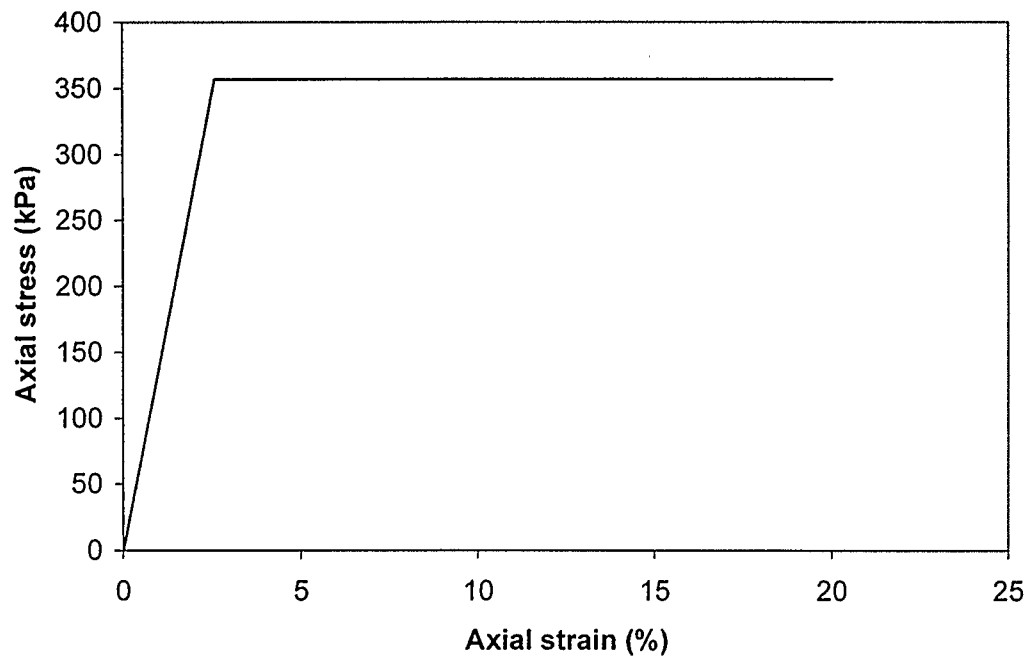


Figure 2-3: Plot of generalized triaxial compression test results

CHAPTER 3: DIRECT SHEAR BOX TESTS

3.1 Introduction

As stated in Chapter 1, the shear stiffness and strength parameters, net confining stress ($\sigma - u_a$), and matric suction ($u_a - u_w$) can be determined by the results of the direct shear box tests. The findings of these parameters allow shear stiffness and strength equations to be developed with two void ratio (e) ranges and three clay content values. The objective of this chapter is to describe the experimental method, present the test results, introduce the shear stiffness and strength equations, and illustrate examples using the proposed equations.

3.2 Description of Soil Samples

Three different soil samples with varying clay contents, expected to display different soil behaviors, are examined in this study. The first soil sample was obtained from a newly developed subdivision in Discovery Ridge Phase II located at the southwest quadrant of the intersection of Glenmore Trail and 69th Street S.W., Calgary. This soil sample contains the highest clay content among the three soil samples. The second soil sample was obtained from ten different locations on the slope at a depth of 0.3 m below surface, which has experienced instability problems on Sunnyside Hill, Calgary. These locations are shown in Figure 3-1. This soil sample was obtained at the time when the soil suction measurements were made from April to November 2001. The third soil sample was taken from test pitting on a slope located at northbound Shaganappi Trail, approximately 300 meters north of 16th Ave. N.W., Calgary. This sample was obtained at depths ranging from 0.3 m to 2.5 m due to the organic content present near the surface.

3.3 Tests and Testing Procedures

3.3.1 Sieve analysis, soil classification, and compaction curves

Soils were initially oven dried at 130 °C for 24 hours. Sieve analysis was then performed by screening soils through U.S. Standard Sieve No.4 (4.75 mm sieve opening) to retain and remove any gravel size material. The presence of gravel in the soil sample is expected to affect the uniformity of the specimens of the direct shear box and triaxial compression tests. Hydrometer tests were then performed on the soils passing this sieve. One set of tests was performed on each of the three soils. Using The Unified Soil Classification System (USCS), the three soils are described as SC-ML (Discovery Ridge), SM-ML (Sunnyside Hill), and SM (UC Site). The composition of the three soil samples are listed in Table 3-1 and the detailed soil gradation tests are shown in Figure 3-3.

Standard Proctor tests (ASTM (1980), Designation D698) were also performed on the three soil samples. The compaction curves results are shown in Appendix A.

3.3.2 Direct shear box tests

A schematic diagram of the direct shear box is illustrated in Figure 3-2. The sample is placed between two porous stones to facilitate drainage. The normal load is applied to the sample by adjusting the air pressure and the shear force is supplied by the piston connected to an electric motor. The horizontal displacement is measured by a horizontal dial gauge and the shear force by a load dial gauge. During the testing process, normal force, horizontal force, vertical, and horizontal displacements are recorded by a computer connected to the direct shear box equipment.

The direct shear box test has several disadvantages with one of them being the limitation of measurement of pore water pressure. In addition, shear stress on the failure plane is not uniform as failure usually occurs progressively from the edges towards the center of

the specimen, but shear stress is recorded at the center of the specimen. Moreover, the area under the shear and vertical loads do not remain constant throughout the test.

Specimens for direct shear box tests could not be brought to full saturation. On the contrary a high degree of saturation could be achieved by immersing specimens in water for a sufficiently long period prior to testing. Alternatively, in this study, soil samples were compacted in various water contents to achieve different degree of saturation. During the testing process, the shearing rate was set to a value of 0.1 mm per minute so that the change of the pore water pressure was negligible.

The testing procedures for the direct shear box tests are summarized as follows:

1. The samples were oven dried overnight at 60 °C.
2. The samples were screened on a 4.75 mm sieve. The portion passing was used.
3. The samples were moisture conditioned to the desired moisture contents.
4. Standard Proctor tests (ASTM (1980), Designation D698) were performed on the samples using the shear box mold.
5. The samples with the mold were placed in the shear box test device for 24 hours after the completion of Standard Proctor tests. The required normal stresses were then applied.
6. The shear rate was set at 0.1 mm per minute and the tests started.
7. After the samples had reached its residual strength, the tests stopped.
8. The samples were taken out with the mold and soil suctions were measured using a soil moisture probe. (Procedures for soil suction measurement are stated in Section 3.3.3.)
9. The samples were oven dried overnight at 130 °C and the moisture contents were determined (ASTM (1992), Designation D2216).

The tests were performed on each of the three soil samples stated in Section 3.2 at five different moisture contents (two below the optimum moisture content, one close to the optimum moisture content, and two above the optimum moisture content) and at four normal stresses (10, 30, 50, and 100 kPa). Therefore, each suite of direct shear box tests on each soil sample required twenty tests at various moisture content and normal stress combinations. Thus, for this study, the total number of direct shear box tests was sixty. The raw data of the tests are presented in Appendix B. Note that the void ratio in Appendix B is determined by assuming the solid densities of the three soils equal to 2650 kg/m³ and using the dry density values obtained from the Standard Proctor tests as presented in Appendix A.

3.3.3 Soil and matric suction measurements

The equipment used for the matric suction measurement was a Soil Moisture Probe, Model 2900FI (Figure 3-5) manufactured by Soil Moisture Equipment Corp. It measures the negative pore water pressure with which water is held in the soil by the soil particles. The measured negative pore water pressure is numerically equal to the matric suction when the pore air pressure is atmospheric. In this study, all measurements using the soil moisture probe are called soil suction and they are numerically equal to the matric suction.

The basic components of the soil moisture probe include a porous ceramic cup, a steel connecting tube, and a vacuum gauge. The ceramic cup is placed in good hydraulic contact with the soil and allows transfer of water into and out of the tube according to the tension in the soil. The vacuum inside the tube equilibrates with the soil water tension and the dial gauge provides a direct readout of the tension or suction in kPa. To calibrate the equipment before each test, the vacuum gauge should read zero when the probe is kept in water.

The first operation for a typical soil suction measurement is to core a hole in the soil with the coring tool to accept the probe. This operation pulls out the soil core and provides a proper sized hole in the soil for insertion of the probe. Prior to removing the probe from the carrying case, the null knob should be turned clockwise as far as it goes and then turned counterclockwise for a half turn. This operation provides the proper range for the null knob when a reading is being taken. The probe is then removed from the carrying case, inserted into the hole made by the coring tool, and pushed in so that the sensing tip is in firm contact with the soil.

After the probe is inserted into the hole, the probe should remain undisturbed for approximately one minute. At the end of this time, the vacuum gauge should be monitored. The null probe is then turned counterclockwise to bring the gauge up to a value, which is one and one-half times the initial reading after the one-minute period. After making the first adjustment, the gauge movement should be monitored after 15 to 30 seconds. Tapping the dial gauge lightly with fingers while observing the pointer movement tends to reduce the normal internal friction so that changes in the pointer position are observable with minimum lapsed time. The recorded suction value is the average of the two trials.

3.4 Data Acquisition and Compilation

3.4.1 Soil-water characteristic curve

Fredlund, et al. (1997) presented a model for the prediction of the soil-water characteristic curve (SWCC), based on the particle-size distribution, dry density, void ratio, and specific gravity of soil. Typical soil-water characteristic curves and grain-size distribution curves for a mixture of sand, silt, and clay were obtained from SoilVision (Fredlund 1996).

Grain-size distribution and soil-water characteristic curves of the three soil samples are shown in Figures 3-3 and 3-4, respectively, and presented with two other soil samples from SoilVision in the same figure for comparison. The soil-water characteristic curves are plotted the graphs of volumetric water content versus matric suction. The volumetric water content is calculated by the ratio of volume of water to total volume and the matric suction is measured by the soil moisture probe.

In Figure 3-3, each of the soil samples presents a unique distribution curve and thus, their soil-water characteristic curves are expected to be different. However, in Figure 3-4, the soil-water characteristic curves of the Sunnyside Hill and UC Site soil samples are similar and the curves of Discovery Ridge and loamy sand soil samples also have relatively the same shape. Hence, the relationships of the grain-size distribution and soil-water characteristic curves in this study are not found to agree with those of the SWCC model. The discrepancy of the results is possibly due to the similar nature of the three soil samples as they all contain significant portions of sand and silt.

3.4.2 Shear stress (τ) versus horizontal displacement (δ_h)

The graph of shear stress versus horizontal displacement illustrates a typical direct shear box test result as shown in Figure 3-6. This figure contains five sets of data series identified by different moisture contents (MC) at a normal stress of 100 kPa. The graphs at varying normal stress and for the other two soil samples are presented in Appendix C.

The initial shear stiffness (k_h) is represented by the initial slope of the graph with the unit of shear stress [kPa] per horizontal shear displacement [mm]. The initial slope is determined by the slope of a straight line drawn from the origin to 50% of the peak stress, shown as dotted line in Figure 3-6. The peak and residual strength are also determined from the graphs. The tests are unloaded after the residual strength has been reached and the slopes of the unloading curve are also measured. In some of the tests, the soils with

high moisture contents do not display residual strengths characteristics and therefore, they are unloaded after their ultimate strength has been reached.

3.4.3 Vertical displacement (δ_v) versus horizontal displacement (δ_h)

The graph of vertical displacement versus horizontal displacement is shown in Figure 3-7. The graph consists of five curves, each representing a different moisture content (MC) at a normal stress of 100 kPa. The maximum dilation rates are determined by the slopes of the curves aligned with the peak shear stress, shown as dotted line in the same figure. On the graphs, negative vertical displacement indicates the occurrence of dilation while the opposite indicate contraction. The term dilation is defined as the increase in volume of a soil sample during shearing and the term contraction is defined as the decrease in volume of a soil sample during shearing. The graphs at varying normal stress and for the other two soil samples are presented in Appendix D.

3.4.4 Shear stiffness (k_h) versus net confining stress ($\sigma - u_a$) and matric suction ($u_a - u_w$)

Experimental studies by Janbu (1963) showed that the relationship between the initial tangent modulus (E_i) and effective confining stress may be expressed as:

$$E_i = K(P_a) \left(\frac{\sigma_c'}{P_a} \right)^n \quad (3.1)$$

where

E_i = initial tangent modulus [kPa],

σ_c' = effective confining stress [kPa],

P_a = atmospheric pressure [101.3 kPa],

K = a modulus number, and

n = the exponent determining the rate of variation of E_i with σ_c' .

The initial tangent modulus is defined as the initial slope of the graph of principal stress difference versus axial strain curve. In a direct shear box test, the initial slope of the graph of shear stress versus horizontal displacement can be expressed as shear stiffness (k_h). Assuming that the shear stiffness follows that of equation (3.1),

$$k_h = K(P_a) \left(\frac{\sigma_c'}{P_a} \right)^n \quad (3.2a)$$

$$k_h = K(101.3\text{kPa}) \left(\frac{\sigma_c'}{101.3\text{kPa}} \right)^n \quad (3.2b)$$

$$k_h = K(101.3\text{kPa}) \left(\frac{1}{101.3} \right)^n \left(\frac{\sigma_c'}{1\text{kPa}} \right)^n \quad (3.2c)$$

$$k_h = K_h \left(\frac{\sigma_c'}{P} \right)^n \quad (3.2d)$$

where

k_h = shear stiffness [kPa/mm],

K_h = constant = $K (101.3) (1 / 101.3)^n$ [kPa/mm],

σ_c' = effective confining stress [kPa],

P_a = atmospheric pressure [101.3 kPa],

P = one unit of pressure [1 kPa],

K = a modulus number [mm⁻¹], and

n = the exponent determining the rate of variation of k_h with σ_c' .

Equation (3.2d) can be used in saturated soil problems as it involves effective confining stress. For unsaturated soil, the two stress state variables, net confining stress ($\sigma - u_a$) and matric suction ($u_a - u_w$) can replace the effective confining stress term in equation (3.2d).

During the initial setup of the direct shear box test, the pore air pressure was present immediately after the testing specimen was compacted in the mold. It is assumed that the pore air pressure gradually reduced to zero during the 24 hours before the start of the test when the soil reached equilibrium with atmosphere. Thus, the net confining stress term becomes (σ) and is equivalent to the applied normal stress in the tests. The matric suction term, $(u_a - u_w)$ becomes $(-u_w)$ and is equivalent to the soil suction value (u_s) measured by the soil moisture probe. The effects of the two stress state variables on the shear stiffness are separated and thus, equation (3.2d) becomes equation (3.3).

$$k_h = K_A \left(\frac{\sigma}{P}\right)^n + K_B \left(\frac{u_s}{P}\right)^m \quad (3.3)$$

where

K_A and K_B = constants [kPa/mm],

σ = net confining stress [kPa],

u_s = soil suction [kPa],

$P = 1$ [kPa], and

n and m = exponents determining the rate of variation of k_h with σ and u_s , respectively.

Since soils display either dilation or contraction behavior with different moisture contents, the test data of each soil samples are divided into two void ratio ranges, representing contraction and dilation. The higher range yields contraction behaviors and the lower range yields dilation behaviors.

The constant, K_A and the exponent, n , are determined from the graphs of shear stiffness (k_h) versus net confining stress (σ) using the data ranges of soil suction values closest to zero in Figures 3-8 to 3-13. Similarly, the constant, K_B and the exponent, m , are determined from the graphs of shear stiffness (k_h) versus suction (u_s) using data points grouped by net confining stress as shown in Figures 3-14 to 3-19. Assuming the effect of

the lowest net confining stresses (10 kPa and 30 kPa) on shear stiffness are negligible, the first term in equation (3.3) becomes zero. The data ranges of this net confining stress are used to determine K_B and m .

3.4.5 Shear strength (τ) versus net confining stress ($\sigma - u_a$) and matric suction ($u_a - u_w$)

Fredlund and Morgenstern (1977) developed the shear strength equation of an unsaturated soil as follows:

$$\tau = c + (\sigma - u_a) \tan \phi' + (u_a - u_w) \tan \phi_\beta \quad (3.4)$$

where

c = cohesion [kPa],

$\phi' = \phi_d + \phi_e$,

ϕ_d = dilation angle; ϕ_e = internal true friction angle, and

ϕ_β = angle indicating the rate of increase in shear strength relative to the matric suction.

Equation (3.4) is simplified to equation (3.5) as the air phase was kept in equilibrium condition during the tests ($u_a = 0$) and the matric suction term ($u_a - u_w$) is replaced by soil suction (u_s).

$$\tau = c + \sigma \tan \phi' + (u_s) \tan \phi_\beta \quad (3.5)$$

The shear strength test data of each soil samples are divided into two void ratio ranges with the higher range yielding contraction behaviors and the lower range yielding dilation behaviors. The angles, ϕ' and ϕ_β in equation (3.5) are determined from the graphs of shear strength (τ) versus net confining stress (σ) using data points grouped by different ranges of soil suction (u_s) as illustrated in Figures 3-20 to 3-25.

In Figures 3-20 to 3-25, slopes of the six graphs are determined and the average value is taken as the value of $\tan \phi'$. Cohesion values of the six data series are also determined from the y-intercept of the graphs and plotted against their corresponding soil suction values as shown in Figures 3-26 to 3-28. Cohesion values of the three soil samples are determined from the best-fit lines that intercept the y-axis and the values of $\tan \phi_p$ are obtained from the slopes of the best-fit lines.

3.5 Data Analysis and Discussion

In Figure 3-6, the initial slopes of the graphs, which represent the initial shear stiffness, increases with decreasing moisture contents. The graphs reach the peak when the test samples reach their maximum strength. The test samples with lower moisture contents tend to reach higher shear strength values. The peak strength, expressed in terms of stress ratio (τ/σ), as well as the initial shear stiffness are summarized in Table 3-2 with respect to their moisture contents and the applied normal stresses. In the table, both the peak strength and the initial shear stiffness increase with increasing normal stresses.

In Figure 3-6 and the figures in Appendix C, most of the test samples with moisture contents below the optimum value display peak and residual strength characteristics. The test samples with moisture contents above the optimum value present different types of curves, which become flatter with little or no difference in peak and residual strengths. This shows the change of soil behavior from brittle to ductile when the moisture contents increase. The residual strength, expressed in terms of stress ratio (τ/σ), is also summarized in Table 3-2.

The three soil samples, each with different clay contents, exhibit different strength characteristics. The Discovery Ridge soil, which contains the highest clay content, display the highest peak strength and initial shear stiffness. The higher clay contents

contribute to higher cohesion and higher matric suction values, and thus, higher shear strength.

Table 3-3 shows the rate of dilation. The test samples with moisture contents below optimum undergo dilation during the shearing process due to their relatively higher dry density. The test samples with higher moisture contents have relatively lower dry density and no dilation characteristic is evident on these test samples. In this study, most of the test samples with moisture contents above the optimum value do not show dilation characteristic.

The relationships among the parameters, shear stiffness, matric suction, and net confining stress are shown in Figures 3-8 to 3-19. These figures show that the shear stiffness increases with increasing matric suction and increasing net confining stress. Thus, based on the correlations, two shear stiffness equations are developed in the form of equation (3.3) as outlined in Section 3.4.4 on each of the three soil samples with two void ranges.

Soil sample: Discovery Ridge

For $0 < u_s < 20$ kPa,

$$k_h = 0.50\left(\frac{\sigma}{P}\right)^{1.30} + 8.30\left(\frac{u_s}{P}\right)^{1.31} \quad e \geq 0.456 \quad (3.6)$$

$$k_h = 3.80\left(\frac{\sigma}{P}\right)^{0.91} + 0.35\left(\frac{u_s}{P}\right)^{2.60} \quad e < 0.456 \quad (3.7)$$

Soil sample: Sunnyside Hill

For $0 < u_s < 35$ kPa,

$$k_h = 0.94\left(\frac{\sigma}{P}\right)^{0.46} + 0.09\left(\frac{u_s}{P}\right)^{2.04} \quad e \geq 0.480 \quad (3.8)$$

$$k_h = 5.93\left(\frac{\sigma}{P}\right)^{0.59} + 0.25\left(\frac{u_s}{P}\right)^{1.97} \quad e < 0.480 \quad (3.9)$$

Soil sample: UC Site

For $0 < u_s < 40$ kPa,

$$k_h = 4.15\left(\frac{\sigma}{P}\right)^{0.02} + 1.97\left(\frac{u_s}{P}\right)^{1.06} \quad e \geq 0.460 \quad (3.10)$$

$$k_h = 2.89\left(\frac{\sigma}{P}\right)^{0.65} + 0.05\left(\frac{u_s}{P}\right)^{2.06} \quad e < 0.460 \quad (3.11)$$

where

e = void ratio,

k_h = shear stiffness [kPa/mm],

σ = net confining stress [kPa],

u_s = soil suction [kPa], and

$P = 1$ [kPa].

Note: Equations (3.6) to (3.11) are only valid in the range of $0 < \sigma < 100$ kPa and the specified soil suction ranges.

The adequacy of a fitted regression model can be expressed by the coefficients of determination (R^2) in equation (3.12). The values of R^2 provide a measure of the relative amount of variation in shear stiffness explained by the regression lines. If the R^2 value is close to 1.00, the regression equation explains most of the variation in the dependent value. When the R^2 value is close to zero, the regression line does not explain the dependent value well.

$$R^2 = \frac{SSR}{SST} = \frac{\sum_{i=1}^n (\hat{y}_i - \bar{y})^2}{\sum_{i=1}^n (y_i - \bar{y})^2} \quad (3.12)$$

where

SSR = regression sum of squares,

SST = total sum of squares,

\hat{y}_i = estimated values from regression lines,

y_i = actual values, and

\bar{y} = mean.

By using equation (3.12), the R^2 values of the shear stiffness equations range from 0.41 to 0.87 as shown in Table 3-4.

To display and compare the correlations, equations (3.6) to (3.11) are shown through three-dimensional graphs in Figure 3-29. The effects of matric suction and net confining stress on the shear stiffness are shown in this figure. The magnitude of the shear stiffness is more dependent on matric suction than net confining stress. The greater effect of matric suction on shear stiffness can be explained by the relatively low net confining stress range applied in the tests as the analyses can only be applied to shallow slope failure problems.

The effects of void ratio and clay content on the shear stiffness are difficult to be compared with other parameters since each soil sample only consists of two void ratio ranges and only three different clay contents are involved. However, from the six graphs in Figure 3-29, the contribution to shear stiffness by void ratio and clay content can still be seen although no numerical correlation can be developed with the available data. From the six graphs, the soil sample with the highest clay content (Discovery Ridge) displays the highest shear stiffness while the other two samples display similar shear stiffness with less clay contents. The lower void ratio ranges also have higher stiffness values than the higher void ratio range and thus, dilation is related to shear stiffness. It is a consequence of shearing and does not contribute to higher shear stiffness. Thus, shear stiffness is a function of matric suction, net confining stress, void ratio, and clay content and it is more dependent on matric suction than on net confining stress.

The unloading test results are not included in the analysis as the three soil samples display similar unloading behavior with respect to different moisture contents and normal stress and thus, no correlation can be developed. The magnitudes of shear stiffness of the unloading curves range from 200 to 800 kPa/mm without displaying representative trends.

In Figures 3-20 to 3-25, the graphs of shear strength (τ) versus net confining stress (σ) show definite correlations. Based on the correlations, two equations are introduced on each of the three soil samples in terms of shear strength, matric suction, and net confining stress in the form of equation (3.5), with the higher void ratio range showing contraction and the lower void ratio range showing dilation behavior during loading.

Soil sample: Discovery Ridge

For $0 < u_s < 20$ kPa,

$$\tau = 22.40 + 1.04 \sigma + 3.40 u_s \quad e \geq 0.456 \quad (3.13)$$

$$\tau = 42.79 + 0.95 \sigma + 3.23 u_s \quad e < 0.456 \quad (3.14)$$

Soil sample: Sunnyside Hill

For $0 < u_s < 35$ kPa,

$$\tau = 11.75 + 0.39 \sigma + 0.13 u_s \quad e \geq 0.480 \quad (3.15)$$

$$\tau = 28.92 + 0.74 \sigma + 1.42 u_s \quad e < 0.480 \quad (3.16)$$

Soil sample: UC Site

For $0 < u_s < 40$ kPa,

$$\tau = 9.20 + 0.27 \sigma + 2.44 u_s \quad e \geq 0.460 \quad (3.17)$$

$$\tau = 0.62 \sigma + 2.90 u_s \quad e < 0.460 \quad (3.18)$$

where

e = void ratio,

τ = shear strength [kPa],

σ = net confining stress [kPa], and

u_s = soil suction [kPa].

Similarly, by using equation (3.12), the R^2 values of the shear strength equations range from 0.33 to 0.91 and are shown in Table 3-4.

The correlations among the parameters in equations (3.13) to (3.18) are illustrated through three-dimensional graphs in Figure 3-30. The effects of matric suction, net confining stress, void ratio, and clay content on the shear strength are shown in this figure. All of the six graphs show increasing shear strength with higher matric suction and higher net confining stress. The effect of matric suction on the shear strength is greater than that of net confining stress.

The effects of void ratio and clay content on shear strength are also shown in Figure 3-30. The soils with higher clay content and lower void ratio tend to have higher shear strength. However, there are not enough data points to develop a numerical correlation between shear strength and void ratio and clay content. Based on the above correlations and trends, it is concluded that shear strength is a function of matric suction, net confining stress, void ratio, and clay content; and it is more dependent on matric suction than on net confining stress.

3.6 Illustrative Examples

The application of the shear stiffness and shear strength equations developed in Section 3.5 are illustrated through the Sunnyside Hill case study in this section. A detailed description of the site is included in Chapter 5.

The shallow landslides in Sunnyside Hill are classified as translational slip with failure depths between 1.5 to 2.0 m. The slide mass soil is classified as sandy silt with trace clay. The net confining stress at the slide surface is calculated from the depth and bulk unit weight of 2.0 m and 20 kN/m^3 , respectively. The unit weight is calculated from the average wet density values obtained from the compaction curves in Appendix A, which is approximately 2000 kg/m^3 . Therefore, the net confining stress in this case is approximately 40 kPa. The void ratio used is greater than 0.48, confirmed by ten density tests on the slopes. Thus, equations (3.8) and (3.15) are used to calculate the corresponding shear stiffness and strength in this example. Atmospheric air pressure is expected near the surface of this natural slope. With the measured soil suction at 20 kPa, the shear stiffness and shear strength are 45.7 kPa/mm and 30.0 kPa, respectively. When the soil suction is reduced to 10 kPa, the shear stiffness and shear strength are reduced to 15.0 kPa/mm and 28.6 kPa, respectively. When soil suction is further reduced to 0 kPa in its fully saturated condition, the shear stiffness and shear strength become 3.7 kPa/mm and 19.6 kPa, respectively, and the net confining stress is reduced to 20 kPa. Figure 3-31 illustrates these shear stiffness and shear strength values with respect to their soil suction.

3.7 Conclusion

The data from direct shear box testing has been used to develop empirical equations to calculate shear stiffness using inputs of matric suction and net confining stress for two void ratio ranges for the three soil samples, Discovery Ridge, Sunnyside Hill, and UC Site. These are equations (3.6) to (3.11). Equations to calculate shear strength using inputs of matric suction and net confining stress for the same three soil samples and two void ratio ranges have also been developed. These are equations (3.13) to (3.18).

The coefficients of determination are determined using equation (3.12) for the shear stiffness and strength equations as shown in Table 3-4. Equations (3.9) and (3.18) have R^2 values of 0.41 and 0.33, respectively, which indicate that more test data are required to

improve the quality of the equations. Note that equation (3.15) has a reliable R^2 value of 0.91 and it is used in the stability analyses in Chapter 5.

The effects of matric suction and net confining stress on the shear stiffness and strength are shown in the six graphs in Figure 3-29 and Figure 3-30, respectively. Both shear stiffness and strength increase with increasing matric suction and net confining stress, but the effects of matric suction are greater than those of net confining stress within the specified net confining stress range. The effects of void ratio and clay content on shear stiffness and strength have not been fully defined due to the limited data, but their effects are also shown in Figure 3-29 and Figure 3-30. As expected, shear stiffness and strength increase with decreasing void ratio and increasing clay content due to the greater friction angles and the presence of cohesion, respectively. Hence, shear stiffness and strength are functions of matric suction and net confining stress. They are more dependent on matric suction than net confining stress.

Section 3.6 illustrates that the shear strength of the Sunnyside Hill soil reduces significantly at a depth of 2.0 m below surface when its soil suction decreases from 20 kPa to 0 kPa. Figure 3-31 shows the effect of the reduction of soil suction on shear strength.

	Discovery Ridge	Sunnyside Hill	UC Site
Sand	33.3%	45.0%	62.4%
Silt	39.7%	39.5%	18.8%
Clay	27.0%	15.5%	18.8%

Table 3-1: Soil classification of the three soil samples

Normal stresses	Discovery Ridge				Sunnyside Hill				UC site			
	100kPa	50kPa	30kPa	10kPa	100kPa	50kPa	30kPa	10kPa	100kPa	50kPa	30kPa	10kPa
Initial tangent loading slope (kPa/mm)												
Test 1	416.7	270	333.3	242.9	350	93.3	225	166.2	192.9	129.5	111.9	106.3
Test 2	214.3	405	222.2	377.8	175	224	144	166.2	135	98.3	90.4	30.9
Test 3	250	192.9	222.2	136	155.6	52.5	55.4	20.8	51.9	21	39.2	17.9
Test 4	187.5	71.1	50	54.4	82.4	11.4	6.2	7.4	17.3	12	5.9	12.1
Test 5	111.1		45.5	27.2	12.7	6.6	3.5	2.9	8.1	1.7	3.8	5.3
τ/σ (peak)												
Test 1	1.609	2.53	3.243	10.17	1.581	1.738	3.233	7.05	1.525	2.266	3.77	13.44
Test 2	1.625	2.852	4.643	11.42	1.43	1.71	2.47	8.42	1.938	2.226	4.16	6.4
Test 3	1.422	2.53	4.347	11.83	1.477	2.056	2.813	5.32	1.25	1.466	2.46	4.16
Test 4	1.313	1.588	1.667	6.17	1.163	0.994	0.987	3.37	0.625	1.12	0.676	3.12
Test 5	1.156		1.727	6	0.616	0.428	0.667	1.37	0.313	0.52	0.276	1.68
τ/σ (residual)												
Test 1	1.313	1.764	2.023	3.08	1.209	1.394	2.05	4.21	1.437	1.814	2.323	5.44
Test 2	1.391	1.676	2.827	3.08	1.291	1.668	1.68	3.53	1.8	1.706	2.53	
Test 3	1.125	1.676	3.72	4.75	1.36	2	1.68	2.95		1.346		
Test 4					1.023			2.53				
Test 5												
Moisture content (%)												
Test 1	9.2	9.0	9.6	9.3	7.1	8.3	8.6	7.7	9.3	8.4	11.0	11.0
Test 2	10.6	11.4	10.8	10.8	10.7	10.3	10.7	10.0	11.5	11.2	13.4	13.4
Test 3	12.7	13.7	13.9	12.3	12.3	14.2	12.4	13.0	13.8	13.4	15.0	15.0
Test 4	14.3	16.2	16.0	14.9	14.7	15.7	15.5	15.6	15.7	15.3	17.6	17.6
Test 5	22.3		17.6	15.4	16.8	17.6	17.6	17.8	17.5	17.2	19.0	19.0

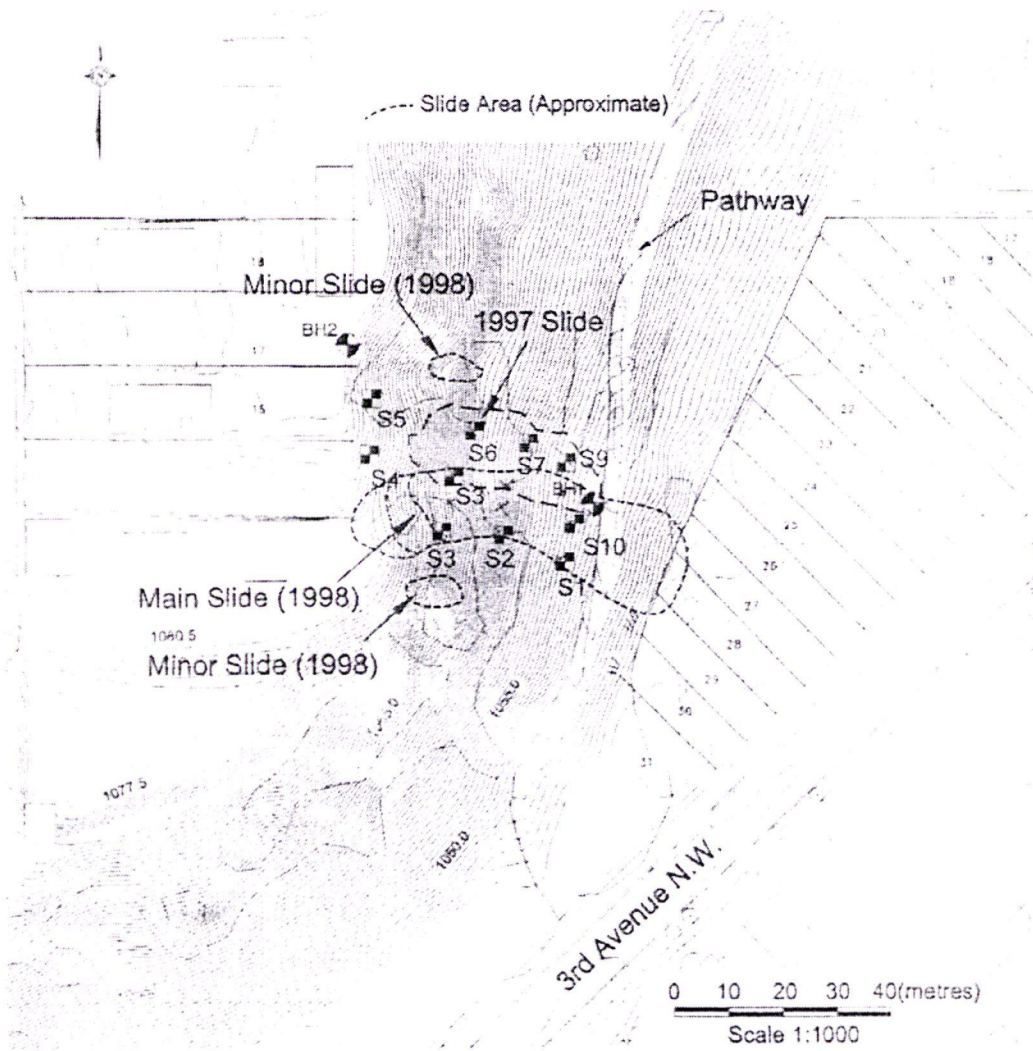
Table 3-2: Summary of results of direct shear box tests of three different soil types

Normal stresses	Discovery Ridge				Sunnyside Hill				UC Site			
	100kPa	50kPa	30kPa	10kPa	100kPa	50kPa	30kPa	10kPa	100kPa	50kPa	30kPa	10kPa
Rate of dilation												
Test 1	-0.05	-0.133	-0.3	-0.529	-0.18	-0.113	-0.1	-0.22	-0.0682	-0.148	-0.14	-0.548
Test 2	-0.0531	-0.182	-0.224	-0.589	-0.17	-0.141	-0.15	-0.46	-0.159	-0.18	-0.207	-0.258
Test 3	-0.0565	-0.076	-0.215	-0.56	-0.167	-0.193	-0.26	-0.195	-0.0297	-0.02	-0.093	-0.156
Test 4	-0.085	-0.125		-0.288	-0.053			-0.08				
Test 5				-0.216								

Table 3-3: Summary of the rate of dilation

Coefficient of Determination, R ²				
Void ratio range	Stiffness		Strength	
	low	high	low	high
Discovery Ridge	0.83	0.74	0.65	0.87
Sunnyside Hill	0.41	0.87	0.81	0.91
UC Site	0.53	0.68	0.33	0.89

Table 3-4: Coefficient of determination (R²) for shear stiffness and strength equations



- Soil suction measurement locations
- Borehole locations

Figure 3-1: Soil suction measurement and borehole locations

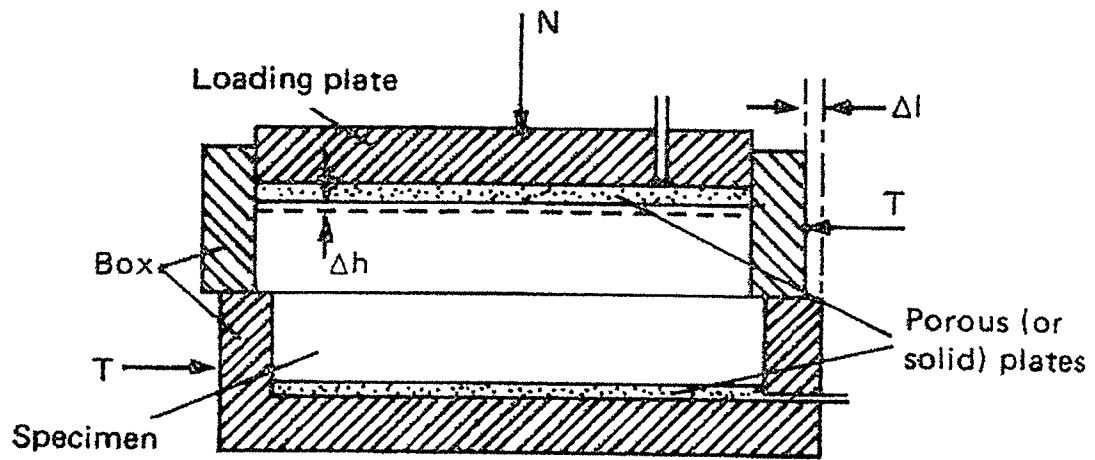


Figure: 3-2: Direct shear box apparatus

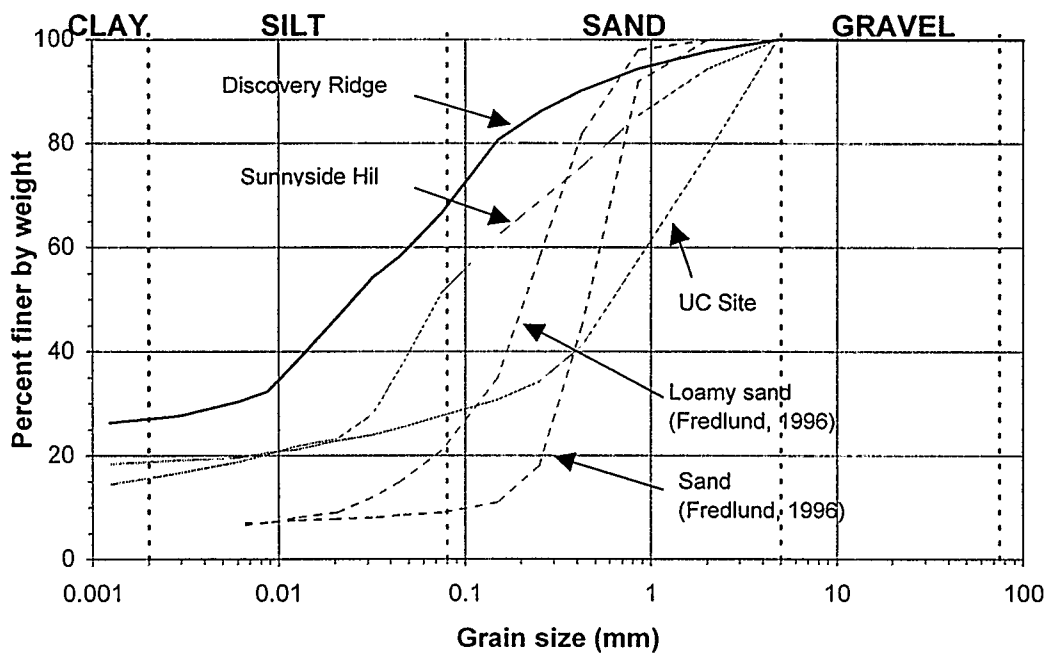


Figure 3-3: Grain size distribution of the three examined soil samples

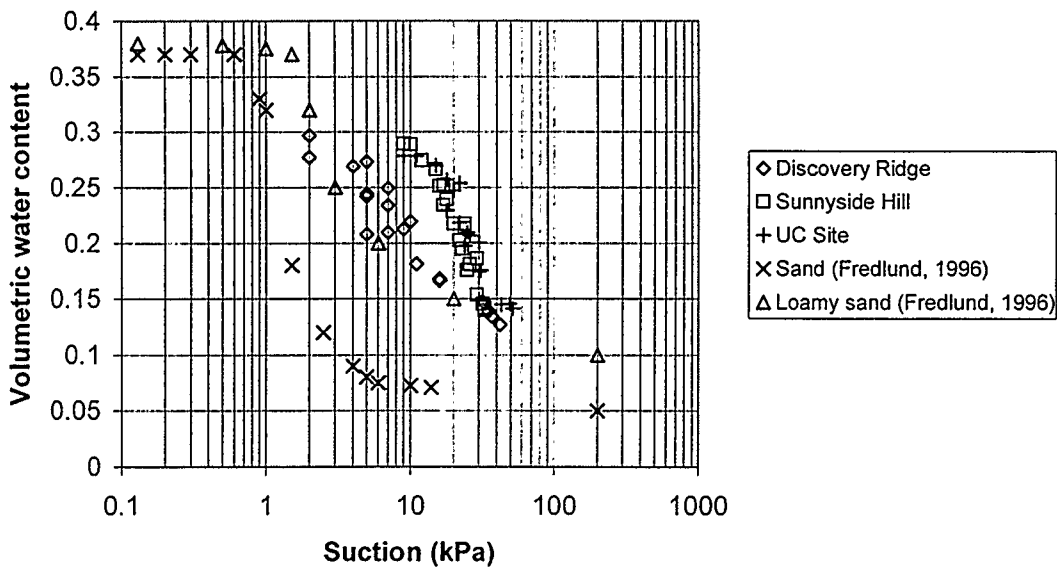


Figure 3-4: Soil-water characteristics curves of the three examined soil samples

"QUICK DRAW" SOILMOISTURE PROBE

11/88

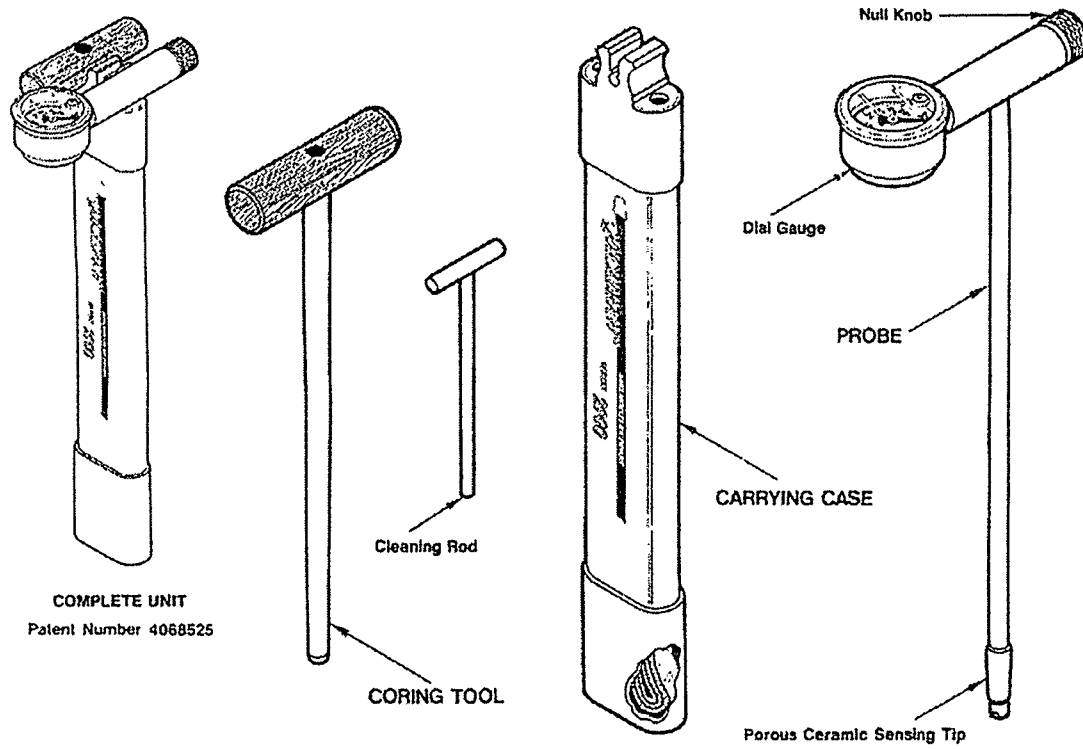


Figure 3-5: Soil moisture probe

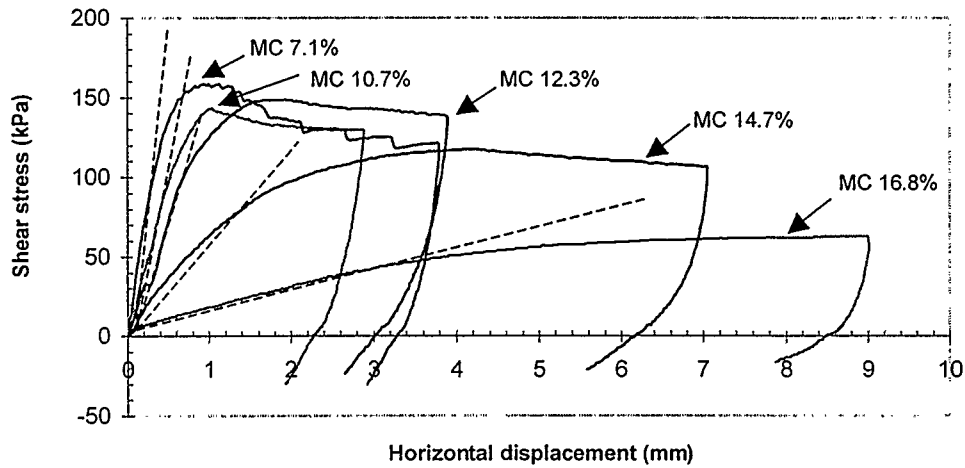


Figure 3-6: Plot of shear stress versus horizontal displacement
(Soil sample: Sunnyside Hill, Normal stress: 100 kPa)

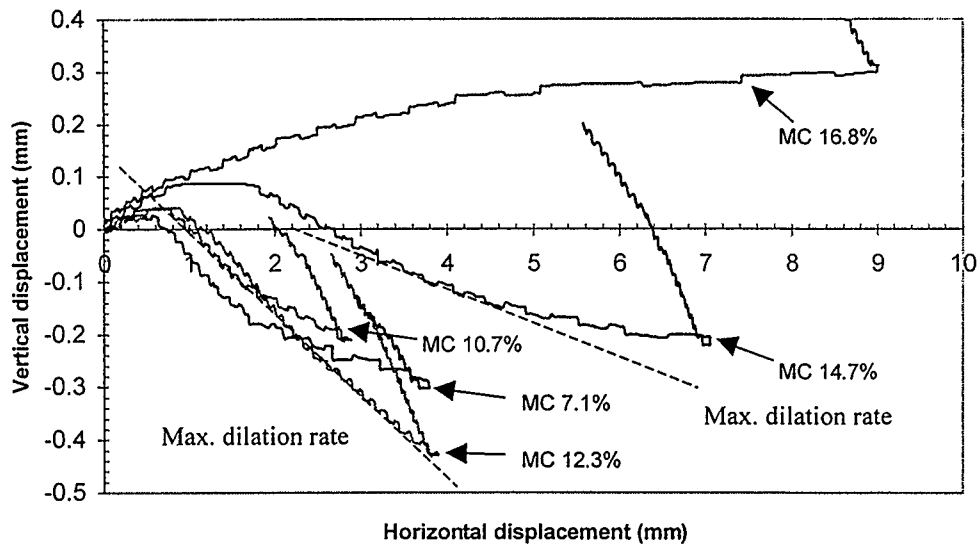


Figure 3-7: Plot of vertical displacement versus horizontal displacement
(Soil sample: Sunnyside Hill, Normal stress: 100 kPa)

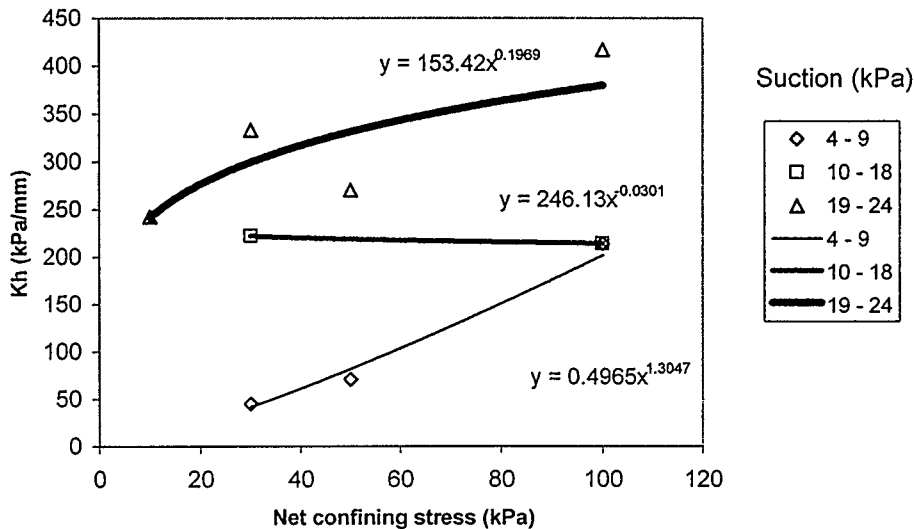


Figure 3-8: Plot of k_h versus σ
 (Soil sample: Discovery Ridge, Void ratio ≥ 0.456)

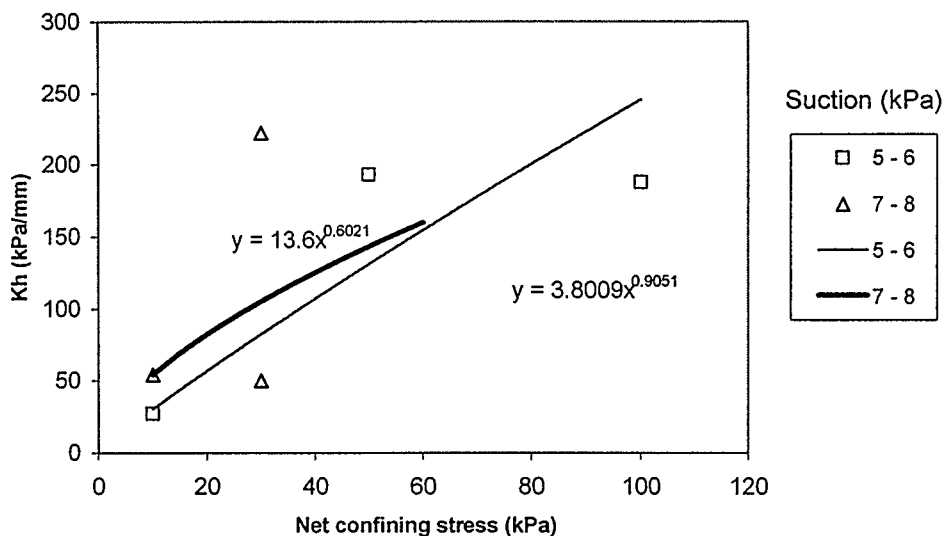


Figure 3-9: Plot of k_h versus σ
 (Soil sample: Discovery Ridge, Void ratio < 0.456)

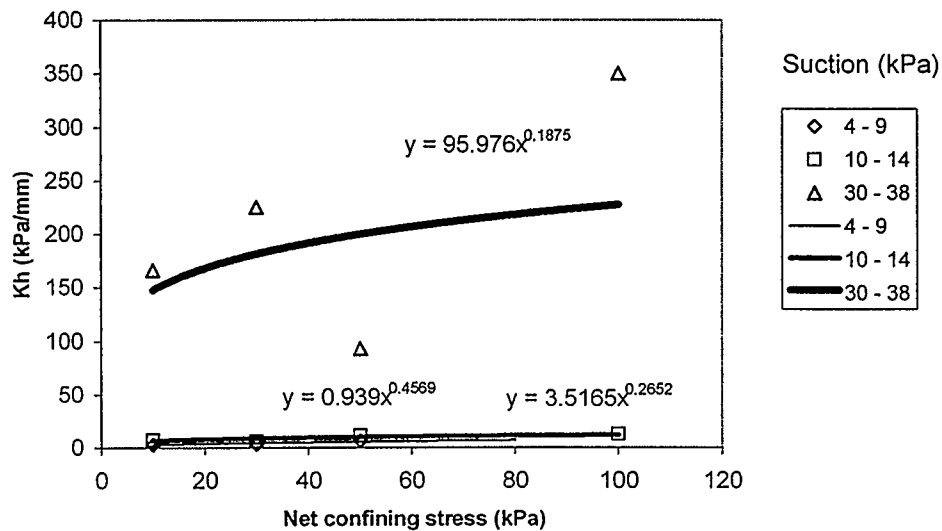


Figure 3-10: Plot of k_h versus σ
(Soil sample: Sunnyside Hill, Void ratio ≥ 0.480)

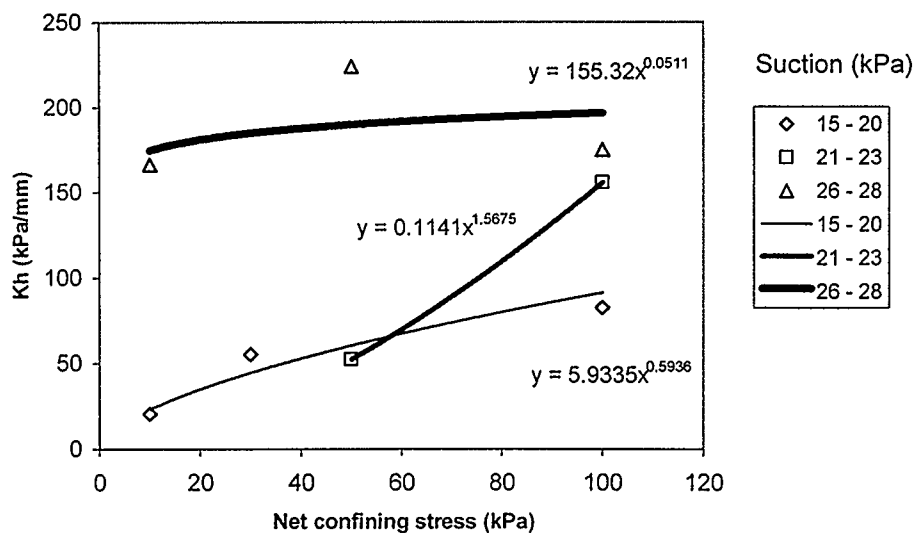


Figure 3-11: Plot of k_h versus σ
(Soil sample: Sunnyside Hill, Void ratio < 0.480)

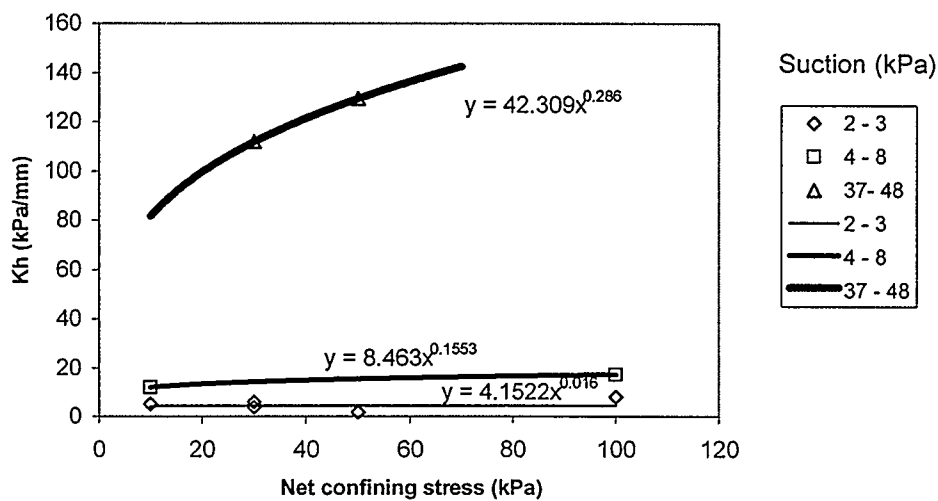


Figure 3-12: Plot of k_h versus σ
(Soil sample: UC Site, Void ratio ≥ 0.460)

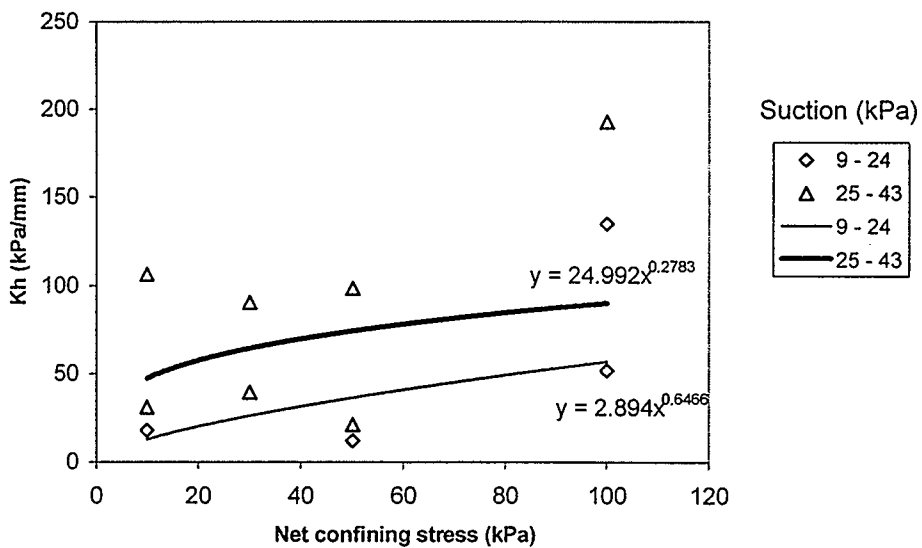


Figure 3-13: Plot of k_h versus σ
(Soil sample: UC Site, Void ratio < 0.460)

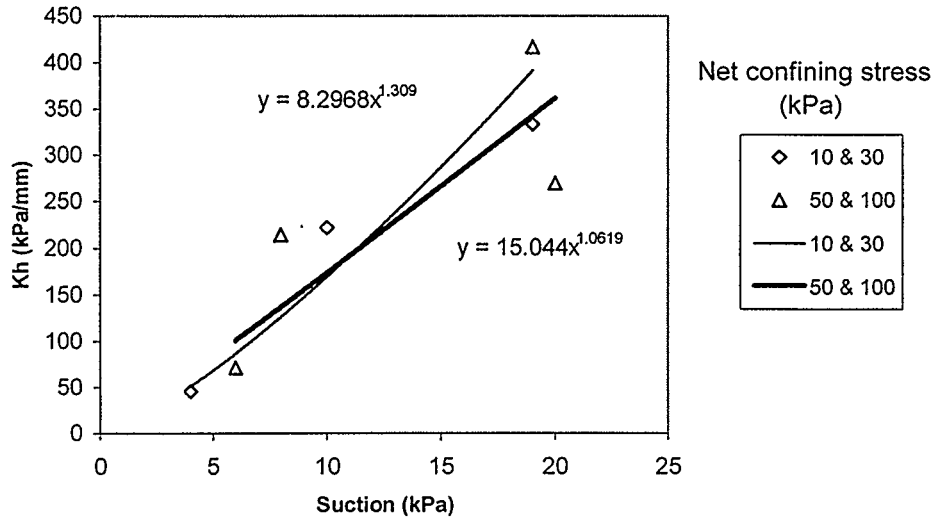


Figure 3-14: Plot of k_h versus u_s
 (Soil sample: Discovery Ridge, Void ratio ≥ 0.456)

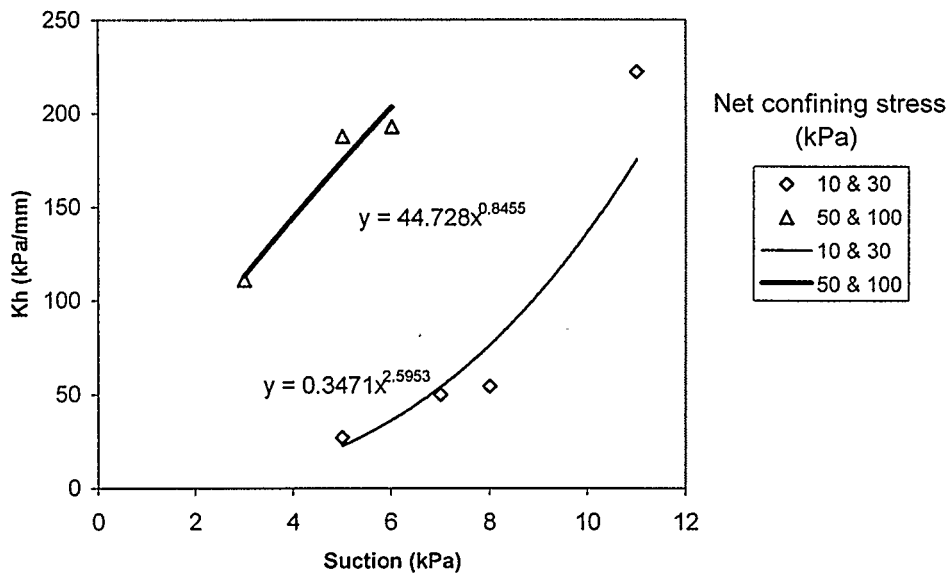


Figure 3-15: Plot of k_h versus u_s
 (Soil sample: Discovery Ridge, Void ratio < 0.456)

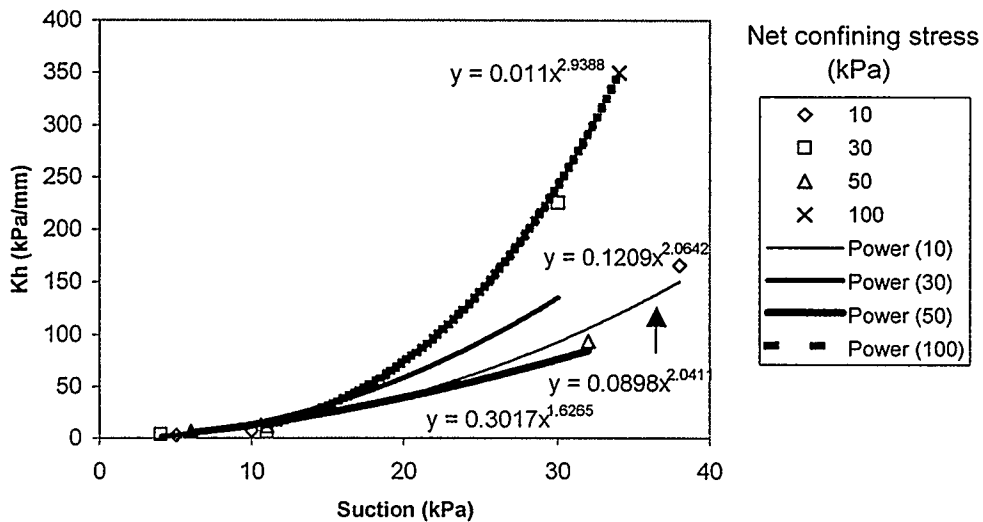


Figure 3-16: Plot of k_h versus u_s
 (Soil sample: Sunnyside Hill, Void ratio ≥ 0.480)

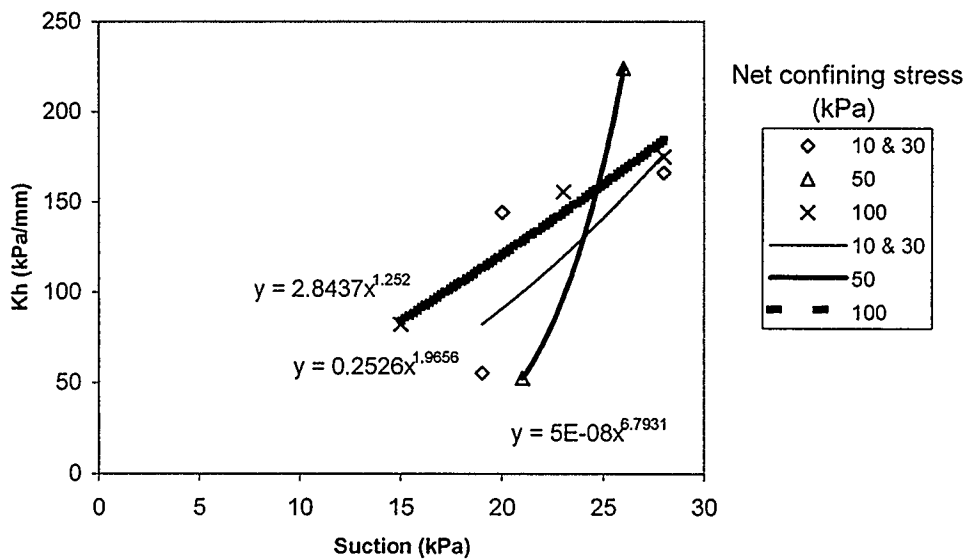


Figure 3-17: Plot of k_h versus u_s
 (Soil sample: Sunnyside Hill, Void ratio < 0.480)

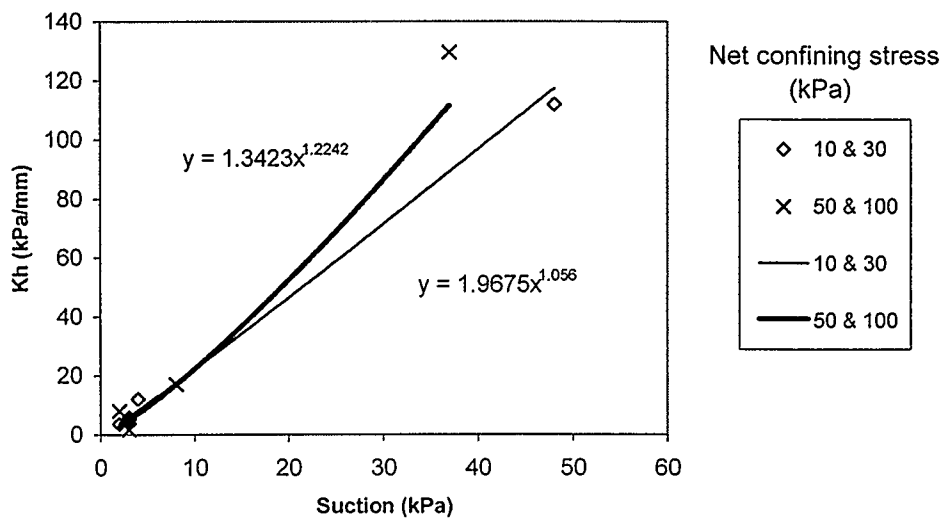


Figure 3-18: Plot of k_h versus u_s
 (Soil sample: UC Site, Void ratio ≥ 0.460)

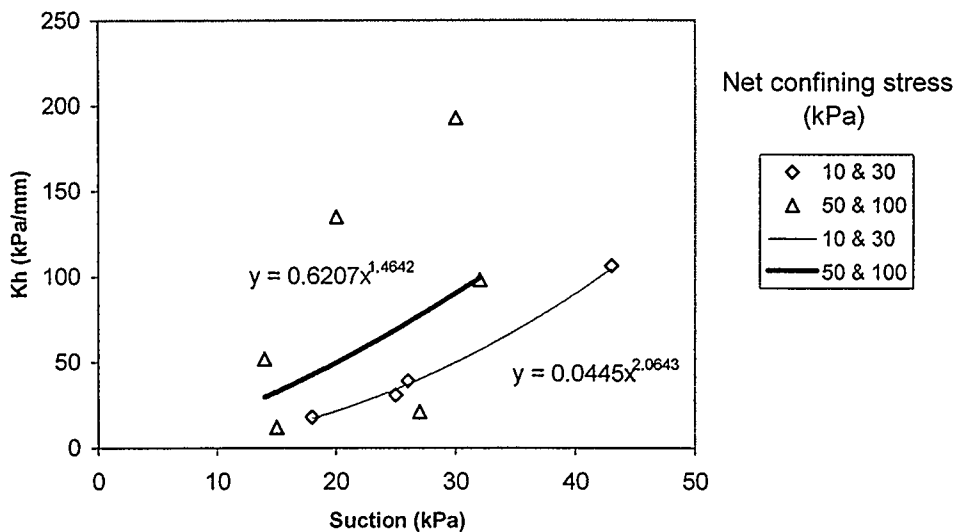


Figure 3-19: Plot of k_h versus u_s
 (Soil sample: UC Site, Void ratio < 0.460)

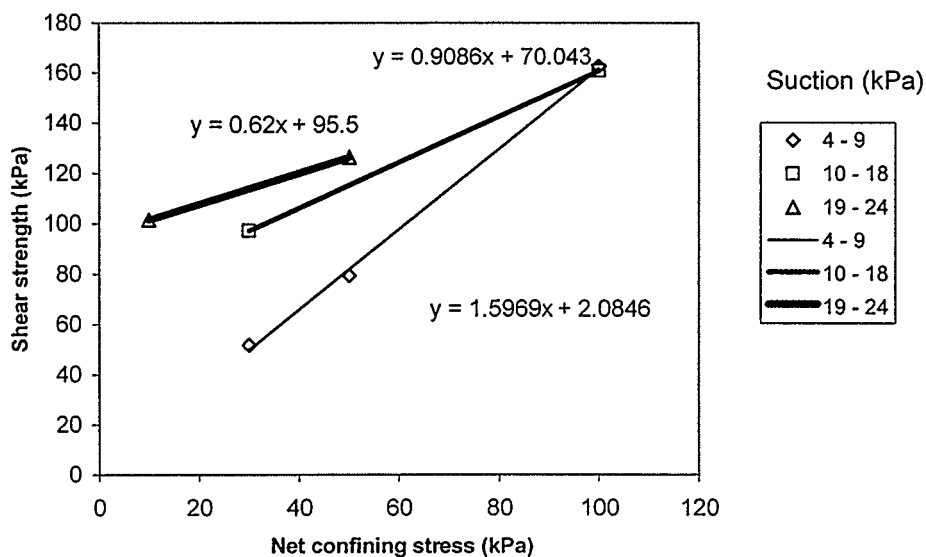


Figure 3-20: Plot of shear strength versus net confining stress (Soil sample: Discovery Ridge, Void ratio ≥ 0.456)

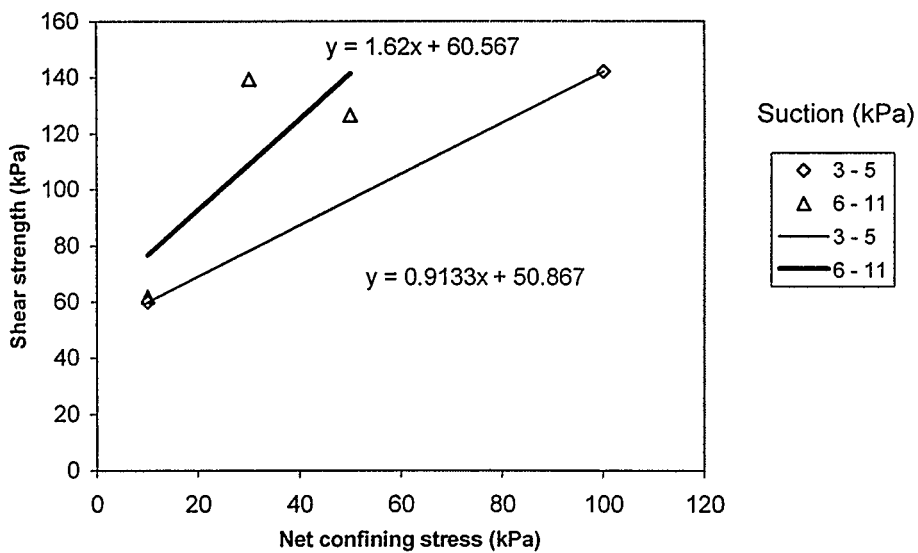


Figure 3-21: Plot of shear strength versus net confining stress (Soil sample: Discovery Ridge, Void ratio < 0.456)

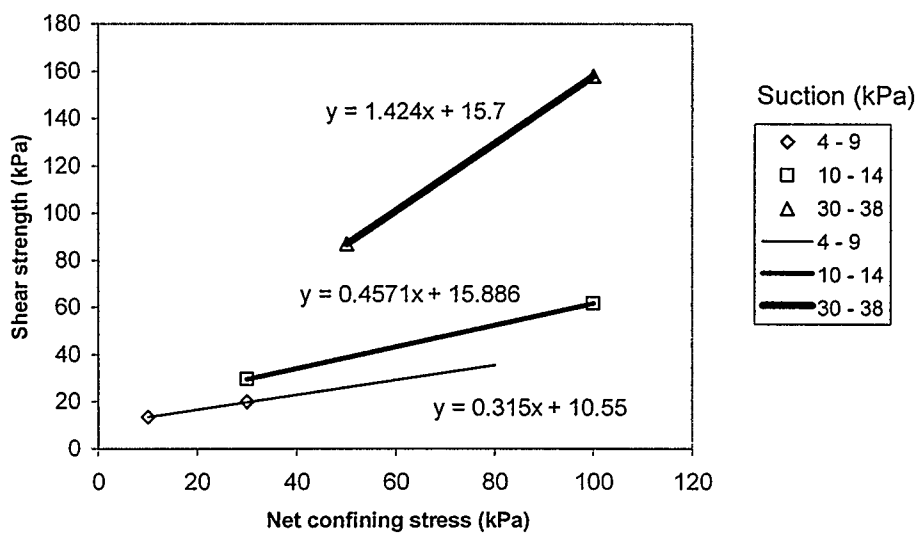


Figure 3-22: Plot of shear strength versus net confining stress (Soil sample: Sunnyside Hill, Void ratio ≥ 0.480)

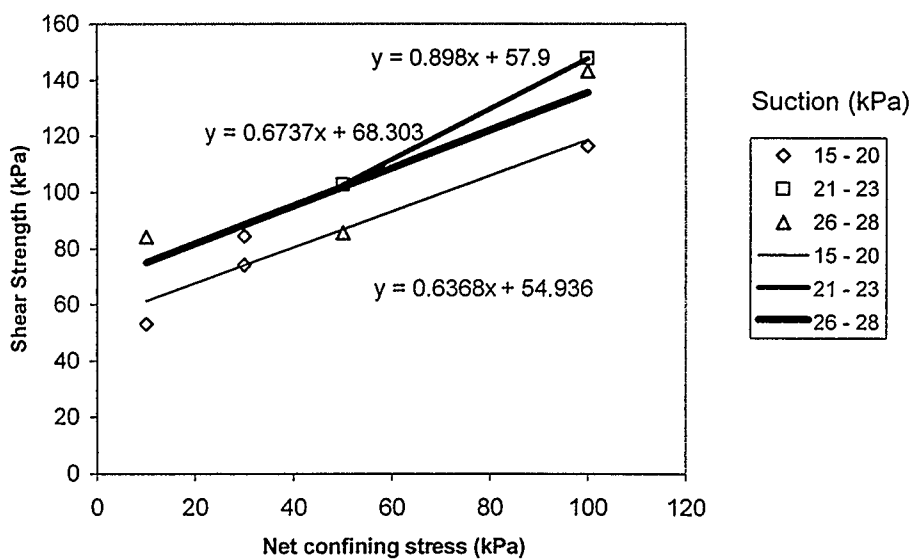


Figure 3-23: Plot of shear strength versus net confining stress (Soil sample: Sunnyside Hill, Void ratio < 0.480)

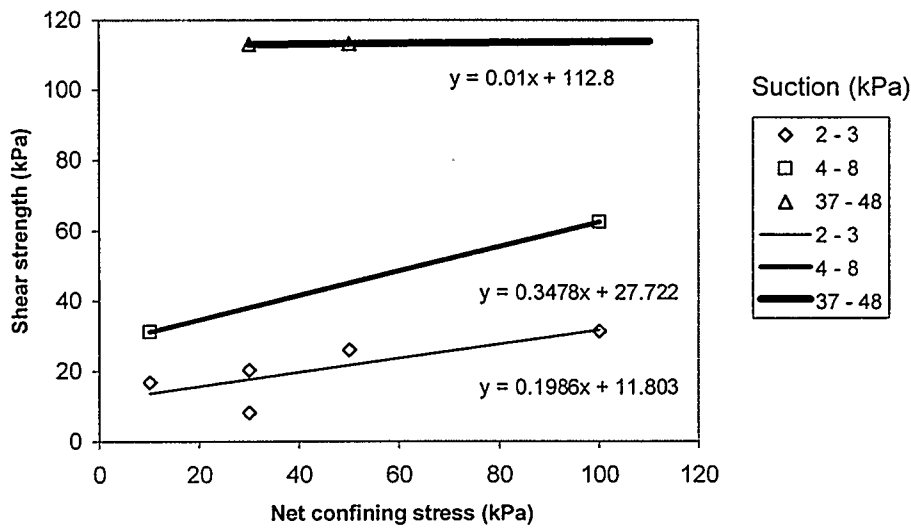


Figure 3-24: Plot of shear strength versus net confining stress (Soil sample: UC Site, Void ratio ≥ 0.460)

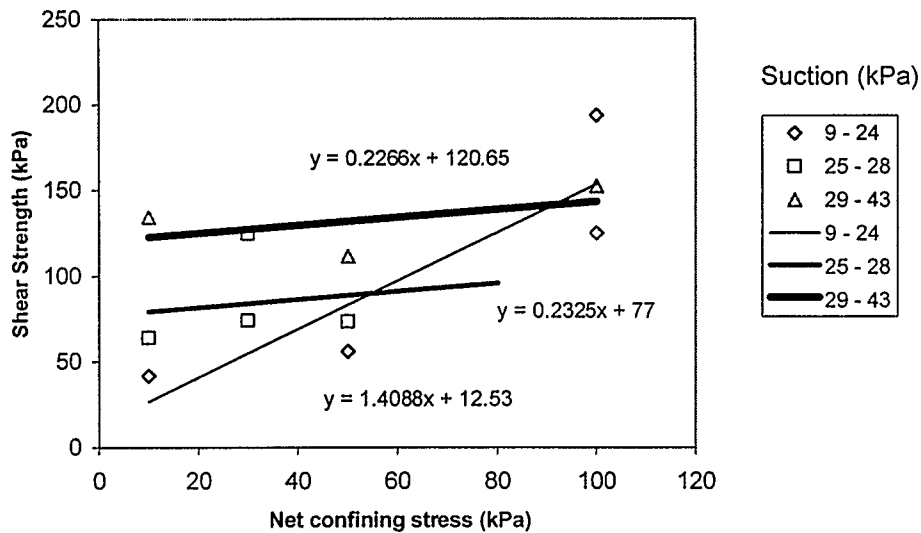


Figure 3-25: Plot of shear strength versus net confining stress (Soil sample: UC Site, Void ratio < 0.460)

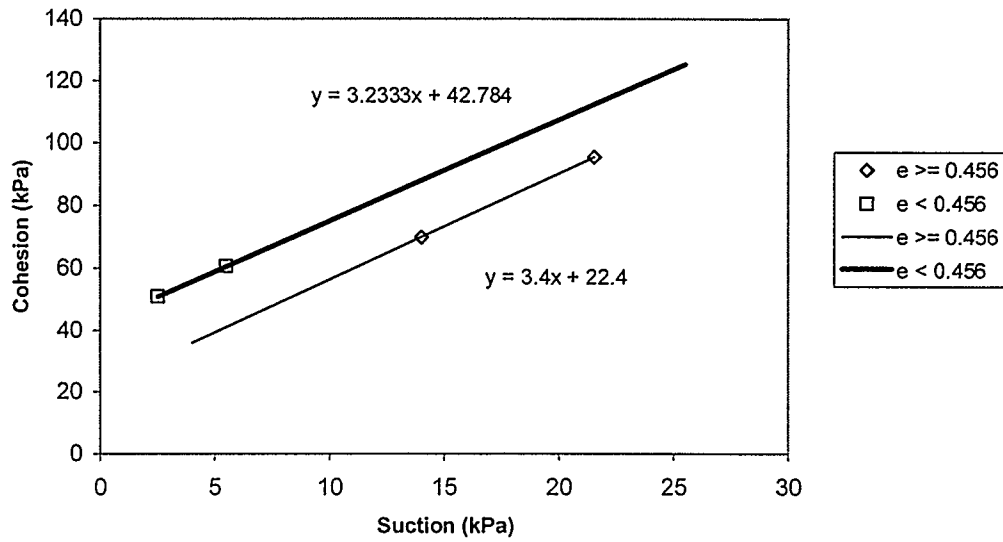


Figure 3-26: Plot of cohesion versus suction
(Soil sample: Discovery Ridge)

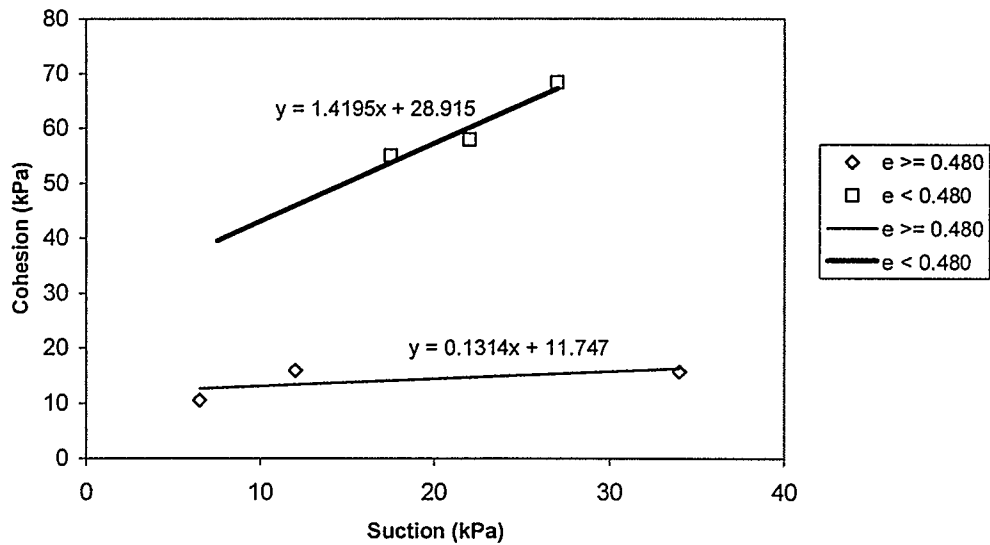


Figure 3-27: Plot of cohesion versus suction
(Soil sample: Sunnyside Hill)

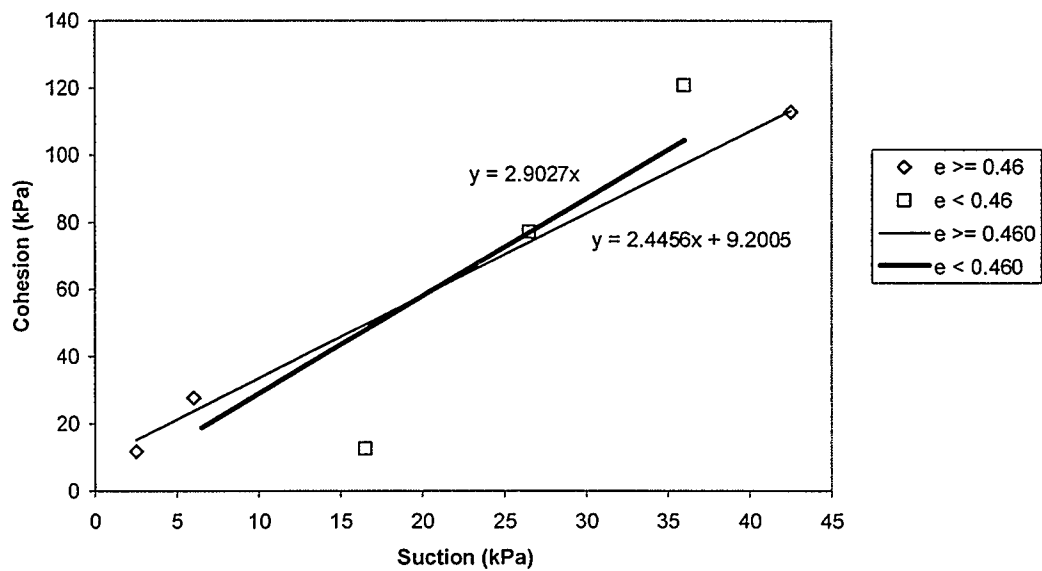


Figure 3-28: Plot of cohesion versus suction
(Soil sample: UC Site)

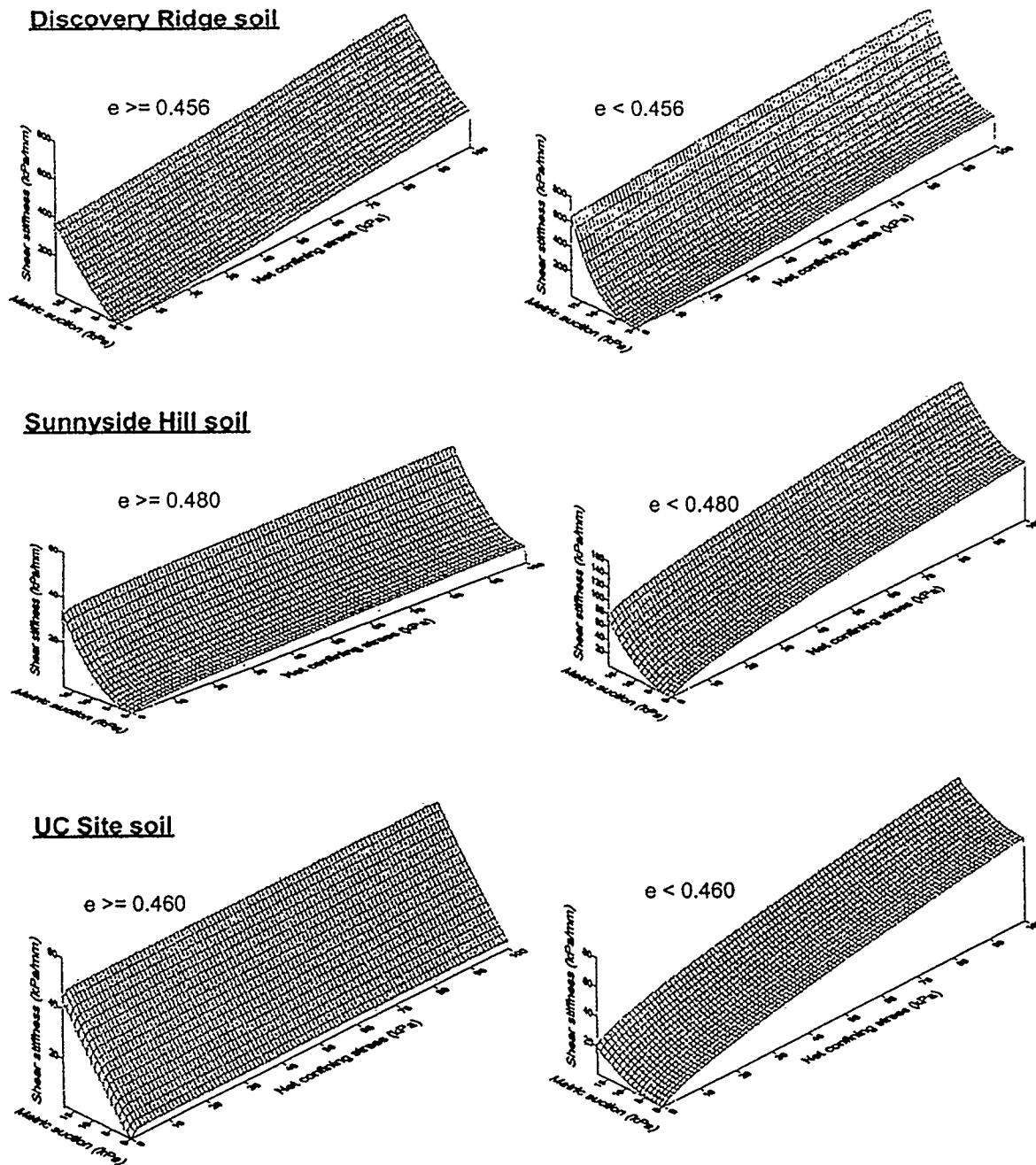


Figure 3-29: Relationships among shear stiffness, net confining stress, and matric suction

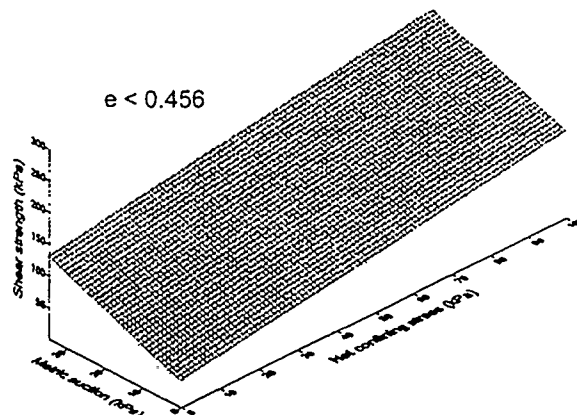
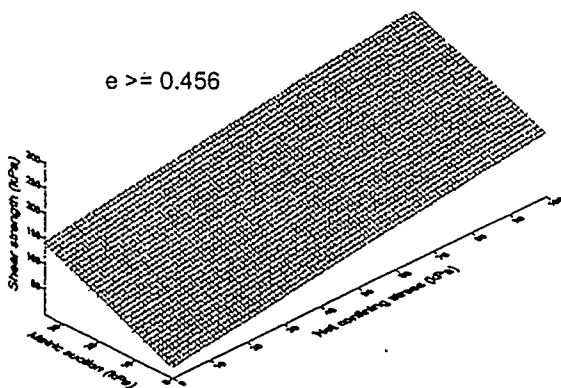
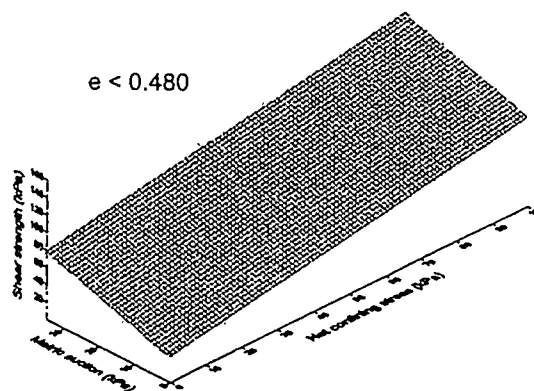
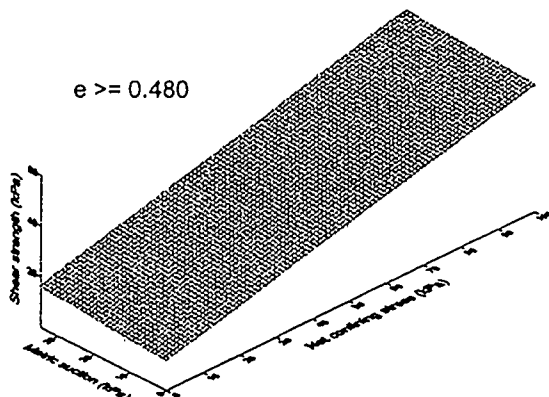
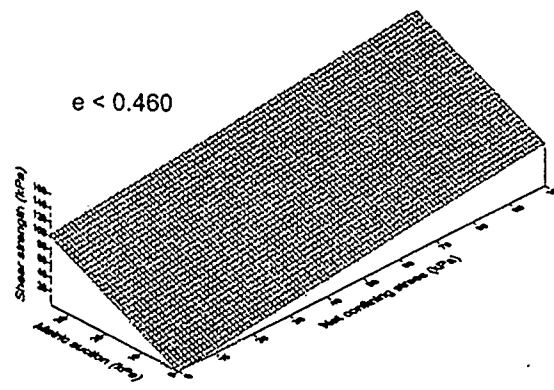
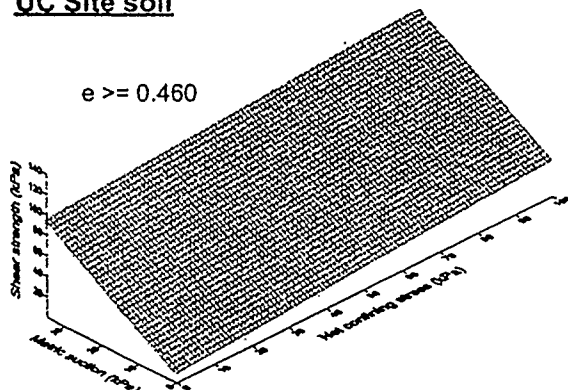
Discovery Ridge soil**Sunnyside Hill soil****UC Site soil**

Figure 3-30: Relationships among shear strength, net confining stress, and matric suction

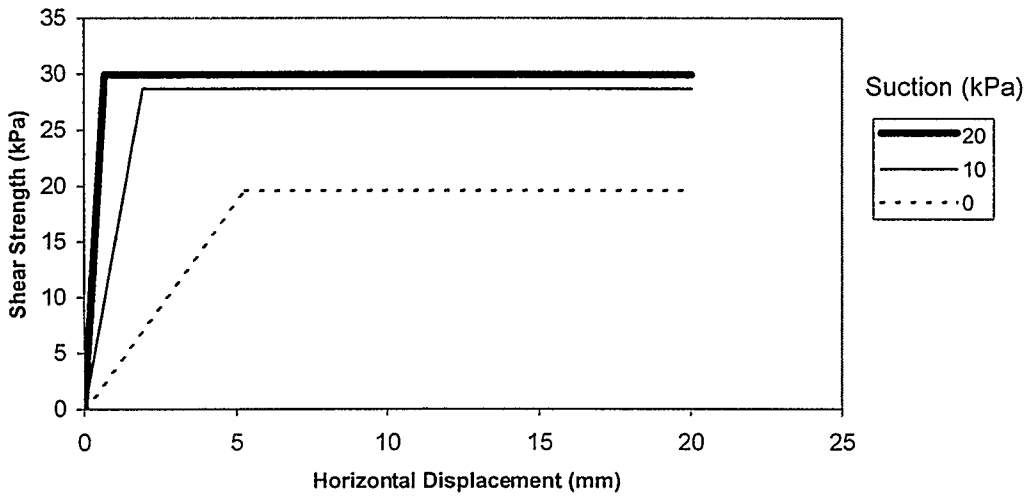


Figure 3-31: Results from the proposed equations for Sunnyside Hill for $\sigma = 40$ kPa

CHAPTER 4: TRIAXIAL COMPRESSION TESTS

4.1 Introduction

A series of triaxial compression tests were performed on the three study soils, described in Section 3.2, to determine the compressive behavior of these soils for development of the slider block-interslice springs model described in Chapters 1 and 2. The objective of the tests is to determine the effects of matric suction ($u_a - u_w$) and net confining stress ($\sigma - u_a$) on compressive stiffness and strength of the soils. By applying the correlations to an established relationship from past experimental studies, compressive stiffness and strength equations are developed in terms of the two parameters for each soil with two void ratio (e) ranges and three clay content values.

4.2 Description of Triaxial Compression Tests

Triaxial compression test has become more popular than direct shear box test as it overcomes several disadvantages of the latter. The triaxial test is more complex than the direct shear box test. It is able to control drainage and there is no rotation of major (σ_1) and minor (σ_3) principal stresses. Stress concentrations still exist, but they are significantly less than in the direct shear test. Complex stress paths can be more effectively modeled in the laboratory with the triaxial test.

A diagram of the triaxial apparatus is shown in Figure 4-1. The major principal stress (σ_1) is applied longitudinally to the sample by a piston that compresses the sample. The minor principal stress (σ_3) or confining stress is applied radially to the sample by placing the water inside the confining cell under pressure. The sample is in a tight fitting rubber membrane to separate the soil from the water in the confining pressure cell. As the axial compressive load is applied, the excess pore pressure in the sample may be measured or

released, depending on the testing protocol. The shear strength of a soil may be accurately measured using a series of triaxial tests on the same soil at different confining pressures.

4.3 Testing Procedures

The detailed testing procedures for the triaxial compression tests are summarized as follows:

1. The samples were oven dried overnight at 60 °C.
2. The samples were screened on a 4.75 mm sieve. The portion passing was used.
3. The samples were moisture conditioned to the desired moisture contents.
4. Standard Proctor tests (ASTM (1980), Designation D698) were performed on the samples.
5. The samples (115 mm in height and 100 mm in diameter) were extruded from the mold and isolated for 24 hours.
6. Soil suction was measured with a soil moisture probe. (Procedures for soil suction measurement are stated in Section 3.3.3.)
7. The samples were then fitted into a rubber membrane and placed in the triaxial cell.
8. The triaxial cell was then filled with water and the confining pressure was adjusted.
9. The tests started with an axial displacement rate of 0.1 mm per minute.
10. During the tests, axial load was measured every 10 seconds for 1 minute, every 20 seconds for another 2 minutes and every 30 seconds for the remainder of the tests until the peak strengths.
11. The samples were removed from the triaxial cell and oven dried overnight at 130 °C to determine the moisture contents (ASTM (1992), Designation D2216).

The tests were performed on each of the three soil samples at five different moisture contents (two below the optimum moisture content, one close to the optimum moisture

content, and two above the optimum moisture content) and at four confining stresses (10, 30, 50, and 100kPa). Therefore, each soil sample required twenty tests at various moisture content and confining stress combinations. Thus, for this study, the total number of triaxial compression tests was sixty. The raw data of the tests are presented in Appendix E. Note that the void ratio in Appendix E is determined by assuming the solid densities of the three soils equal to 2650 kg/m^3 and using the dry density values obtained from the Standard Proctor tests as presented in Appendix A.

4.4 Data Acquisition and Compilation

The raw data presented in Appendix E are further manipulated to deviator stress ($\sigma_1 - \sigma_3$) and compressive stiffness (k_h) as shown in Table 4-1 and presented in the graphs in Sections 4.4.1 to 4.4.3.

4.4.1 Deviator stress ($\sigma_1 - \sigma_3$) versus vertical displacement (δ_v)

One of the graphs of deviator stress ($\sigma_1 - \sigma_3$) versus vertical displacement (δ_v) is presented in Figure 4-2. The graph has five curves, one for each different moisture content. The graphs for other net confining stresses and other two soil samples are presented in Appendix F.

The initial tangent slope represents the initial compressive stiffness (k_h). The initial compressive stiffness is determined by the slope of a straight line drawn from the origin to 50% of the maximum deviator stress. The peak stresses, residual stresses, and the slopes of the unloading curves are also determined. The results are summarized in Table 4-1.

4.4.2 Compressive stiffness (k_h) versus net confining stress ($\sigma - u_a$) and matric suction ($u_a - u_w$)

The equation developed by Janbu (1963) is used to examine the relationship between the tangent modulus and effective confining stress as that of shear box test. It is assumed that the compressive stiffness also follows that of equation (3.1) as the following.

$$k_h = K_h \left(\frac{\sigma_c'}{P} \right)^n \quad (4.1)$$

where

k_h = compressive stiffness [kPa/mm],

K_h = constant = $K (101.3) (1 / 101.3)^n$ [kPa/mm],

σ_c' = effective confining stress [kPa],

P = one unit of pressure [1 kPa],

K = a modulus number [mm⁻¹], and

n = the exponent determining the rate of variation of k_h with σ_c' .

For unsaturated soil, the two stress state variables, net confining stress ($\sigma - u_a$) and matric suction ($u_a - u_w$) are used to replace the effective confining stress term in equation (4.1). The matric suction term, ($u_a - u_w$) becomes ($-u_w$) and is equivalent to the soil suction value (u_s) taken in this study since the pore air pressure is atmospheric. The effects of the two stress state variables on the shear stiffness are separated and thus, equation (4.1) becomes equation (4.2) as follows:

$$k_h = K_A \left(\frac{\sigma}{P} \right)^n + K_B \left(\frac{u_s}{P} \right)^m \quad (4.2)$$

where

K_A and K_B = constants [kPa/mm];

σ = net confining stress [kPa]

u_s = soil suction [kPa]

$P = 1$ [kPa]

n and m = exponents determining the rate of variation of k_h with σ and u_s , respectively.

To investigate the effects of void ratio on the compressive stiffness, the test data of each soil samples are divided into two void ratio ranges. The criteria for dividing the data is based on the brittle and ductile behaviors displayed in the graphs of deviator stress versus vertical displacement as shown in Figure 4-2 and the graphs in Appendix F. Two compressive stiffness equations are developed on each of the soil samples, one for each void ratio range that also represents brittle or ductile behavior.

The constant, K_A , and the exponent, n , are determined from the graphs of compressive stiffness (k_h) versus net confining stress (σ) using the data ranges of suction values close to zero in Figures 4-3 to 4-8. Similarly, the constant, K_B , and the exponent, m , are determined from the graphs of compressive stiffness (k_h) versus suction (u_s) using test data grouped by the lowest net confining stress (10 kPa) as shown in Figures 4-9 to 4-14. It is assumed that the net confining stresses of 10 kPa and 30 kPa are close to unconfined condition so that their effects on compressive stiffness are negligible.

4.4.3 Compressive strength ($\sigma_1 - \sigma_3$) versus net confining stress ($\sigma - u_a$) and matric suction ($u_a - u_w$)

The compressive strength of an unsaturated soil can be written as (Fredlund and Rahardjo 1993):

$$\sigma_1 - \sigma_3 = (\sigma_1 + \sigma_3 - 2u_a) \sin \phi' + 2c \cos \phi' + (u_a - u_w) \tan \phi_\beta \cos \phi' \quad (4.3)$$

where

σ_1 = major principal stress [kPa],

σ_3 = minor principal stress [kPa],

u_a = pore air pressure [kPa],

c = cohesion [kPa],

$\phi' = \phi_d + \phi_e$,

ϕ_d = dilation angle; ϕ_e = internal true friction angle, and

ϕ_β = angle indicating the rate of increase in compressive strength relative to the matric suction.

Since the air phase was kept in equilibrium condition during the tests, u_a is equal to zero. Let $a = \sin \phi'$, $b = \sin \phi_\beta$ and $c_o = 2c \cos \phi'$, equation (4.3) becomes equations (4.3a) to (4.3d) as follows:

$$\sigma_1 - \sigma_3 = (\sigma_1 + \sigma_3) a + c_o + (u_s) b \quad (4.3a)$$

$$\sigma_1 (1 - a) = \sigma_3 (1 + a) + c_o + (u_s) b \quad (4.3b)$$

$$\sigma_1 = \sigma_3 \left(\frac{1+a}{1-a} \right) + \frac{c_o}{1-a} + u_s \left(\frac{b}{1-a} \right) \quad (4.3c)$$

$$\sigma_1 - \sigma_3 = \frac{c_o}{1-a} + \sigma_3 \left(\frac{1+a}{1-a} - 1 \right) + u_s \left(\frac{b}{1-a} \right) \quad (4.3d)$$

Let $c_1 = \frac{c_o}{1-a}$, $S_1 = \frac{1+a}{1-a} - 1$, and $S_2 = \frac{b}{1-a}$, and $\sigma_3 = (\sigma - u_a) = \sigma$, equation (4.3d) becomes (4.3e).

$$\sigma_1 - \sigma_3 = c_1 + \sigma S_1 + (u_s) S_2 \quad (4.3e)$$

The test data of each soil samples are divided into two void ratio ranges as described in the previous section. S_1 and S_2 in equation (4.3e) are determined from the graphs of compressive strength ($\sigma_1 - \sigma_3$) versus net confining stress (σ_c) using data points grouped by different ranges of suction (u_s) as illustrated in Figures 4-15 to 4-20.

In Figures 4-15 to 4-20, slopes of the graphs in each figure are determined and the average value is taken as the value of S_1 . Cohesion values of the data series are also determined from the y-intercept of the graphs and then plotted against their corresponding suctions as shown in Figures 4-21 to 4-23. Best-fit lines are drawn and cohesions of the three soil types are determined from the y-intercepts, respectively. The values of S_2 are obtained from the slopes of these best-fit lines. Based on the results, two compressive strength equations, each presenting a different void ratio range, are developed for each of the three soil samples in the form of equation (4.3e) in Section 4.5.

4.5 Data Analysis and Discussion

From the graphs of deviator stress ($\sigma_1 - \sigma_3$) versus vertical displacement (δ_v), shown in Figure 4-2, the initial slopes for both loading and unloading curves, and peak compressive stresses are determined and summarized in Table 4-1. The initial slopes of the loading curves, representing the compressive stiffness, tend to increase with increasing net confining pressure and decreasing moisture contents. The trends indicate the effects of net confining stress and matric suction on the compressive stiffness. The test samples with moisture contents above the optimum value present different types of curves. These curves become flatter after they have reached their peak strengths. This shows the change of soil behavior from brittle to ductile when the moisture content increases.

The shape of all unloading curves are similar for the three soil samples, despite each has different matric suction, void ratio, and net confining stress, as shown in the data in Table 4-1. This data shows that matric suction, net confining stress, void ratio, and clay content do not have significant influences on the behavior of unloading curves.

The deviator stress values ($\sigma_1 - \sigma_3$) of the tests are also summarized in Table 4-1. The peak stress ratio displays similar trends as the compressive stiffness; it increases with

increasing net confining stress and decreasing moisture contents. The trends are more obvious on the soil samples with less clay content as the soil samples from Sunnyside Hill and UC Site lose their compressive strength significantly when their moisture contents increase above their optimum moisture values.

The correlations between the compressive stiffness and matric suction as well as net confining stress can be seen in Figures 4-3 to 4-8. This data shows the compressive stiffness generally increases with increasing matric suction and net confining stress. Based on these correlations, two compressive stiffness equations are developed in the form of equation (4.2) on each of the three soil samples. One equation is for soils with the higher void ratio range and ductile behavior, and the second equation is for soils with the lower range and brittle behavior.

Soil sample: Discovery Ridge

For $0 < u_s < 20$ kPa,

$$k_h = 0.18\left(\frac{\sigma}{P}\right)^{1.58} + 16.3\left(\frac{u_s}{P}\right)^{0.69} \quad e \geq 0.456 \quad (4.4)$$

$$k_h = 7.30\left(\frac{\sigma}{P}\right)^{0.33} + 4.07\left(\frac{u_s}{P}\right)^{1.67} \quad e < 0.456 \quad (4.5)$$

Soil sample: Sunnyside Hill

For $0 < u_s < 35$ kPa,

$$k_h = 0.22\left(\frac{\sigma}{P}\right)^{0.87} + 0.0012\left(\frac{u_s}{P}\right)^{3.49} \quad e \geq 0.480 \quad (4.6)$$

$$k_h = 0.83\left(\frac{\sigma}{P}\right)^{1.09} + 0.0013\left(\frac{u_s}{P}\right)^{3.54} \quad e < 0.480 \quad (4.7)$$

Soil sample: UC Site

For $0 < u_s < 40$ kPa,

$$k_h = 5.45\left(\frac{\sigma}{P}\right)^{0.09} + 0.05\left(\frac{u_s}{P}\right)^{2.23} \quad e \geq 0.406 \quad (4.8)$$

$$k_h = 7.61\left(\frac{\sigma}{P}\right)^{0.53} + 0.04\left(\frac{u_s}{P}\right)^{2.45} \quad e < 0.406 \quad (4.9)$$

where

e = void ratio,

k_h = compressive stiffness [kPa/mm],

σ = net confining stress [kPa],

u_s = soil suction [kPa], and

$P = 1$ [kPa]

Note: Equations (4.4) to (4.9) are valid in the range of $0 < \sigma < 100$ kPa.

The adequacy of the fitted regression model above can be expressed by the coefficients of determination (R^2). By using equation (3.12), the R^2 values of the compressive stiffness equations range from 0.40 to 0.85 as shown in Table 4-2. No R^2 value can be determined for equation (4.9) as it was derived with insufficient test data.

Equations (4.4) to (4.9) are shown graphically in three-dimension in Figure 4-24. Each of the graphs shows a trend of increasing compressive stiffness with increasing matric suction and increasing net confining stress, and decreasing void ratio. Data in Figure 4-24 show matric suction is more influential on compressive stiffness than net confining stress. Void ratio and clay content also show influence on the compressive stiffness; however, there is insufficient data to conduct a numerical correlation. From the six graphs, the soil sample with the highest clay content (Discovery Ridge sample) displays the highest compressive stiffness while the other two samples display similar

compressive stiffness with less clay contents. The test samples with lower void ratio also have higher stiffness than those with higher void ratio.

Based on the correlations displayed in the graphs of compressive strength ($\sigma_1 - \sigma_3$) versus net confining stress (σ), two equations are developed for each of the three soil samples in terms of compressive stress, matric suction, and net confining stress in the form of equation (4.3e), with two void ratio ranges for ductile and brittle behaviors.

Soil sample: Discovery Ridge

For $0 < u_s < 20$ kPa,

$$\sigma_1 - \sigma_3 = 30.71 + 2.06 \sigma + 4.64 u_s \quad e \geq 0.456 \quad (4.10)$$

$$\sigma_1 - \sigma_3 = 46.52 + 4.79 \sigma + 4.14 u_s \quad e < 0.456 \quad (4.11)$$

Soil sample: Sunnyside Hill

For $0 < u_s < 35$ kPa,

$$\sigma_1 - \sigma_3 = 1.77 \sigma + 6.11 u_s \quad e \geq 0.452 \quad (4.12)$$

$$\sigma_1 - \sigma_3 = 2.10 \sigma + 7.63 u_s \quad e < 0.452 \quad (4.13)$$

Soil sample: UC Site

For $0 < u_s < 40$ kPa,

$$\sigma_1 - \sigma_3 = 0.92 \sigma + 7.37 u_s \quad e \geq 0.406 \quad (4.14)$$

$$\sigma_1 - \sigma_3 = 3.99 \sigma + 4.50 u_s \quad e < 0.406 \quad (4.15)$$

where

e = void ratio,

$\sigma_1 - \sigma_3$ = compressive strength [kPa],

σ = net confining stress [kPa], and

u_s = soil suction [kPa].

By using equation (3.12), the R^2 values of the compressive strength equations range from 0.39 to 0.91 as shown in Table 4-2. No R^2 value can be determined for equation (4.15) as it was derived with insufficient test data.

In equations (4.10) to (4.15), the two soil samples from Sunnyside Hill and UC Site are cohesionless due to their low clay contents. To display and compare the correlations, equations (4.10) to (4.15) are shown in three-dimensional graphs in Figure 4-25. The correlation of the three parameters ($\sigma_1 - \sigma_3$, u_s , σ) is shown on this figure. All six graphs consist of relatively flat, but inclined surfaces that display increasing compressive strength with increasing suction and net confining stress. There is a definite correlation between void ratio and compressive strength. However, there is no correlation between the clay content and compressive strength.

4.6 Illustrative Examples

The application of the compressive stiffness and compressive strength equations developed in Section 4.5 are also demonstrated through the Sunnyside Hill case study as the examples for shear equations in Section 3.6. The net confining stress at the center of the sliding blocks is 40 kPa, given the same parameters in Section 3.6. Equations (4.6) and (4.12) are used to calculate the corresponding compressive stiffness and compressive strength. When the soil suction was at 20 kPa, the compressive stiffness and compressive strength were 47.1 kPa/mm and 193.0 kPa. When the soil suction was reduced to 10 kPa, the compressive stiffness and compressive strength decreased to 9.2 kPa/mm, 131.9 kPa, respectively. When the soil suction was further reduced to 0 kPa in its fully saturated condition, the compressive stiffness and compressive strength decreased to 3.0 kPa/mm, 35.4 kPa, respectively, and the net confining stress is reduced to 20 kPa. Figure 4-26 illustrates these compressive stiffness and compressive strength values according to their soil suction values.

4.7 Comparison of Strength Parameters from Direct Shear Box and Triaxial Compression Tests

The shear stiffness, shear strength, compressive stiffness and compressive strength equations are developed from the data of direct shear box and triaxial compression tests. These equations are shown in Sections 3.5 and 4.5, respectively.

Table 4-3 shows the strength parameters derived from direct shear box tests. Soils with lower void ratios dilate first as they are compressed. Soils with higher void ratios simply compress when loaded. Consequently the shear strength equations are different for different void ratio ranges. The Discovery Ridge soil sample with the highest clay content shows the highest cohesion values. The Sunnyside Hill and UC Site soil samples also show relatively less or no cohesive values.

Table 4-4 shows the strength parameters derived from triaxial compression tests. The Discovery Ridge soil sample also shows the highest cohesion values and they are comparative to those in Table 4-3. The Sunnyside Hill and UC Site soil samples are cohesionless. The internal friction angles are also compared between the two tables and are relatively similar. The difference between the angles is possibly due to the dilation effects during the shearing processes.

From past experimental studies, the ϕ' values for silt and clay typically range from 20° to 30° (Fredlund and Rahardjo 1993). However, in Fredlund and Rahardjo experiments, the applied net confining stresses range from 200 to 450 kPa which are much higher than those used in this study (10 to 100 kPa). At such a low stress level, a linear Mohr Coulomb failure envelope assumed by Fredlund and Rahardjo may not be appropriate. A highly non-linear failure envelope as shown in Figure 4-27 is contributed by the high shear dilation at low stress level. A bilinear envelope can be used to approximate the non-linear envelope, i.e., a high friction angle at low stress and a low friction angle at high stress.

In the same experimental studies by Fredlund and Rahardjo (1993), the ϕ_{β} values range from 15° to 22° , which are lower than their corresponding ϕ' values. At low matric suctions, the soil specimen remains saturated and the effects of pore water pressure and total normal stress on the shear strength are characterized by the internal friction angle, ϕ' . As a result, an increase in matric suction causes an increase in shear strength in accordance with the ϕ' angle. The shear stress versus matric suction envelope has a slope angle ϕ_{β} equal to ϕ' . However, in this study, the ϕ_{β} values are typically much higher than the ϕ' values that contradict with Fredlund and Rahardjo's works. The discrepancies of the ϕ_{β} values can be explained as follows:

- 1) Recent shear strength test results on unsaturated soils also indicate some nonlinearity in the shear strength versus matric suction failure envelope (Gan, 1986 and Escario and Sáez, 1986). The ϕ_{β} angle is a function of matric suction. It appears to decrease to a lower value at higher matric suctions. In this study, tests were conducted at low matric suction range and this explains the high ϕ_{β} angle. A bilinear envelope illustrated in Figure 4-28 can be used to interpret the discrepancies.
- 2) The first scenario was also encountered and explained in Fredlund and Rahardjo's experiments. However, in their experiments, the ϕ_{β} values are found to be equal or less than the ϕ' values at low matric suction ranges similar to those used in this study. It is apparent that the higher than expected ϕ_{β} values in this study are related to the variation of matric suction during the tests. The volumetric water content or matric suction at failure may have changed due to the pore water being drawn out and an increase in total volume due to dilation. A decrease of volumetric water content results in an increase of matric suctions as shown in the soil-water characteristic curves in Figure 3-4. Due to the limitation of the tests, the matric suctions were not measured during the tests at failure. The actual matric suction values, which should be used to determine the ϕ_{β} values, could be higher than those measured in this study and thus, should be lower. Assuming the actual ϕ_{β} values are equal to the ϕ' values at

low matric suctions as suggested in Fredlund and Rahardjo's experiments, Tables 4.5 and 4.6 summarize the changes of volumetric water contents at failure during the tests in this study.

- 3) As shown in Figures 3-18 to 3-23 and Figures 4-15 to 4-20, the ϕ' values vary slightly at different matric suction ranges. Since the ϕ' value is related to the physical properties of a soil, it could be affected by a change of void ratio, but should not be affected by a change of matric suction. In this study, average ϕ' values are taken from the different matric suction ranges. If these average ϕ' values are lower than the actual ϕ' values, the determined ϕ_β values are then higher than the actual values to balance the soil strength.
- 4) The assumption of pore air pressure equal to atmospheric pressure is valid only when the air phase is continuous in unsaturated soil. The air pressure is larger than the atmospheric pressure if the air phase is discontinuous and contractile undrained shearing occurs. In contrast, the air pressure drops below the atmospheric pressure value for the case of dilative undrained shearing. If either of these two conditions happened during the tests, the determined ϕ' values and ϕ_β values might not reflect the actual soil properties.

4.8 Conclusion

The data from triaxial compression tests has been used to develop equations to calculate compressive stiffness (equations 4.4 to 4.9) and strength (equations 4.10 to 4.15) in terms of matric suction and net confining stress for the three soil samples, Discovery Ridge, Sunnyside Hill, and UC Site.

The coefficients of determination are determined using equation (3.12) for the compressive stiffness and strength equations as shown in Table 4-2. Equations (4.5),

(4.12), and (4.13) have R^2 values of 0.40, 0.31, and 0.39, respectively, which indicate that more test data are required to improve the quality of the equations. More triaxial compression tests are required for the UC Site soil with void ratio less than 0.406 as equations (4.9) and (4.15) were derived with insufficient test data.

The three-dimensional graphs presented in Figure 4-24 show that the increase of matric suction and the increase of net confining stress cause an increase of compressive stiffness of the three soil samples. The effects of void ratio and clay content on compressive stiffness have not been fully defined due to the limited data. However, the effects of void ratio and clay content on compressive stiffness are shown in Figure 4-24. Hence, compressive stiffness is functions of matric suction, net confining stress, void ratio, and clay content. It is more dependent on matric suction than net confining stress.

The compressive strengths of the three soil samples are shown on the three-dimensional graphs in Figure 4-25. The graphs show that matric suction is more influential on compressive strength than net confining stress. The effects of void ratio and clay content on shear strength have not been fully defined due to the limited data, although the effects of void ratio on compressive strengths is also shown in Figure 4-25. Hence, compressive strengths are functions of matric suction, net confining stress, and void ratio. The influence of matric suction is the most dominant parameter.

Based on the results presented in Section 4.6, compressive stiffness and strength of the soil in Sunnyside Hill reduce significantly when soil suction decreases from 20 kPa to 0 kPa.

The parameters in the strength equations derived from direct shear box and triaxial tests are compared in Section 4.7. The parameters are also compared with those from Fredlund and Rahardjo's experimental studies. The difference in the parameters suggests that the internal friction angle at low stress level due to shear dilation effect could be

higher than that at high stress level, yielding a non-linear failure envelope. However, the unexpected high ϕ_β angles (much greater than the ϕ' angles) both in low and high void ratio requires further investigation.

Net Confining Stress	Discovery Ridge				Sunnyside Hill				UC Site			
	100kPa	50kPa	30kPa	10kPa	100kPa	50kPa	30kPa	10kPa	100kPa	50kPa	30kPa	10kPa
k_h (compressive stiffness) (kPa/mm)												
Test 1	259.3	208.3	178.6	116.7	333.3	285.7	238.1	200	266.7	333.3	238.1	250
Test 2	250	185.2	192.3	181.8	250	193.5	131.6	178.6	181.8	263.2	200	151.2
Test 3	156.3	151.2	294.1	125	125	58.8	38	131.4	46.9	100	46.2	63.6
Test 4	93.8	34.5	47.6	100	11.7	9.7	19.2	100	6.9	13.8	20	25.8
Test 5	43.5	8.5	19.4	13.8	3.75	2	6.7	30	1.6	6.2	7.5	7.3
$\sigma_1 - \sigma_3$ (peak axial stress) (kPa)												
Test 1	435	350	309	190	440	385	324	265	430	400	324	350
Test 2	383	345	366	263	365	300	261	267	315	380	300	277
Test 3	292	270	384	257	300	210	177	226	155	255	153	160
Test 4	178	170	129	166	115	100	135	212	65	110	114	138
Test 5	112	80	72	82	55	35	69	135	35	50	48	63
Slope of unloading curve (kPa/mm)												
Test 1	555.6	555.6	487.8	200	566	500	461.5	151.5	454.5	500	555.5	215.1
Test 2	555.6	526.3	454.5	285.7	566	500	394.9	238.1	454.5	500	555.5	416.7
Test 3	480.8	444.4	588.2	296.3	333.3	500	394.9	200	373.1	400	300	250
Test 4	347.2	363.6	312.5	242.4	312.5	322.6	394.9	236.2	219.6	333.3	300	317.5
Test 5	373.1	300	222.2	222.2	333.3	500	235.3	238.1	333.3	400	300	285.7
Moisture content (%)												
Test 1	8.5	8.1	7.3	7.8	8.8	8.1	8.3	8.1	9.4	8.0	8.1	7.8
Test 2	10.2	10.5	9.6	9.5	9.7	9.9	11.3	10.5	11.2	9.3	10.9	9.4
Test 3	11.3	11.5	11.9	12.1	11.5	11.3	12.7	11.2	13.2	11.3	11.5	12.3
Test 4	13.2	13.0	13.1	12.5	13.6	14.5	13.6	12.1	13.9	13.2	13.2	12.9
Test 5	14.5	14.3	16.4	14.9	16.3	16.5	15.3	12.6	15.0	14.0	14.9	14.9

Table 4-1: Summary of results of triaxial tests of three different soil types

Coefficient of Determination, R^2				
Void ratio range	Stiffness		Strength	
	low	high	low	high
Discovery Ridge	0.40	0.84	0.80	0.91
Sunnyside Hill	0.50	0.81	0.39	0.31
UC Site	n/a	0.85	n/a	0.50

Table 4-2: Coefficient of multiple determination (R^2) for compressive stiffness and strength equations

Direct Shear Box Test							
Void ratio range	c (kPa)		ϕ' (°)		ϕ_β (°)		No. of data used in correlation
	low	high	low	high	low	high	
Discovery Ridge	42.8	22.4	43.5	46.1	72.8	73.6	4
Sunnyside Hill	28.9	11.8	36.5	21.3	54.8	7.4	6
UC Site	0	9.2	31.8	15.1	71.0	67.7	6

Table 4-3: Parameters in strength equations from direct shear box test results

Triaxial Compression Test							
Void ratio range	c (kPa)		ϕ' (°)		ϕ_β (°)		No. of data used in correlation
	low	high	low	high	low	high	
Discovery Ridge	46.5	30.7	44.9	30.5	71.1	69.6	4
Sunnyside Hill	0	0	30.9	28.0	77.3	73.9	5
UC Site	0	0	41.8	18.4	71.7	75.6	5

Table 4-4: Parameters in strength equations from triaxial compression test results

Volumetric Water Contents at failure and (at start) of direct shear box tests										
Initial matric suction (kPa)	10		20		30		40		50	
Void ratio range	low	high								
Discovery Ridge	0.15 (0.18)	0.15 (0.18)	0.12 (0.16)	0.12 (0.16)	0.12 (0.14)	0.12 (0.14)	0.11 (0.12)	0.11 (0.12)	0.11 (0.12)	0.11 (0.12)
Sunnyside Hill	0.28 (0.29)	0.12 (0.29)	0.19 (0.22)	0.10 (0.22)	0.14 (0.15)	0.10 (0.15)	0.13 (0.14)	0.10 (0.14)	0.12 (0.13)	0.10 (0.13)
UC Site	0.14 (0.29)	0.11 (0.29)	0.13 (0.22)	0.11 (0.29)	0.11 (0.15)	0.11 (0.29)	0.11 (0.14)	0.11 (0.29)	0.11 (0.14)	0.11 (0.29)

Table 4-5: Change of volumetric water contents from start to failure during direct shear box tests for initial matric suctions ranging from 10 to 50 kPa

Volumetric Water Content at failure and (at start) of triaxial compression tests										
Initial matric suction (kPa)	10		20		30		40		50	
Void ratio range	low	high								
Discovery Ridge	0.14 (0.18)	0.15 (0.18)	0.12 (0.16)	0.12 (0.16)	0.12 (0.14)	0.11 (0.14)	0.11 (0.12)	0.10 (0.12)	0.11 (0.12)	0.10 (0.12)
Sunnyside Hill	0.12 (0.29)	0.12 (0.29)	0.11 (0.22)	0.11 (0.22)	0.10 (0.15)	0.10 (0.15)	0.10 (0.14)	0.10 (0.14)	0.10 (0.13)	0.10 (0.13)
UC Site	0.15 (0.29)	0.11 (0.29)	0.14 (0.22)	0.11 (0.29)	0.13 (0.15)	0.11 (0.29)	0.12 (0.14)	0.11 (0.29)	0.11 (0.14)	0.11 (0.29)

Table 4-6: Change of volumetric water contents from start to failure during triaxial compression tests for initial matric suctions ranging from 10 to 50 kPa

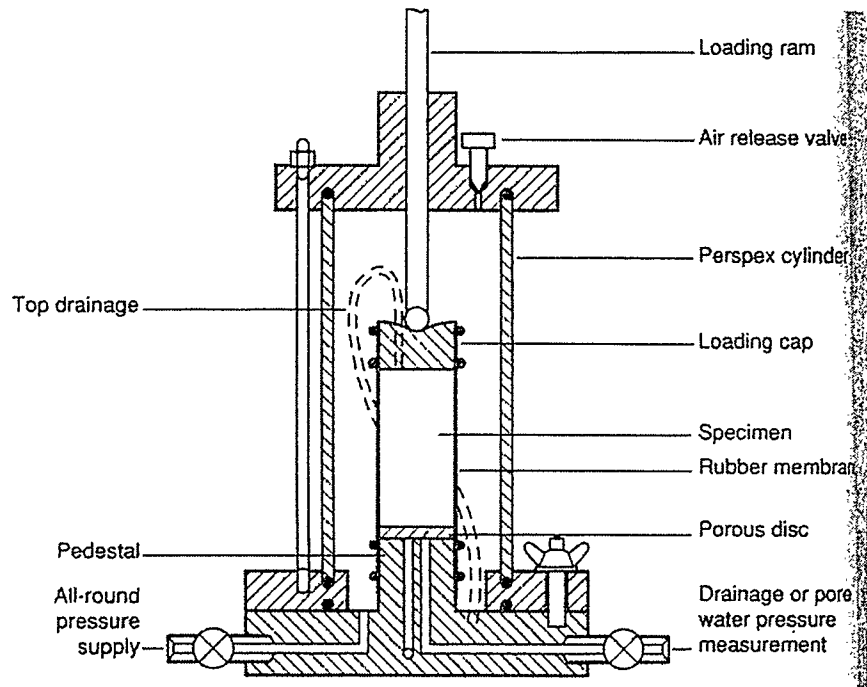


Figure 4-1: Schematic diagram of a triaxial cell

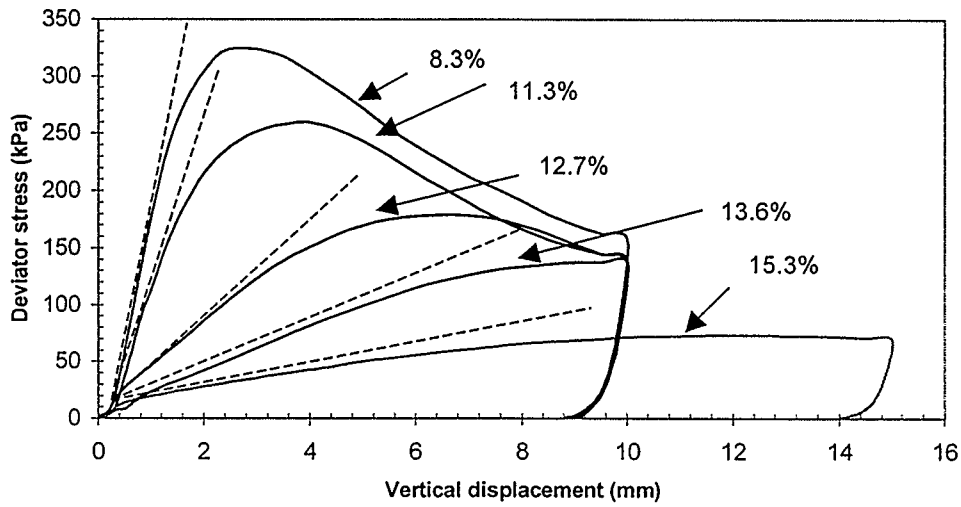


Figure 4-2: Deviator stress versus vertical displacement
(Soil sample: Sunnyside Hill, Net confining stress: 30 kPa)

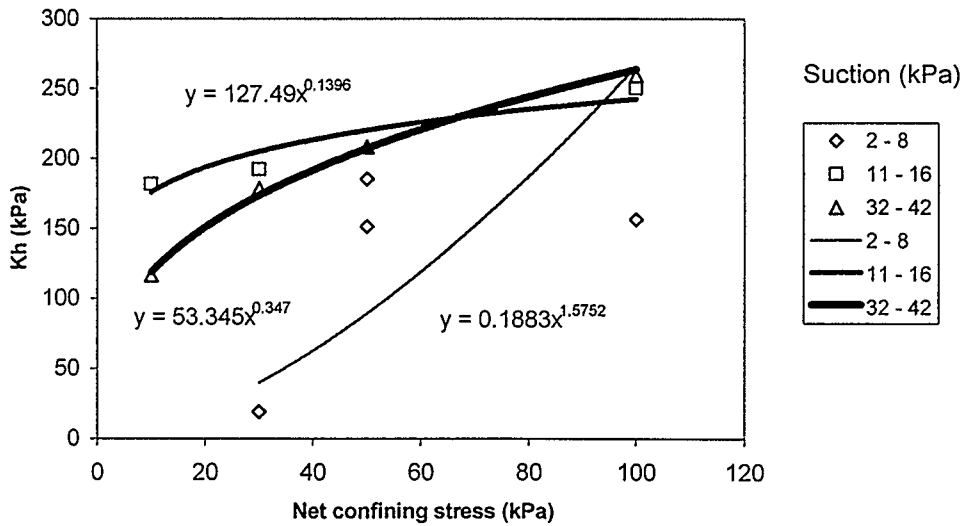


Figure 4-3: Compressive stiffness versus net confining stress
(Soil sample: Discovery Ridge, Void ratio ≥ 0.456)

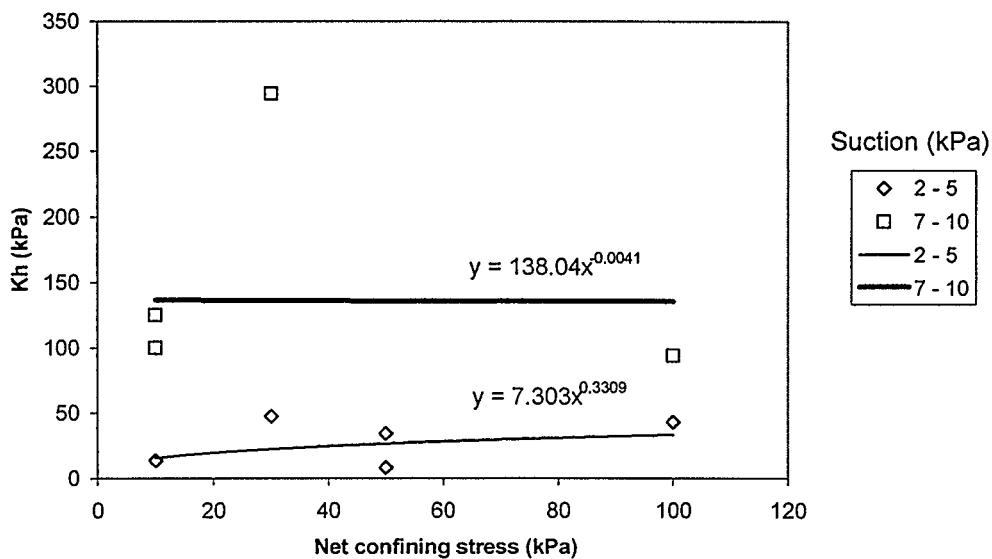


Figure 4-4: Compressive stiffness versus net confining stress
(Soil sample: Discovery Ridge, Void ratio < 0.456)

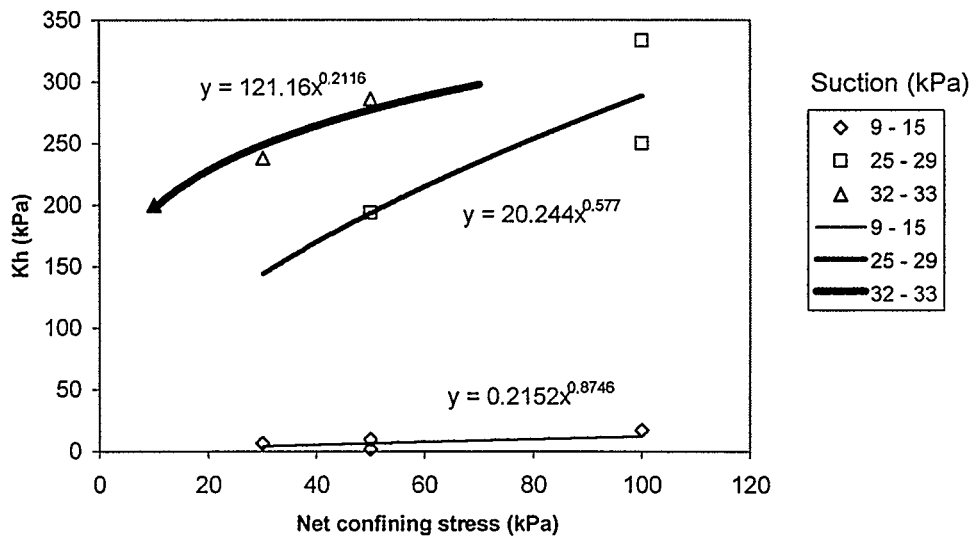


Figure 4-5: Compressive stiffness versus net confining stress
(Soil sample: Sunnyside Hill, Void ratio ≥ 0.452)

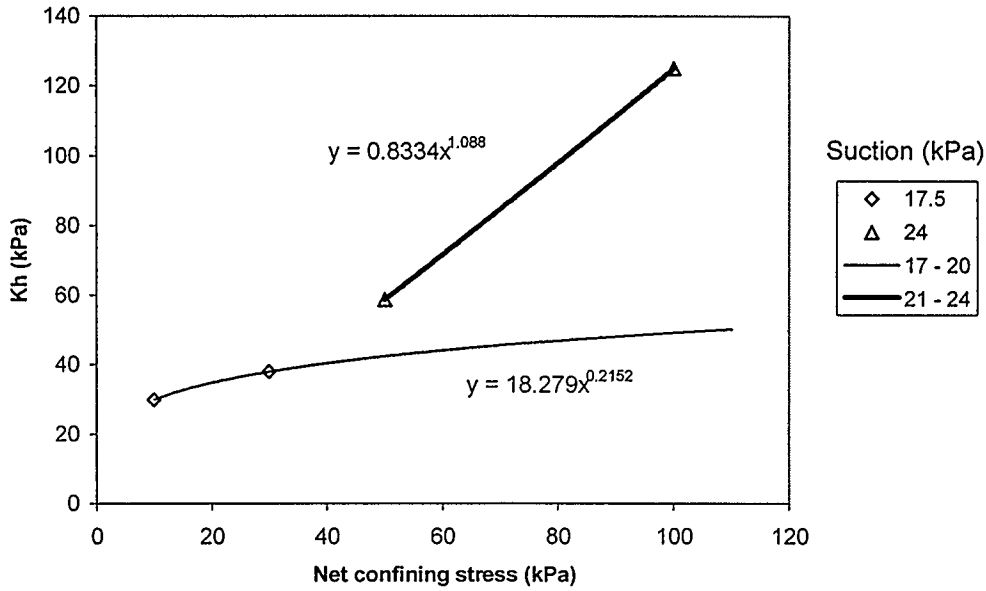


Figure 4-6: Compressive stiffness versus net confining stress (Soil sample: Sunnyside Hill, Void ratio < 0.452)

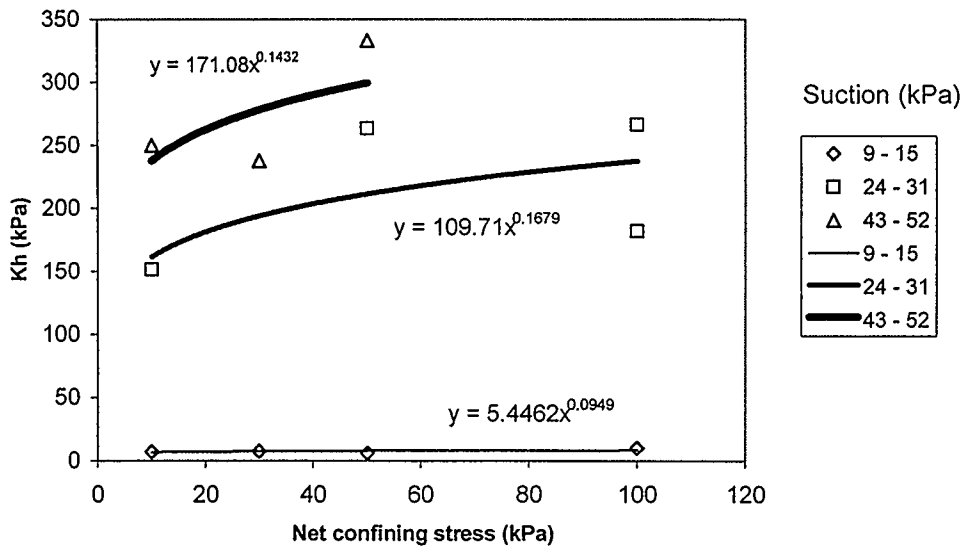


Figure 4-7: Compressive stiffness versus net confining stress (Soil sample: UC Site, Void ratio >= 0.406)

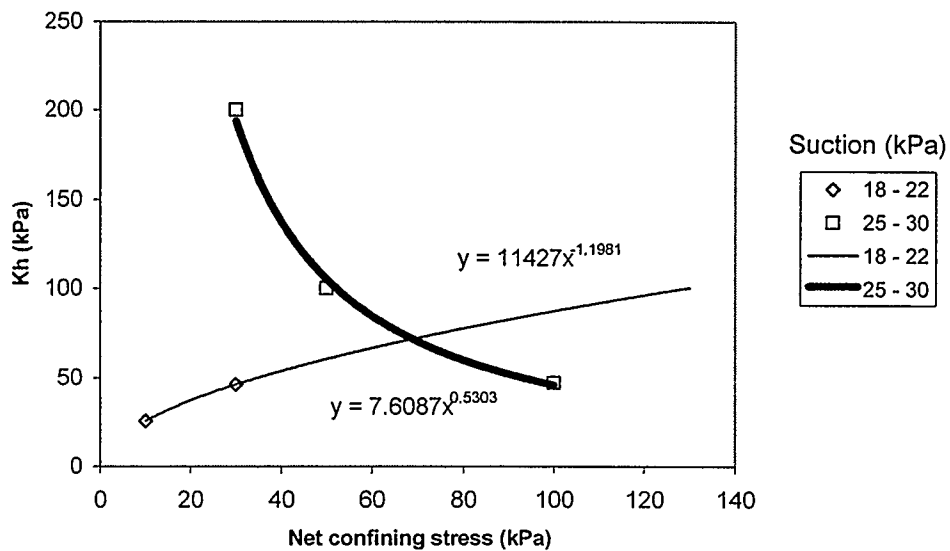


Figure 4-8: Compressive stiffness versus net confining stress
(Soil sample: UC Site, Void ratio < 0.406)

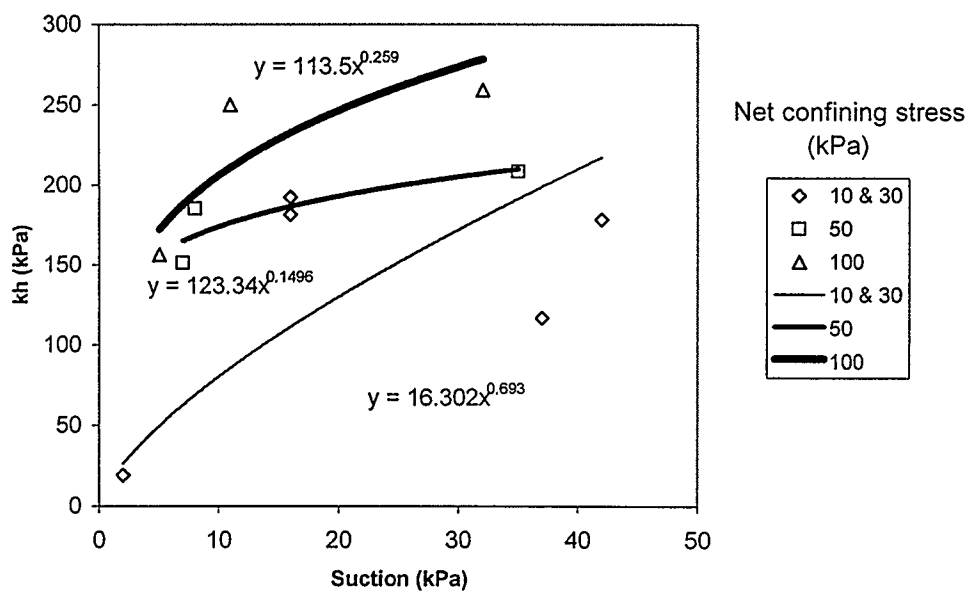


Figure 4-9: Compressive stiffness versus suction
(Soil sample: Discovery Ridge, Void ratio >= 0.456)

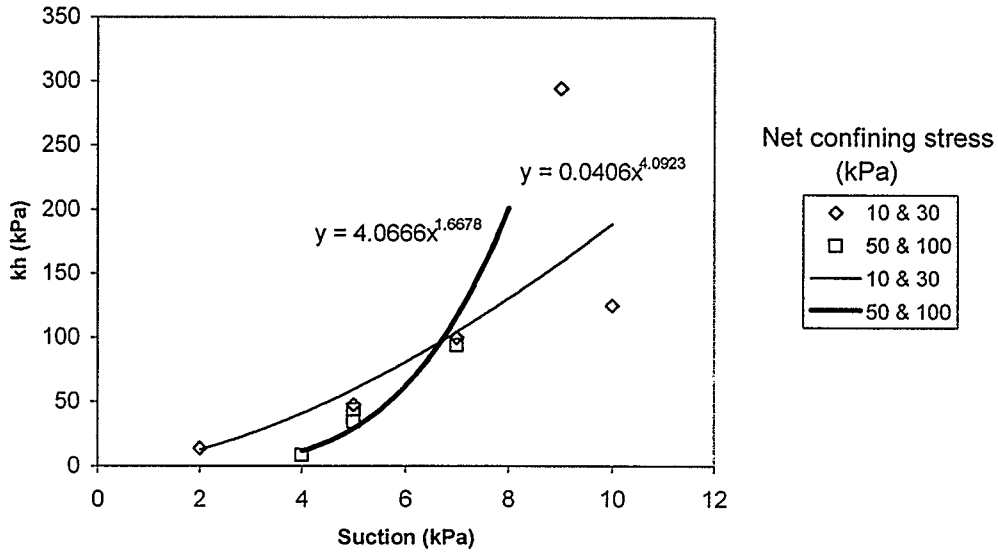


Figure 4-10: Compressive stiffness versus suction
 (Soil sample: Discovery Ridge, Void ratio < 0.456)

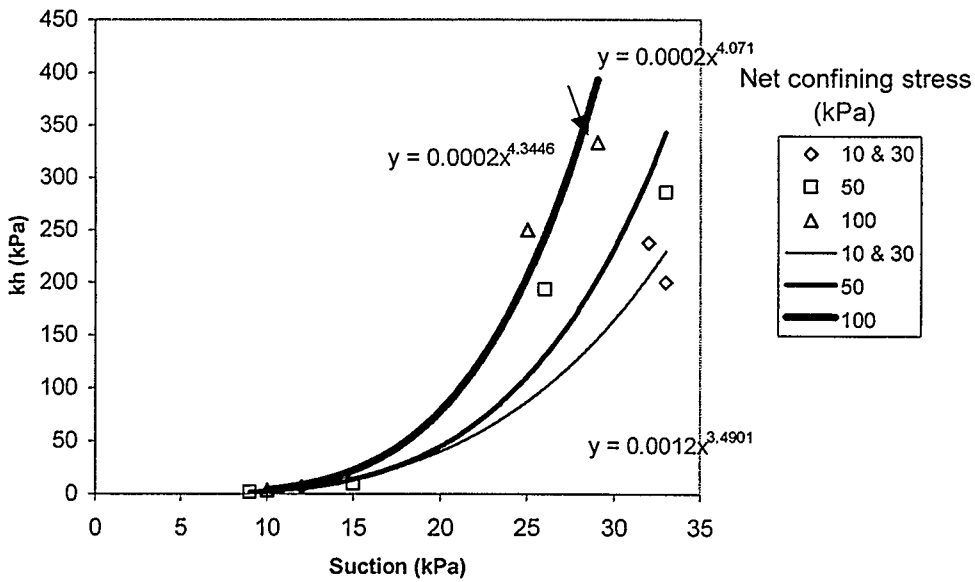


Figure 4-11: Compressive stiffness versus suction
 (Soil sample: Sunnyside Hill, Void ratio ≥ 0.452)

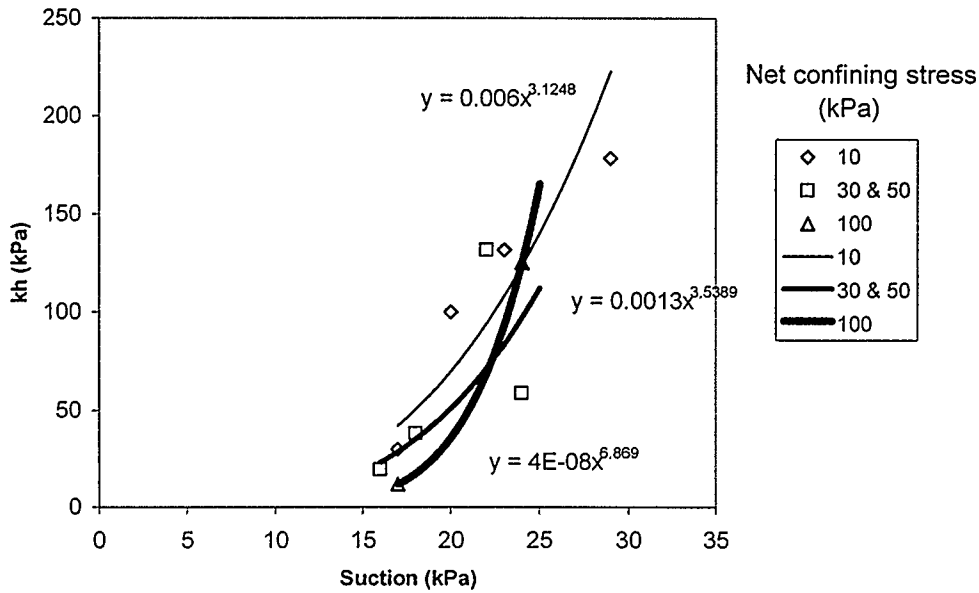


Figure 4-12: Compressive stiffness versus suction (Soil sample: Sunnyside Hill, Void ratio < 0.452)

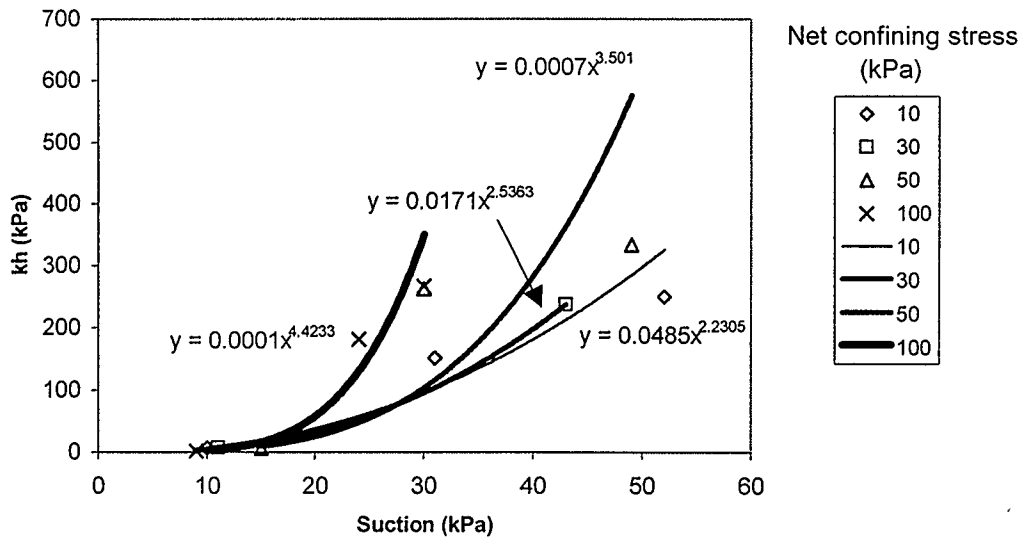


Figure 4-13: Compressive stiffness versus suction (Soil sample: UC Site, Void ratio ≥ 0.406)

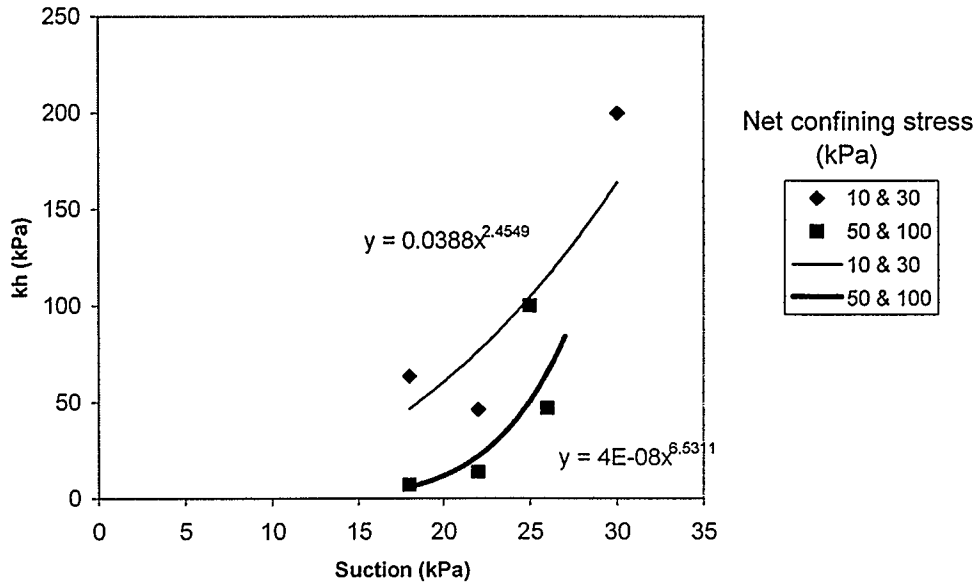


Figure 4-14: Compressive stiffness versus suction
(Soil sample: UC Site, Void ratio < 0.406)

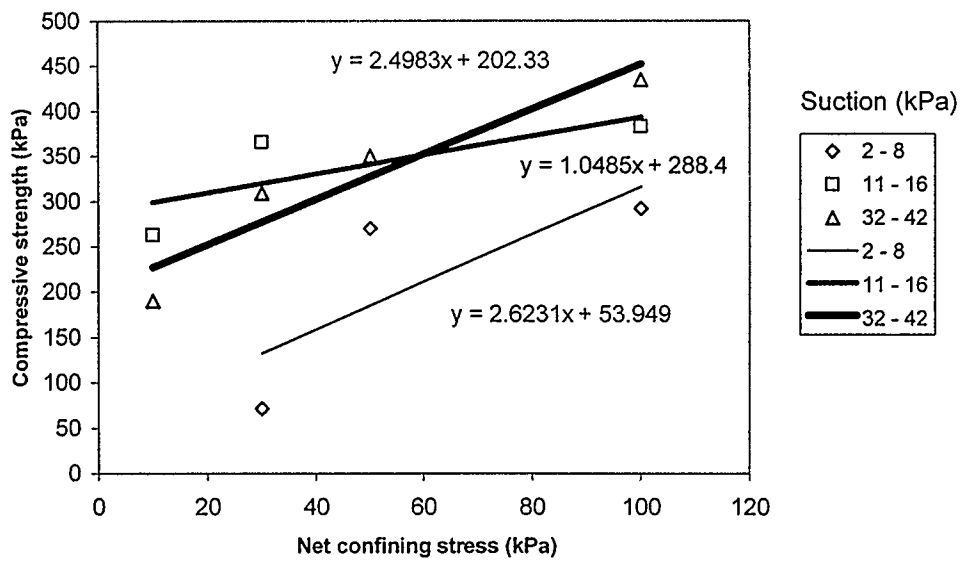


Figure 4-15: Compressive strength versus net confining stress
(Soil sample: Discovery Ridge, Void ratio ≥ 0.456)

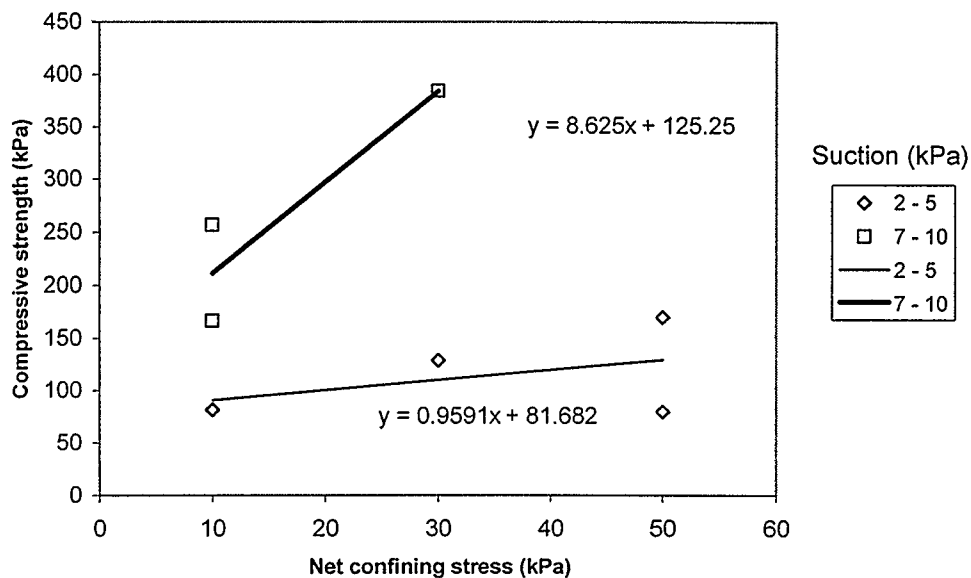


Figure 4-16: Compressive strength versus net confining stress (Soil sample: Discovery Ridge, Void ratio < 0.456)

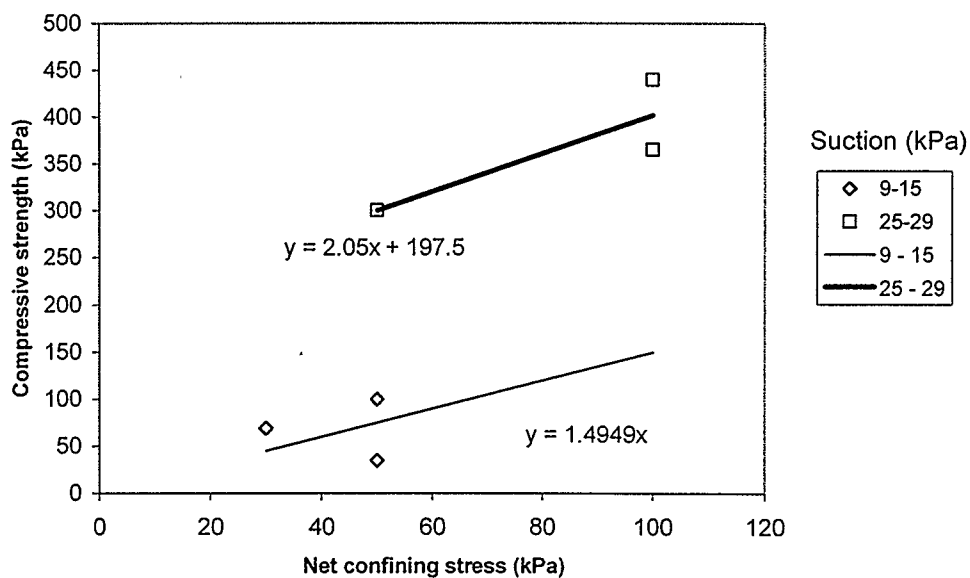


Figure 4-17: Compressive strength versus net confining stress (Soil sample: Sunnyside Hill, Void ratio ≥ 0.452)

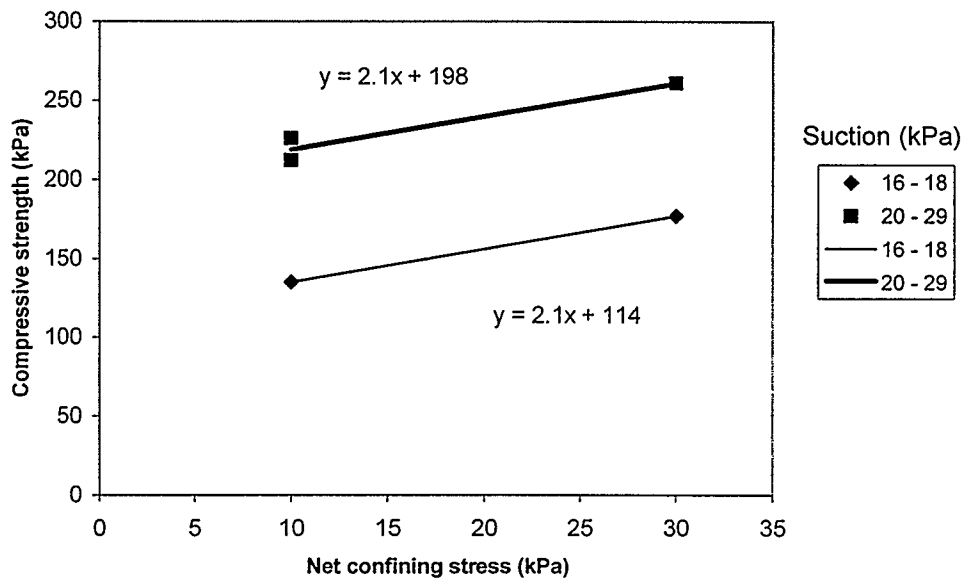


Figure 4-18: Compressive strength versus net confining stress
(Soil sample: Sunnyside Hill, Void ratio < 0.452)

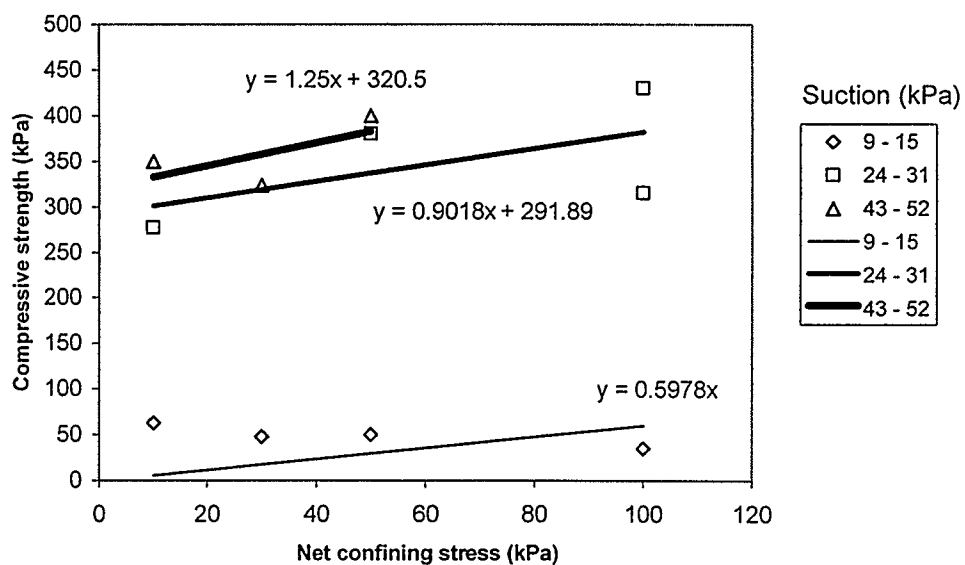


Figure 4-19: Compressive strength versus net confining stress
(Soil sample: UC Site, Void ratio ≥ 0.406)

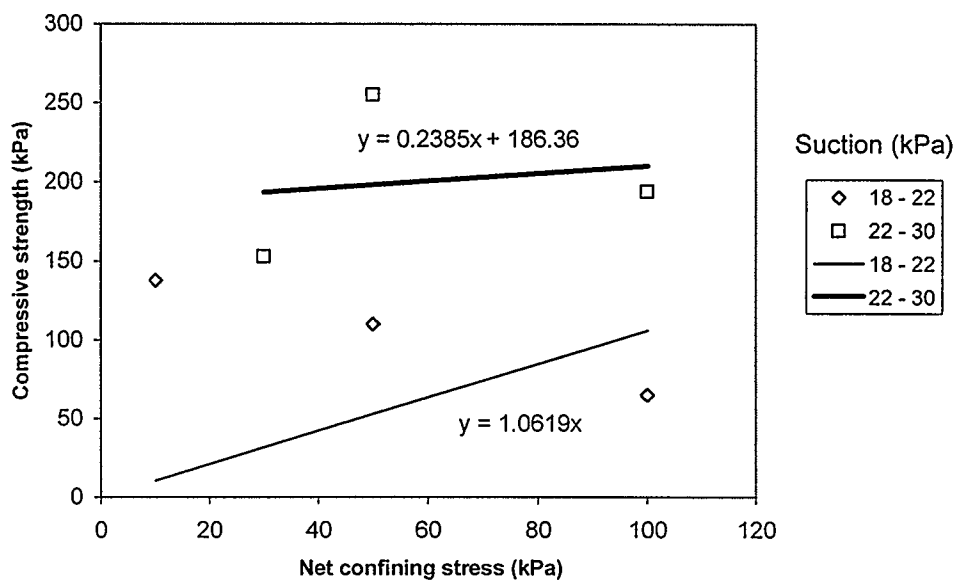


Figure 4-20: Compressive strength versus net confining stress
(Soil sample: UC Site, Void ratio < 0.406)

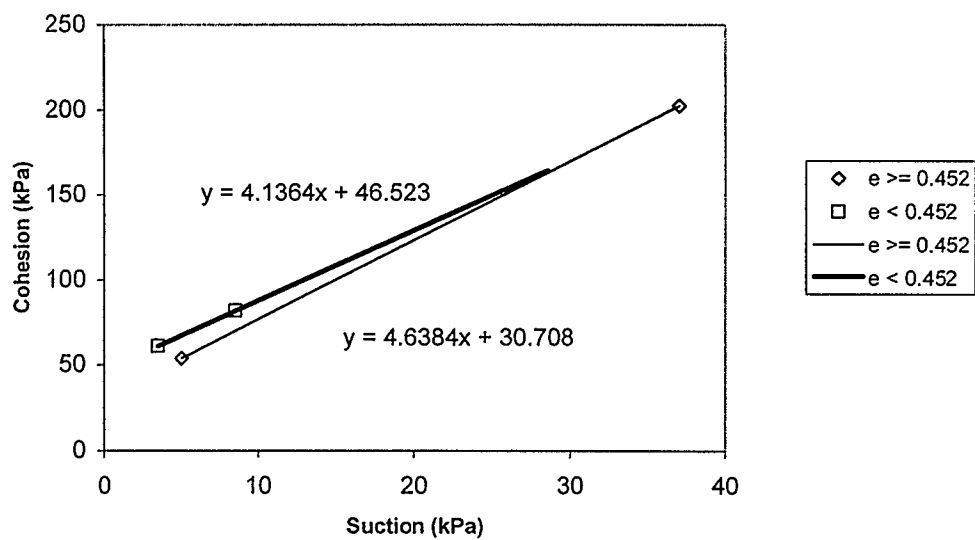


Figure 4-21: Cohesion versus suction
(Soil sample: Discovery Ridge)

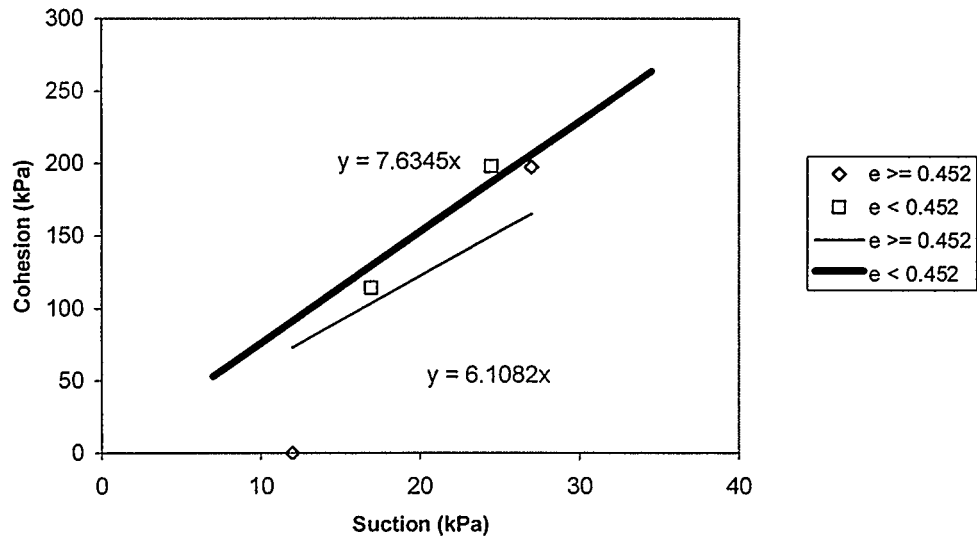


Figure 4-22: Cohesion versus suction
(Soil sample: Sunnyside Hill)

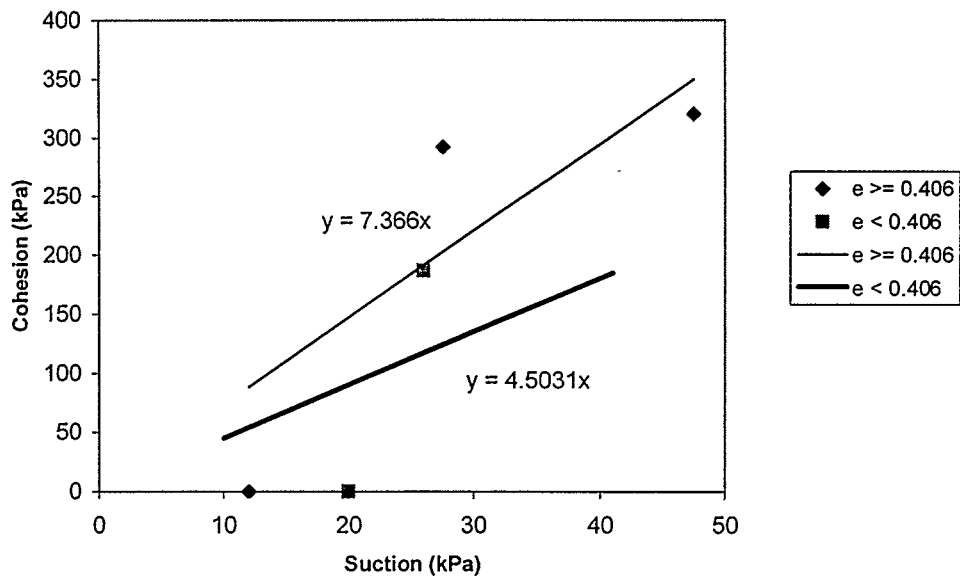
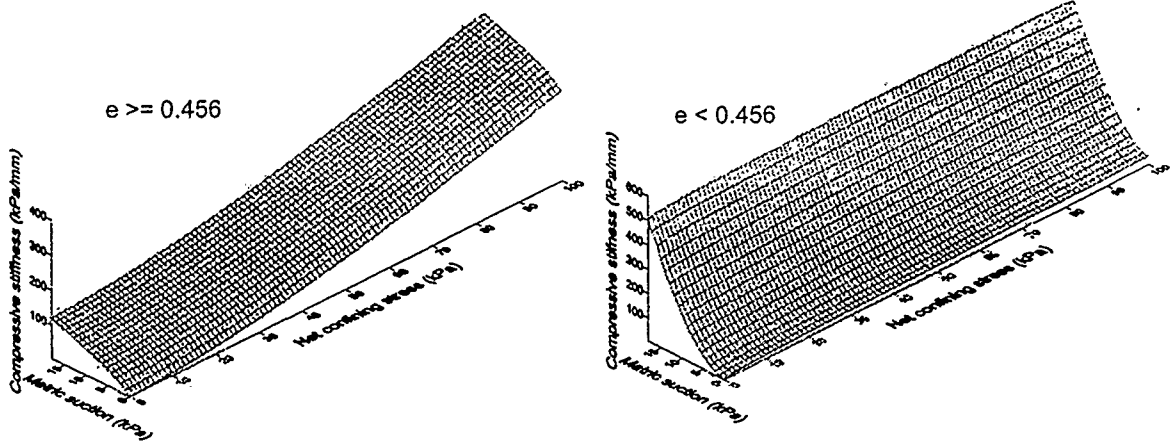
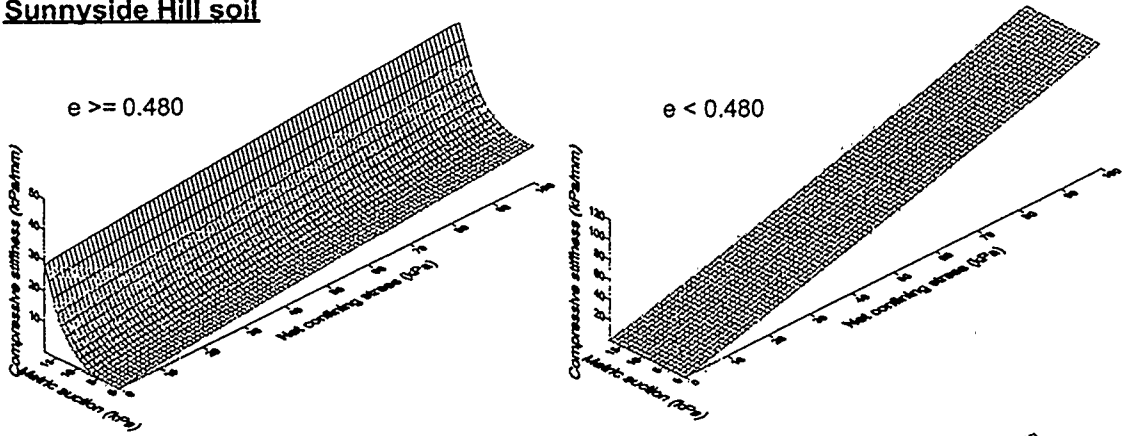


Figure 4-23: Cohesion versus suction
(Soil sample: UC Site)

Discovery Ridge soil



Sunnyside Hill soil



UC Site soil

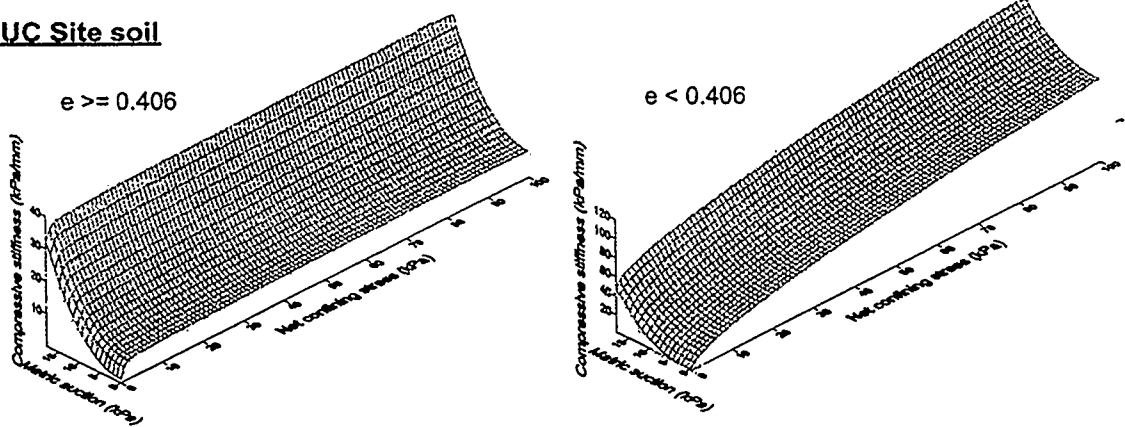


Figure 4-24: Relationships among compressive stiffness, net confining stress, and matric suction

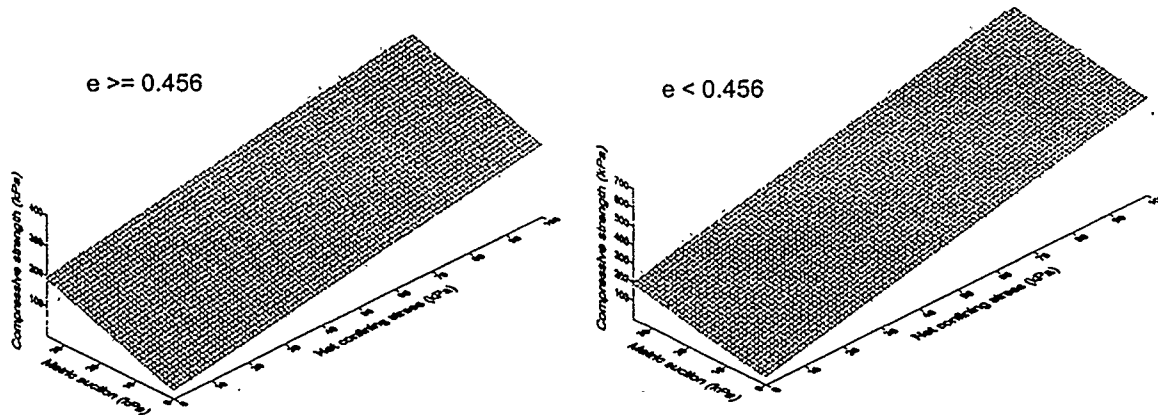
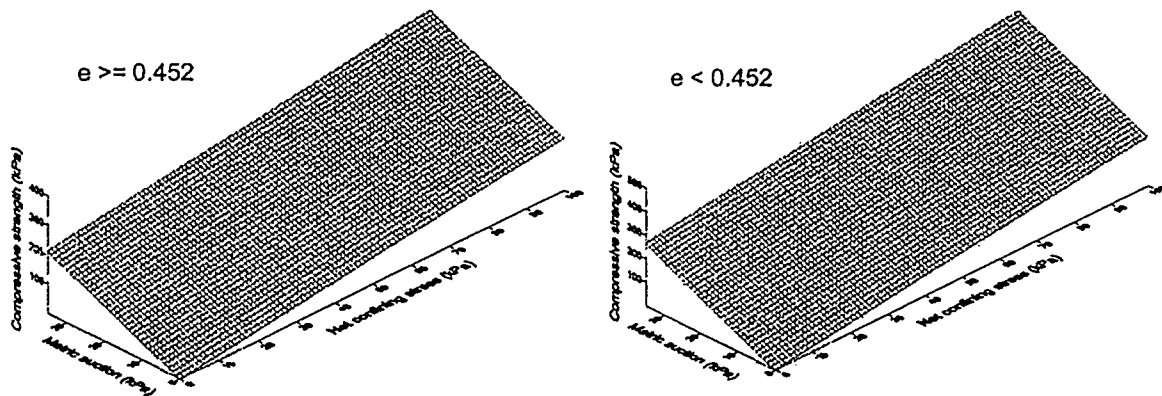
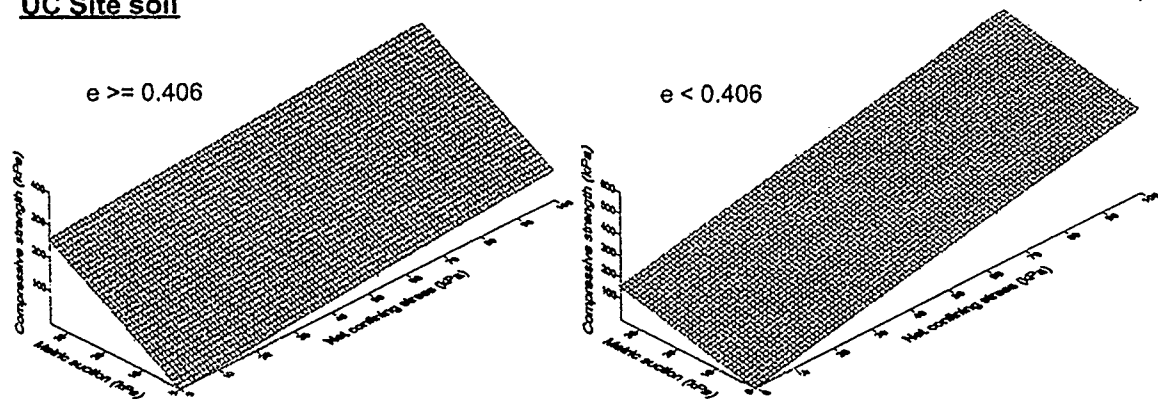
Discovery Ridge soilSunnyside Hill soilUC Site soil

Figure 4-25: Relationships among compressive strength, net confining stress, and matric suction

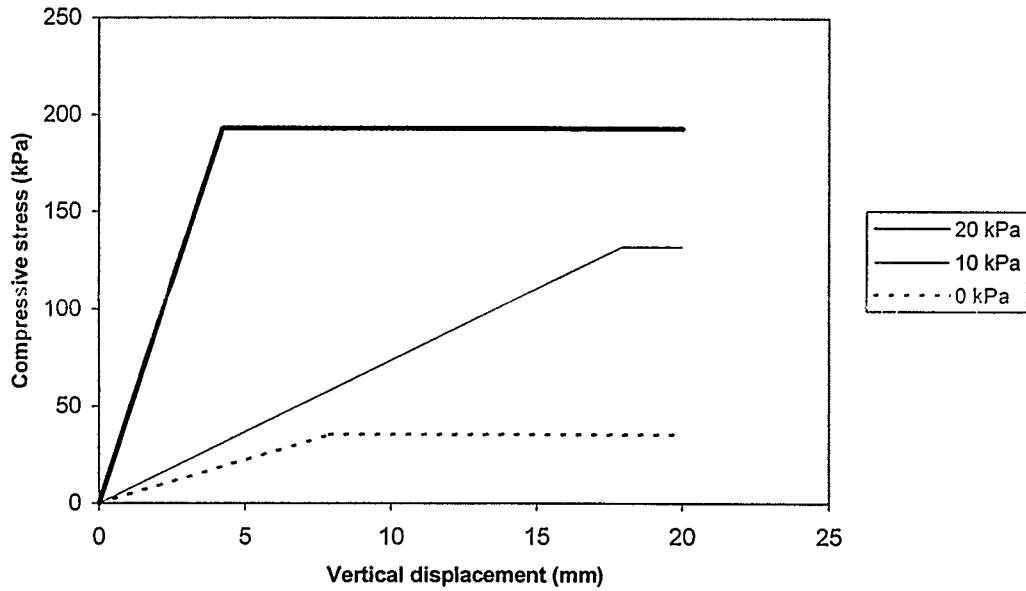


Figure 4-26: Results from the proposed equations for Sunnyside Hill for $\sigma = 40$ kPa for sample length = 115 mm, diameter = 110 mm

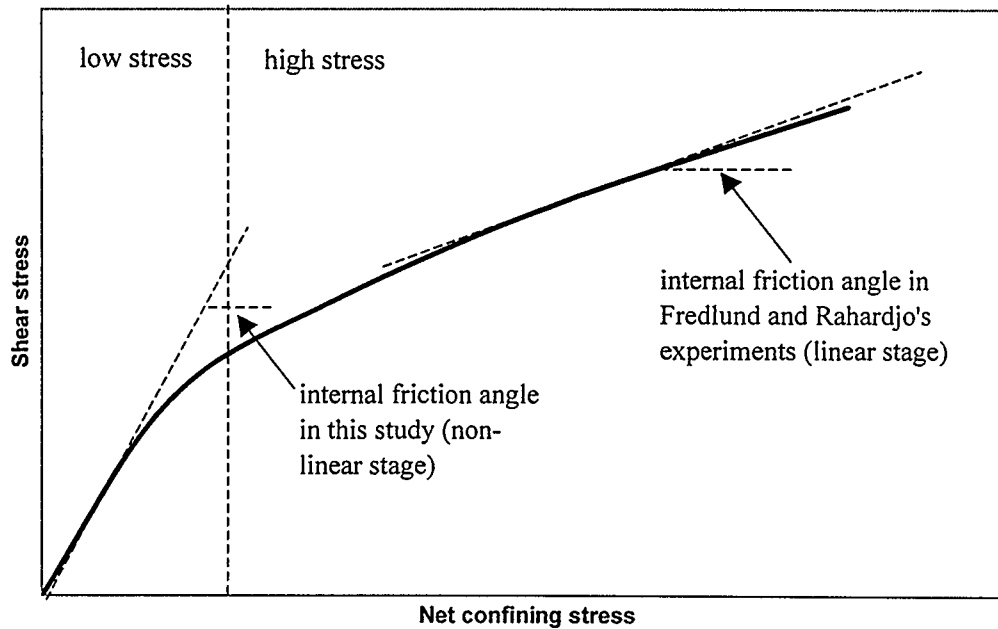


Figure 4-27: Internal friction angles (ϕ') at non-linear and linear stages

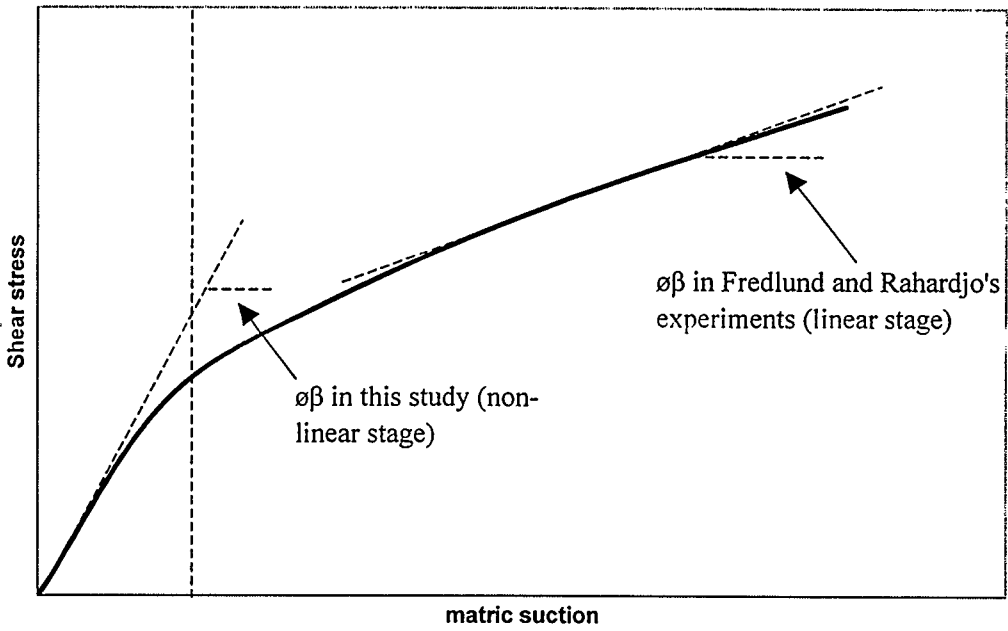


Figure 4-28: Angles relative to matric suction ($\phi\beta$) at non-linear and linear stages

CHAPTER 5: CASE STUDY

5.1 Introduction

In order to provide a thorough understanding of the application and effectiveness of the shear strength equation (Equations (3.15)) correlated from the direct shear box tests in this study, stability analyses are conducted on the slope located at Sunnyside Hill between 5th and 6th Street N.W. Calgary, Alberta.

Golder Associates Ltd. (Golder) performed field investigations and stability analysis at the above site in March, 1998. In April, 2001, Golder initiated a series of field works, including the measurement of soil suction. The first two measurements were performed by one of their engineers, Karen Moffit, and was continued on May 2001 by the author for nine more measurements in a one-year span. The purpose of the field work was to monitor the seasonal soil suction variation near the surface for a year.

Changing conditions of the soil mass in the Sunnyside Hill active landslide made it difficult to measure seasonal variations in soil suction because the measured values were affected by the physical disturbance of the soil mass. Therefore, a test pit program to monitor seasonal variations of suction with depth was done on a similar, yet stable slope at the University of Calgary campus (UC Site) along northbound Shaganappi Trail, approximately 300 m north of 16th Ave. The purpose of the test pit program is to delineate the subsurface soil suction profile, which cannot be done on the slopes at Sunnyside Hill due to difficult access conditions.

Slope stability analyses are presented with the use of the shear strength equations and the findings from the field programs. From the results of the analyses, possible factors that triggered the previous slope slides are discussed and a conclusion is drawn.

5.2 Description of the Site

5.2.1 Surface conditions

Sunnyside Hill is located along the north escarpment of the Bow River overlooking downtown Calgary as shown in Figure 5-1. The slope angle is approximately 22° to 26°. Private residences are located on the top and toe of the slope. A paved pathway separates the residences at the toe of the slope.

5.2.2 Subsurface conditions

The surficial geology consists of lacustrine sands, silts, and clays overlying till and bedrock (Moran, 1986). The lacustrine soil is approximately 20 to 35 m thick and the till is approximately 5 to 20 m thick. Bedrock is as shallow as 5 m below the surface towards the toe of the slide.

The groundwater conditions consist of a perched water table existing in the upper sand seams and exposing at various depths in the slope while the measured piezometric levels correspond to 15 to 30 m above the toe elevation (Meyboom, 1961).

Sieve analysis and hydrometer tests were performed on the soil samples obtained from ten different locations at depths between 200 mm and 300 mm. The soil on the upper portion of the slope contains 18.8% clay, 38.2% silt and 43.0% sand and gravel while the soil on the lower portion contains 12.1% clay, 39.7% silt and 48.2% sand and gravel.

5.3 Slope Instability

5.3.1 Instability history

Records of instability of the hillside started in the 1930's and coincided with urban development of the area. Stabilization measures were implemented in the 1930's,

1940's, 1950's and 1960's, nonetheless, instabilities continued. Slides in 1997 and 1998 brought awareness that additional measures were required to preserve the integrity of adjacent private property (Mahmoud and Burwash 1998).

5.3.2 Description of previous slope failures and remedial measures

A major slide occurred in the summer of 1948. The cause of the slide was due to unfavorable climatic conditions that led to the sudden release of pore pressures behind a frozen crust which was blocking a major seepage zone. Horizontal drains was installed, but became ineffective when the drains became plugged and impossible to service by backwashing. Other stabilization measures included slope re-grading and toe land construction as well as vertical drains and gravel blanket, which were done in the 90s to control silt erosion (Hardy, 1963; Materials Testing Laboratories, 1964; Hardy and Associates Ltd., 1974).

The slide in 1997 was approximately 40 m long, 15 m wide, and 1.5 to 2.0 m deep. It happened in June following a particularly heavy rain period and runoff from the previous winter's heavy snowfall (Mahmoud and Burwash 1998). The slide debris covered a portion of the paved pathway near the toe of the slope.

A protection barrier was constructed shortly after the slide. The barrier was about 50 m long located along the upslope of the pathway. It was designed as a catchment to prevent slide debris from encroaching on the pathway and private property downslope of the pathway. The tension cracks were filled with bentonite pellets to minimize the infiltration of surface water and thus, the risk of additional slope movement.

The Golder's analysis (Mahmoud and Burwash 1998) of the 1997 and 1998 slides suggested that there were two potential failure conditions: deep seated failure and shallow instability. The deep seated failure was initiated by increasing water table level. The

shallow instability was initiated by saturated surficial conditions following spring runoff or periods of prolonged rainfall.

5.4 Field Investigation

5.4.1 Boreholes drilling program

Golder drilled two boreholes, located at the top of the escarpment and near the toe in November, 1997. Borehole BH-1 encountered refusal in bedrock at a depth of 10.4 m and Borehole BH-2 was advanced to a depth of 34.3 m in the glacial till. Two pneumatic piezometers separated by bentonite seals were installed in each borehole. The two borehole logs are shown in the cross-section in Figure 5-2.

5.4.2 Soil suction measurement program

The soil suction profile was determined in Sunnyside Hill from April 2001 to May 2002. At the beginning of each month during the period, soil suction measurements were made on ten different locations at approximately 0.3 m below the surface on the slope in Sunnyside Hill with the use of a soil moisture probe, which is designed to conduct field soil suction measurement. The measurement locations are shown in Figure 3-2. Following each suction measurement, a disturbed sample was taken from the soil at the field suction measurement position. The samples were taken to the laboratory for testing of water content.

The soil suction profile was also determined in UC Site during the test pit program on July 8, 2001, November 2, 2001, and May 2, 2002. Soil suctions were measured every 0.5 m using the soil moisture probe. The subsurface condition was visually logged and disturbed samples were obtained every 0.5 m in depth.

5.4.3 Field density tests

Field density tests were undertaken at the ten locations as shown in Figure 3-2 (S1 to S10) using a densiometer, which is capable to measure the soil dry density at 0.3 m below surface. The results are presented in Appendix G. The average dry density from the surface to 0.3 m below on the slope in Sunnyside Hill is 1765 kg/m³.

5.5 Laboratory Investigations

Soil samples were collected in sealed plastic bags from each of the testing locations and taken immediately to the laboratory. The soil samples were oven dried at 130 °C to determine their moisture contents (ASTM (1992), Designation D2216). The dried samples were homogenized and used as the testing material for the direct shear box and triaxial compression tests described in Chapters 3 and 4.

5.6 Field Data Analysis

The field data, presented in Appendix G, are soil suction measurements and their corresponding soil moisture contents, and field density tests.

The soil suction profile fluctuated in Sunnyside Hill, especially during the high precipitation periods as the silt soil are not impervious, but moderately permeable. Soil suction decreased significantly at most of the test locations from May to June in both 2001 and 2002 as shown in Figures 5-3 to 5-7. In Figure 5-8, the precipitation records show that May, June, and July are the highest precipitation months in 2001. During this high precipitation period, the silt soil on the slope surface became wetter and had lower soil suction values.

The field soil suction measurements are also compared to the laboratory measurements in Figure 5-9, and the two data sets are consistent.

Additional soil suction measurements were taken in UC site as shown in Figure 5-10 to better define the seasonal changes in suction and water content with depth in test pits on a similar, but more accessible slope. Two test pits (TP 1 and TP 2) located on the slope were 30 m apart. The two test pits were grassed at the surface, but the second test pit (TP 2) had trees planted nearby it. Vegetation has a significant influence on soil suction near the surface as shown in Figures 5-11. Grasses, trees, and other plants growing on the ground surface dry the soil by applying a tension to the pore water through evapotranspiration (Dorsey 1940). In TP 2, soil suction near the surface was much higher than that in TP 1, but the difference in the soil suction readings between the two test pits became less significant at greater depths.

The field suction measurements are also compared to the laboratory readings based on the different moisture contents in Figure 5-12 and the two data sets are consistent.

5.7 Slope Stability Analyses

Stability analyses for the specified slope at Sunnyside Hill might be carried out using the force equilibrium method:

$$\text{Factor of safety} = \frac{\Sigma F_R}{\Sigma F_D} \quad (5.1)$$

where

F_R = resisting forces = $c + (\sigma - u_a) \tan \phi' \cos \psi$,

c = apparent cohesion = $c' + (u_a - u_w) \tan \phi_\beta$,

c' = true cohesion,

$u_a - u_w$ = matric suction,

ϕ_β = angle indicating the rate of increase in shear strength with respect to suction,

$\sigma - u_a$ = net confining stress,

ϕ' = internal angle of friction,

ψ = slope angle = 22-26°,

F_D = driving forces = $\gamma h \sin \psi$,

γ = unit weight = 20 kN/m³, and

h = depth of slides = 1.5 - 2.0 m.

Typical strength parameters for sandy silts in Calgary include an internal angle of friction (ϕ') ranging from 27° to 36° and a true cohesion ranging from 0 to 7 kPa (Hardy et al., 1980). In this study, these parameters were determined from laboratory testing and found to be within the above ranges. The angles, ϕ_β and ϕ' , and true cohesion in equation (5.1) were obtained from equation (3.15). The maximum depth of the 1997 and 1998 slope slides of 2.0 m was chosen for the calculation. The unit weight was determined by the density tests conducted on the slopes, which was approximately equal to 20 kN/m³. Thus, the corresponding net confining stress was approximately equal to 40 kPa. The factors of safety for different soil suction values are shown in Table 5-1.

Note that the calculated factors of safety are based on using soil parameters obtained from laboratory testing of remolded samples from the site. Consequently, the calculated factors of safety are estimated, which assume that insitu and remolded soil properties are similar. It is beyond the scope of this research to correlate insitu and remolded soil properties.

In Table 5.1, the factor of safety values of one or less than one indicate an unstable slope condition. The data shows factors of safety for unstable slopes when soil suction values are between 0 kPa and 5 kPa. Soil suction values within this range were measured in the field at a depth of 300 mm. It is possible that during periods of higher infiltration, much of the soil near the surface has suction values less than 5 kPa. Therefore, higher water contents, and thus lower suction values, most likely caused the shallow landslides in 1997

and 1998. The factor of safety values are plotted against soil suction with slope angles of 22°, 24°, and 26° in Figure 5-13.

In Golder's report (Mahmoud and Burwash 1997), a similar analysis was reported; however, the angles, ϕ' and ϕ_β were estimated from past experiences. In this study, the angles were determined from laboratory testing. Both studies calculated that the slope becomes unstable when soil approached the saturated condition (i.e. suction approached zero) during the summer months. It is proven that the reduction of soil suction can lead to unstable condition and movements on the slopes in Sunnyside Hill.

In the illustrative examples presented in Sections 3.7 and 4.6, the stiffness and strength values reduced significantly as soil suction decreased. Although the factors of safety were generally above the unity with soil suction above 5 kPa, some movement was anticipated on the slope as illustrated in Figures 3-31 and 4-26. In Figure 3-31, the slope moved slightly when soil suction reduced from 20 kPa to 10 kPa and the movement began to exaggerate when soil suction further reduced to 0 kPa.

5.8 Discussion

The slopes in Sunnyside Hill were constructed at angles between 22° to 26°, which were larger than the soil effective friction angle of 21.3° obtained from equation (3.15) and presented in Table 4-3. The friction component of the strength alone would not have been sufficient to maintain the stability. Soil in Sunnyside Hill has some apparent cohesive strength contributed by soil suction. Since the slopes have had continual instability problems, it would appear that the cohesive component of the strength must have decreased with time.

This study has shown, and Figure 5-13 illustrates, that soils strength and thus the slope factor of safety are sensitive to changes in soil suction values. Specifically, the slope

becomes unstable and shallow landslides occur when soil suction values are near or less than 5 kPa. The reduction of soil suction can be associated with different sources. Saturation of surficial materials following heavy or prolonged rainfall, and during snowmelt or thawing cycles is a common phenomenon in a typical Calgary spring. Thawing of segregated ice lenses in spring is another source of high water contents. Freezing temperatures, frost active soils, like those on the Sunnyside Hill and a water table within about 4 m of surface are conditions present on parts of Sunnyside Hill. During winter, free water moves from the water table to the freezing isotherm in the soil as water particles tend to move from high to low temperature. Over time, several layers or lenses of varying thickness of segregated ice form. When the segregated ice thaws in spring, the soil water contents in nearby soils increase and approach saturation values. Such high water contents can trigger shallow landslides (Mahmoud and Burwash 1998).

The suction readings collected during the one-year span indicate a significant reduction in soil suction in the silt material during the summer months. In the precipitation bar charts from 1997 and 2002 presented in Figure 5-8, the months between May and July have the highest precipitation. In 1997 and 1998 when the slides occurred, the precipitation from May to July was significantly higher than the same period in other years. Therefore, the cause of the 1997 and 1998 slides is likely the result of high precipitation which leads to the reduction of soil suction near the surface.

5.9 Conclusion

The slopes on Sunnyside Hill were initially stable owing to the apparent cohesive strength of the soil combined with its frictional strength. However, the soil lost its cohesive strength as the soil became saturated and the remaining frictional strength was not sufficient to maintain stability. Golder's stability analysis (Mahmoud and Burwash 1998) shows that the 1997 and 1998 slope failures were triggered by extremely adverse weather conditions leading to a reduction in suctions in the silt deposits near the surface.

In this study, soil suction measurements during a one-year period found low values during the wetter months of May to July. According to the strength equations developed in Chapters 3 and 4, the apparent cohesive strength due to soil suction is more influential than the frictional strength in total soil strength. Thus, the reduction of soil suction on the slope in Sunnyside Hill caused the decrease in shear strength during the summer months and led to the slope slides in 1997 and 1998, which agreed with Golder's conclusions (Mahmoud and Burwash 1998).

The soil suction values measured in UC Site did not demonstrate a definite pattern throughout the year as those taken on Sunnyside Hill due to different soil types and different site conditions between the two sites. The slope in UC Site was grassed and that prevented the underlying soil by adversely affected under unfavorable weather conditions. In contrary, soil exposed in Sunnyside Hill due to the previous slides and was significantly affected by the weather conditions. Although the suction measurements in UC Site did not provide a plausible correlation with the field measurements taken at Sunnyside Hill, the results showed the soil suction profile at various depths.

Soil suction, u_s (kPa)	Factor of safety		
	Slope angle 22°	Slope angle 24°	Slope angle 26°
0	0.97	0.88	0.80
5	1.16	1.05	0.97
10	1.36	1.24	1.13
15	1.56	1.42	1.30
20	1.75	1.60	1.47
25	1.95	1.78	1.64
30	2.14	1.96	1.80

Table 5.1 – Factors of safety for the specified slope at Sunnyside Hill

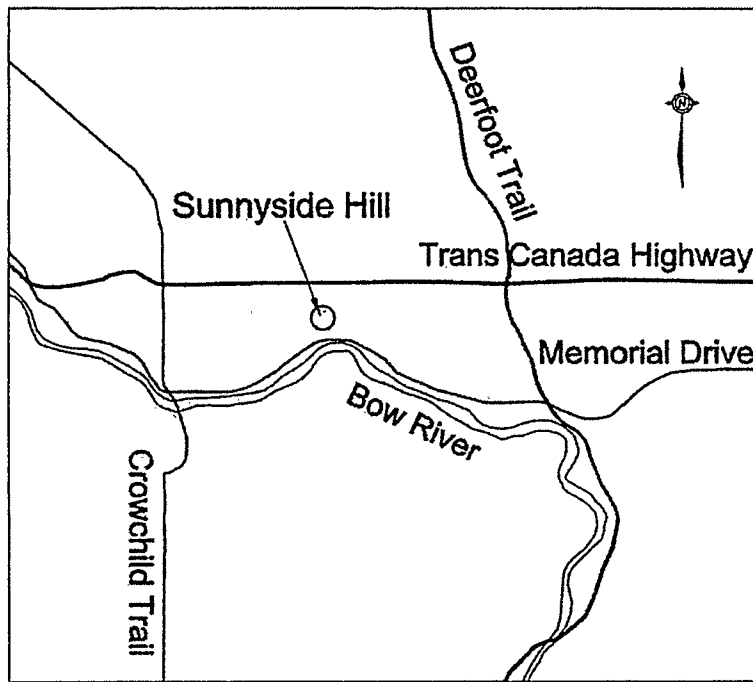


Figure 5-1: Location of Sunnyside Hill

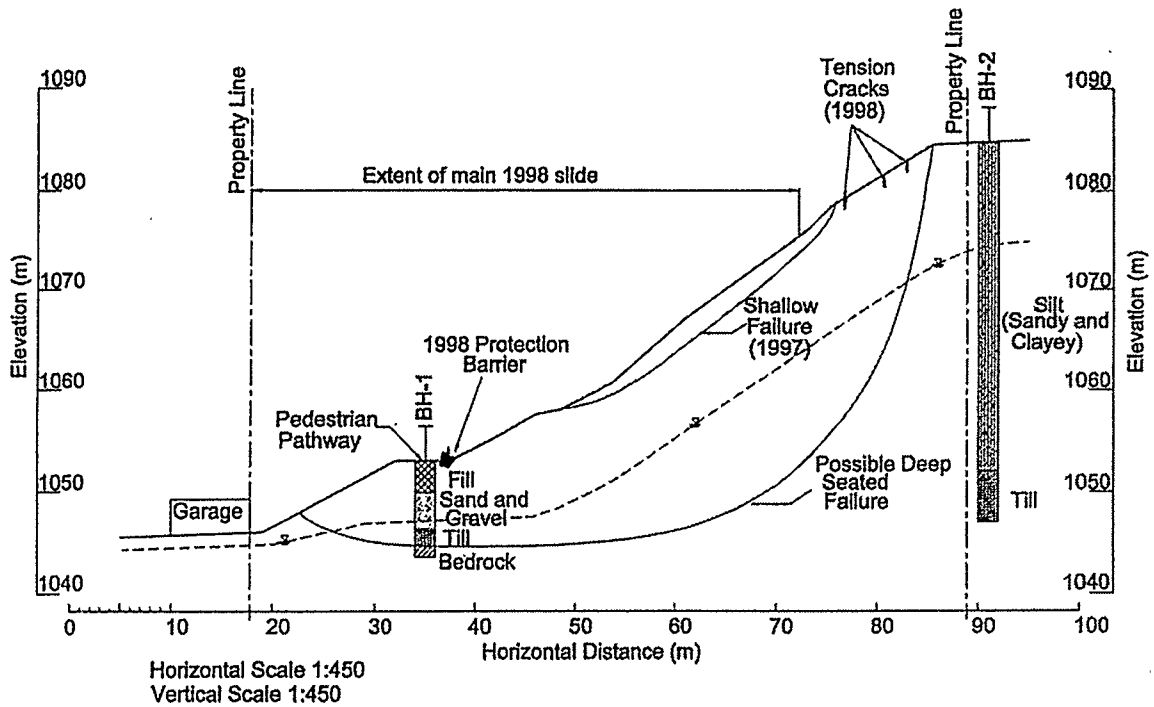


Figure 5-2: Cross-section of slides in Sunnyside Hill
(Modified from Golder Associates Ltd. report,
'Stability of Sunnyside Hill in Calgary, Alberta.')

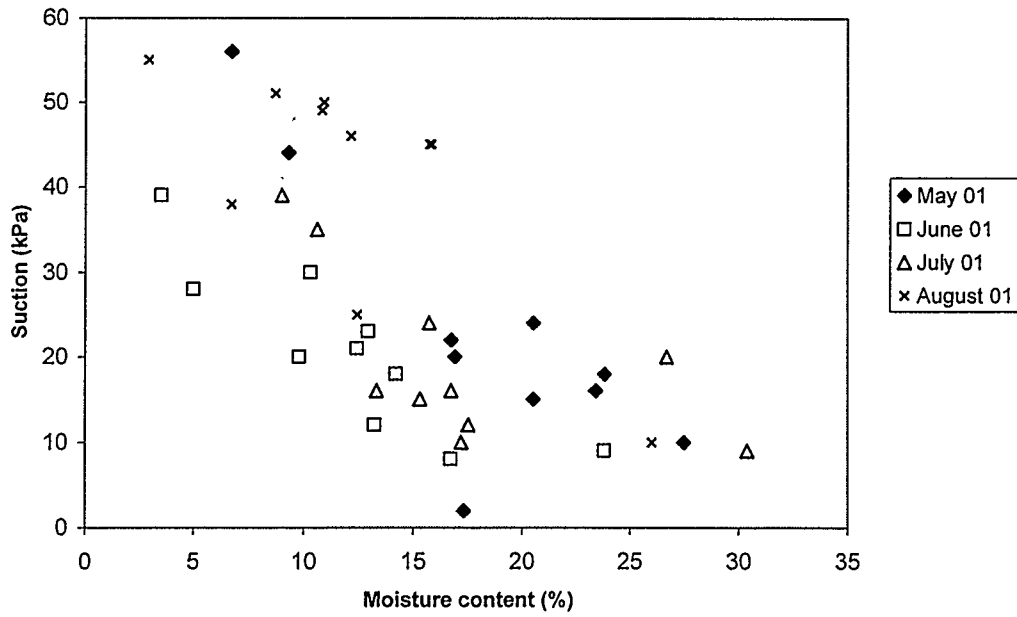


Figure 5-3: Suction versus moisture content at 0.3 m from surface in Sunnyside Hill (May to August 2001)

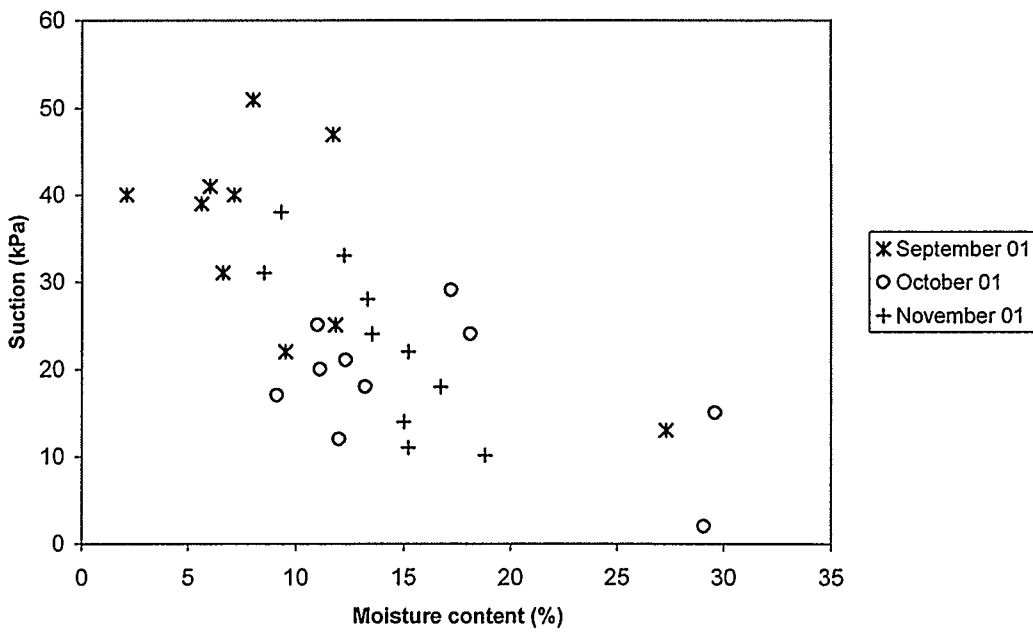


Figure 5-4: Suction versus moisture content at 0.3 m from surface in Sunnyside Hill (September to November 2001)

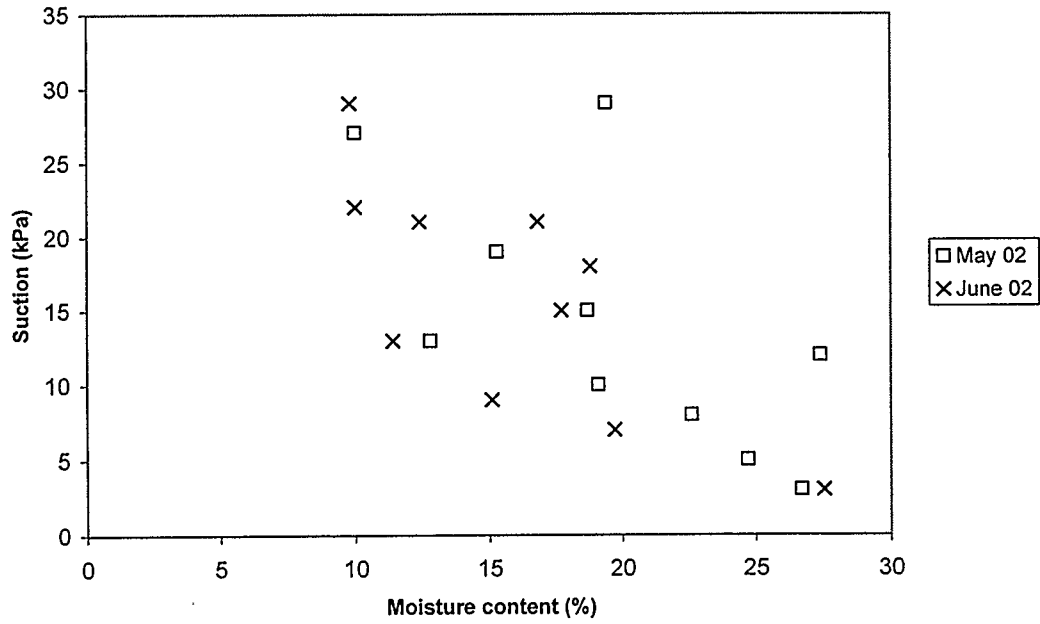


Figure 5-5: Suction versus moisture content at 0.3 m from surface in Sunnyside Hill (May and June 2002)

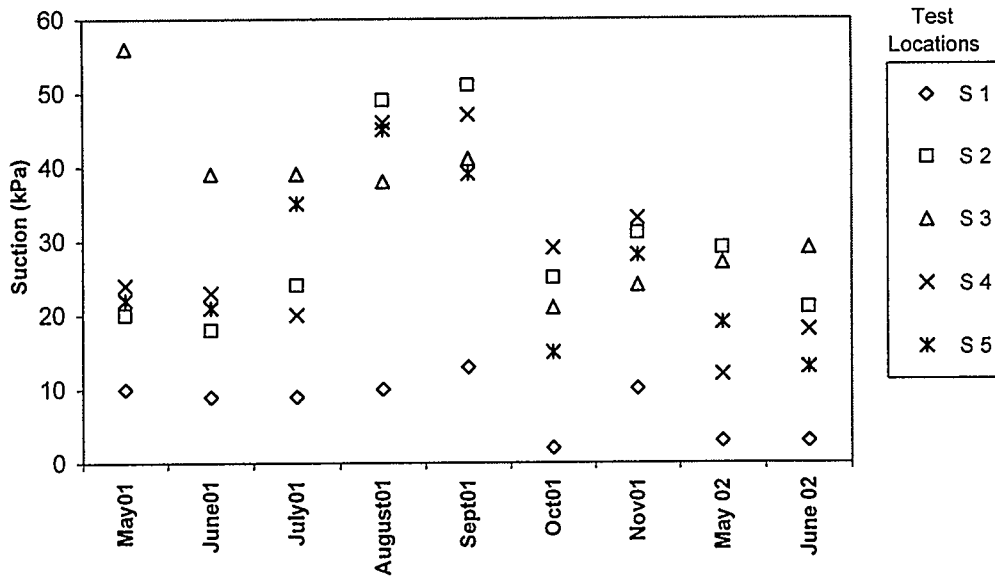


Figure 5-6: Change of suction at 0.3 m from surface in Sunnyside Hill throughout the year (Locations S1 to S5)

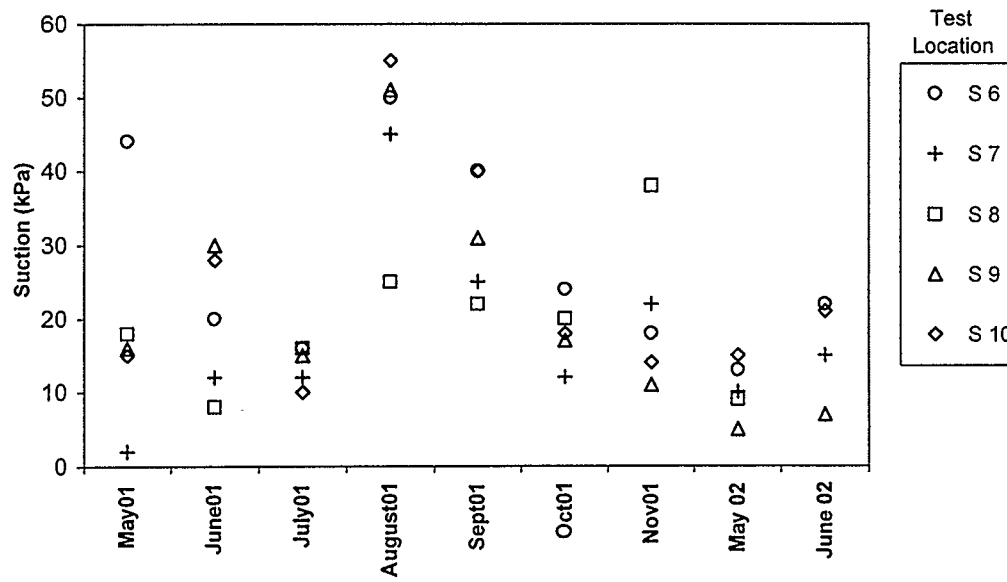


Figure 5-7: Change of suction at 0.3 m from surface in Sunnyside Hill throughout the year (Locations S6 to S10)

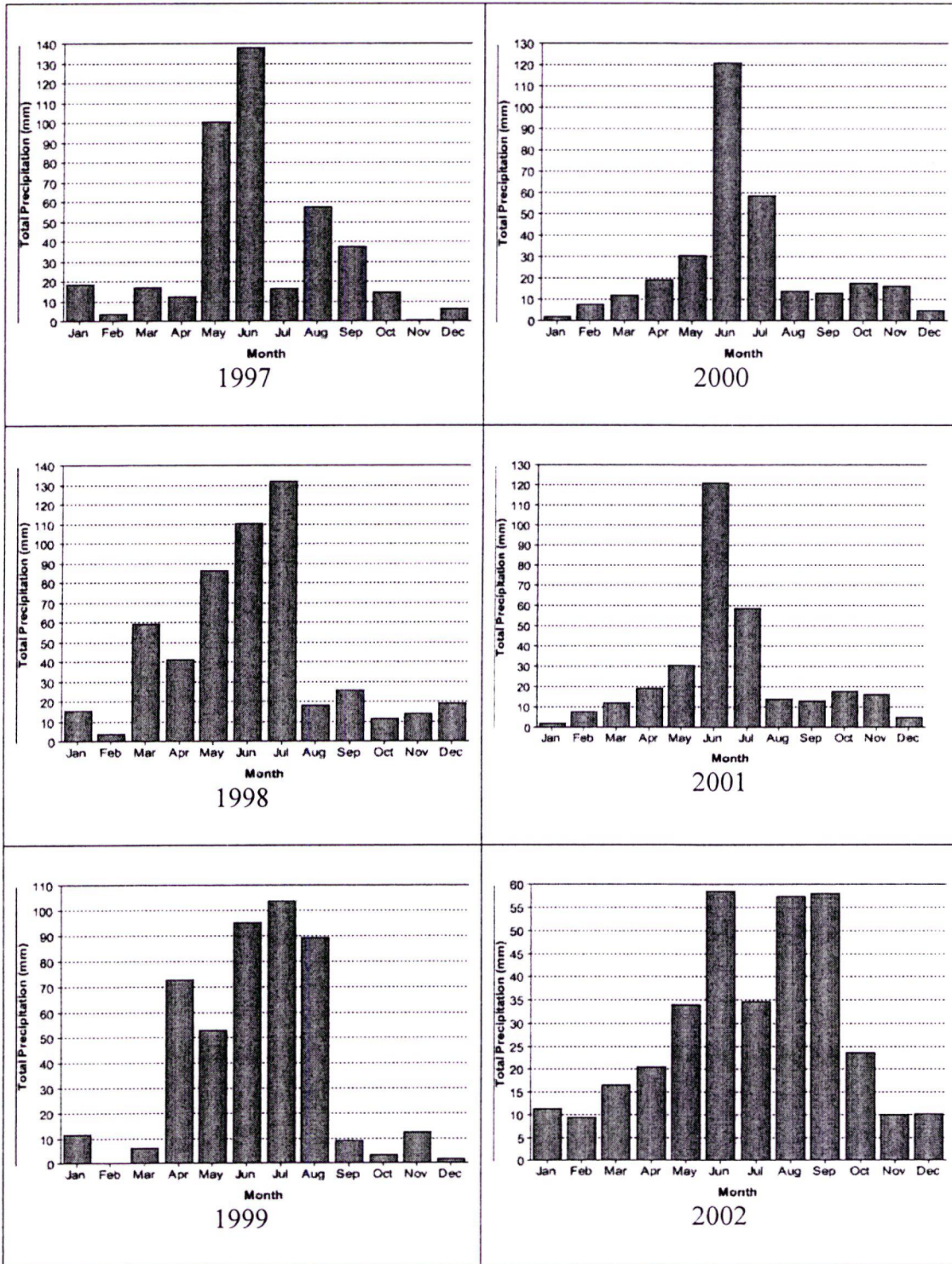


Figure 5-8: Precipitation records at Calgary International Airport from 1997 to 2002

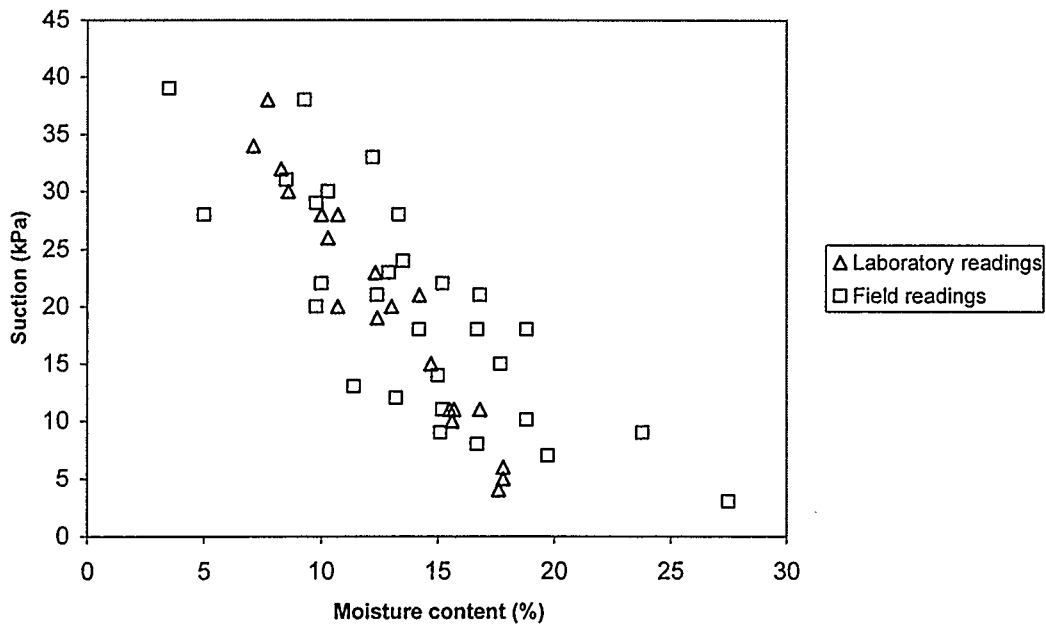


Figure 5-9: Comparison of laboratory and field suction readings in Sunnyside Hill
(All moisture contents were determined in laboratory)

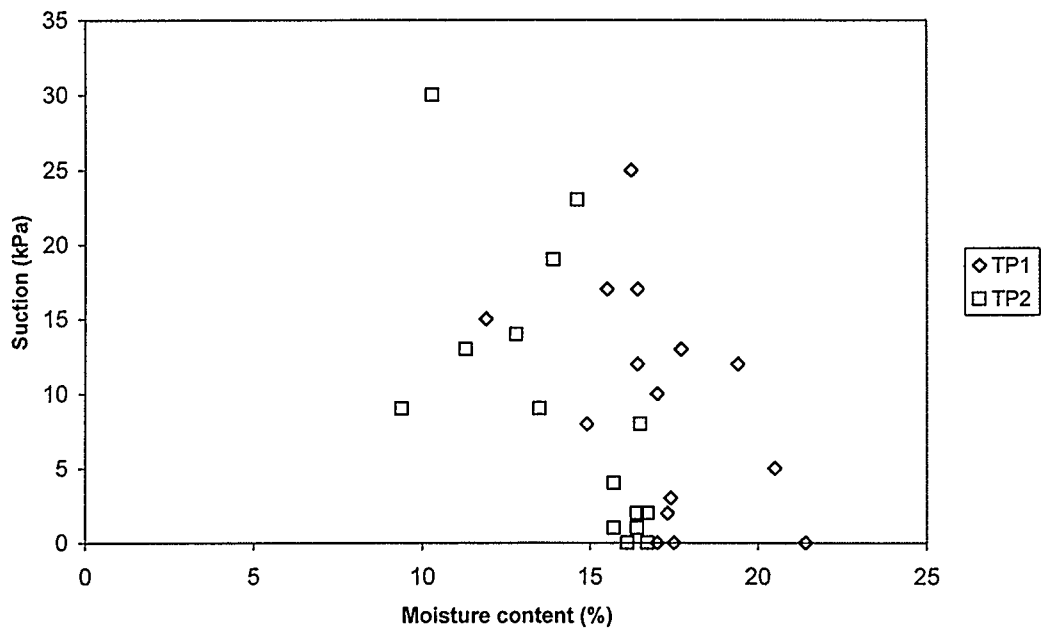


Figure 5-10: Suction versus moisture content in UC site

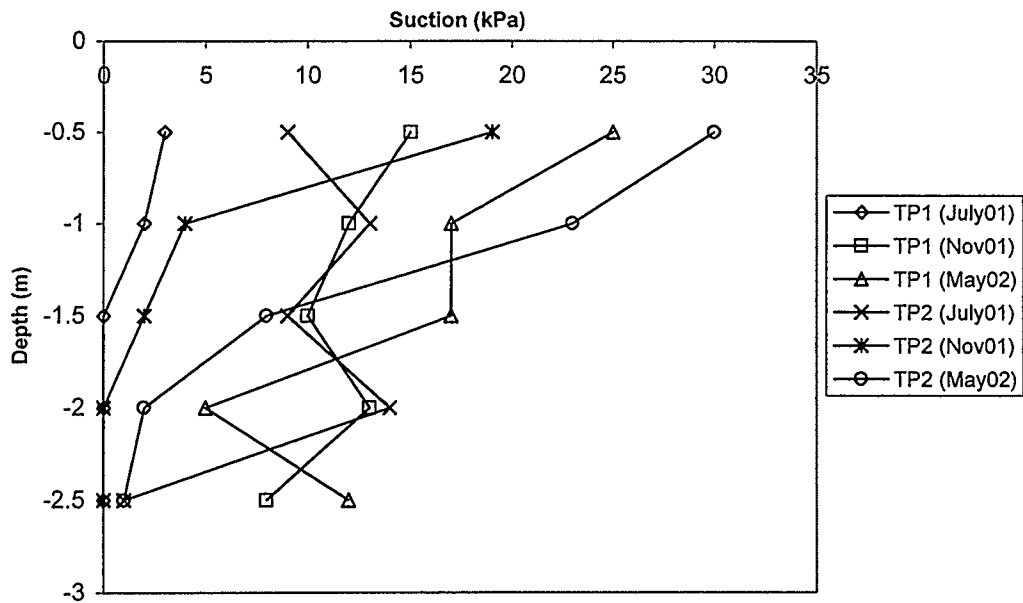


Figure 5-11: Soil suction profile in UC site

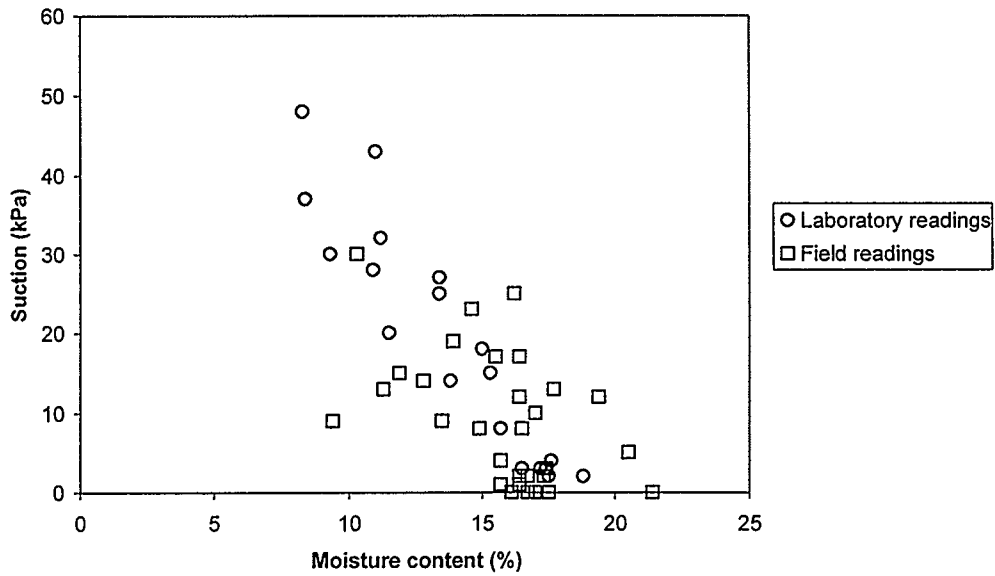


Figure 5-12: Comparison of laboratory and field suction readings in UC Site

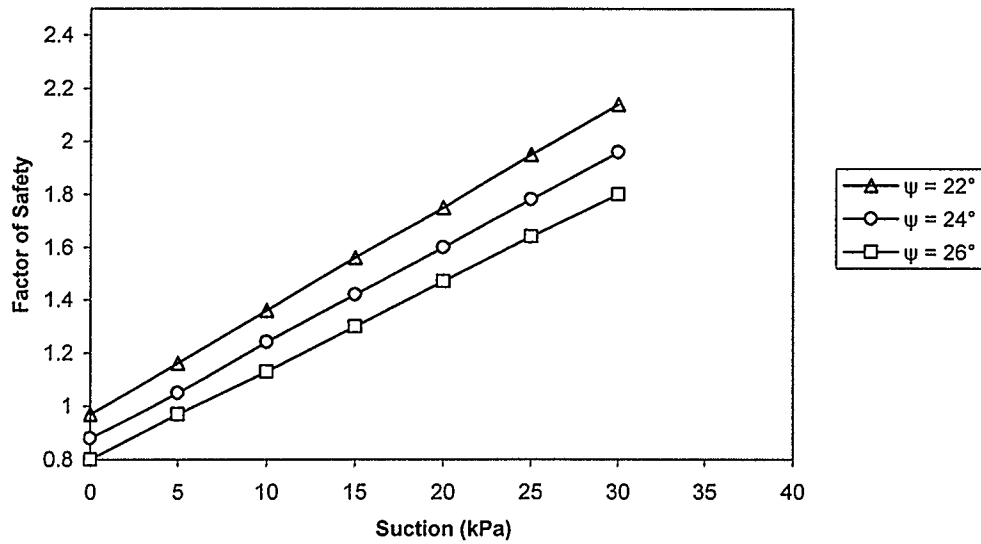


Figure 5-13: Factors of safety with slope angle (ψ) ranging from 22-26°

CHAPTER 6: CONCLUSIONS AND RECOMMENDATION FOR FUTURE WORK

6.1 Conclusions

The objective of this research is to perform laboratory testing on disturbed samples of three soils to determine shear and compressive stiffness and strength parameters and correlate these parameters with measurable parameters to calculate stiffness and strength. Through a series of direct shear box and triaxial compression tests, the parameters, matric suction ($u_a - u_w$) are found to be more influential on stiffness and strength than net confining stress ($\sigma - u_a$). Shear stiffness, shear strength, compressive stiffness, and compressive strength equations are developed in terms of matric suction and net confining stress with two void ratio ranges (e) and three clay contents. The parameters void ratio and clay contents, which govern the physical properties of the soils, also show their effects on stiffness and strength, despite no numerical correlation is developed. Note that these equations are designed for shallow slope failure problems with net confining stress values ranging from 10 to 100 kPa as demonstrated in a case study in Chapter 5.

The qualities of the proposed stiffness and strength equations are expressed as coefficients of determination (R^2) and shown in Tables 3-2 and 4-2. Most of the equations have reliable R^2 values in the range of 0.50 to 1.00. More test data are required for the equations with R^2 values less than 0.50 before qualitative equations can be developed. These equations are equation (3.9), (3.18), (4.5), (4.12), and (4.13). More triaxial compression tests are also required for the UC Site soil with void ratio less than 0.406 as equations (4.9) and (4.15) were derived with insufficient test data and no R^2 value can be determined. Equation (3.15) has a relatively reliable R^2 value of 0.91 and is used in the slope stability analyses in Chapter 5.

Chapter 5 presents a case study at an existing area of shallow slope slides on Sunnyside Hill, Calgary. Slope stability analyses are carried out by using the soil suction measurements obtained at this site and inputting the data into equation (3.15) to calculate the resisting forces in equation (5.1) and in turn, the factors of safety. From the stability analyses, the factors of safety, approach and drop below 1.0 when soil suction decreases to 5 kPa or lower. By comparing the field soil suction measurements from 2001 to 2002 and correlating them to the precipitation records from 1997 to 2002, it is concluded that the increase in soil moisture content and the corresponding reduction of soil suction is the cause of shallow slope slides on Sunnyside Hill in 1997 and 1998. From the soil suction measurements in the two test pits in UC Site, it is found that vegetation could be a mean to prevent the reduction of soil suction near the slope surface.

The proposed stiffness and strength equations (equations (3.6) to (3.11), equations (3.13) to (3.18) and equations (4.4) to (4.15)) determine the relationships among the unknown force components, $R_{(n-1,n)}$, $R_{(n, n+1)}$, F_n , and N_n' , in equations (2.1) to (2.6). With the findings of these unknown force components, the equilibrium equations of Wong's landslide model may be used to characterize the movement of soil mass in shallow landslides during the failure process.

6.2 Recommendation for Future Work

The behaviors of slider block-basal and interslice springs are examined by direct shear box and triaxial compression tests in this study. Some of the proposed equations require additional experiment data to improve the qualities. Similar experiments on other soils types are recommended to establish similar stiffness and strength equations for use in slope stability analysis using this method.

The slider-block model for analysis of shallow slope slides on Sunnyside Hill has been shown to estimate slope stability. This study has defined the shear stiffness and shear

strength parameters for the soils in the slopes. Further, this study has found shallow slope slides occur as soil suction values are near or below 5 kPa. The City of Calgary could install soil suction monitoring system at slopes areas nearest residential housing and slopes with potential stability problems. System monitoring allows for detection of soil suction values approaching 5 kPa, and thus the warning to do more visual monitoring and take other actions to protect those using the slopes and nearby property at the base of the slopes.

The reduction of soil suction can be controlled by landscaping topsoil and grass, plant trees and shrubs with deep and shallow root systems on potential failure slopes, which is proven to be effective from the soil suction measurements in UC Site. The use of vegetation on slopes act as a reinforcing system to increases shear strength and most importantly, to maintain the soil suction values near the slope surface due to evapotranspiration. The stability of a steep fine-grained soil slope could also conceivably be maintained by covering the slope with an impermeable membrane or installing trench drains and collector drain to collect and convey the seepage away from the hillside. This would prevent the infiltration and absorption of moisture and prevent the consequential loss of suction. The effectiveness of these methods would require some future works to confirm.

It is recommended to install some practical monitoring systems for slope movement such as slope indicator, and compare the practical data to the results from the landslide model using the proposed equations in this study.

It is also recommended to conduct undrained direct shear box and triaxial compression tests, and measure the change of pore pressure during the tests as some shallow slope instability problems may relate to both soil suction and pore pressure.

REFERENCES

- Aitchison, G.D. (1961), 'The Quantitative Description of the Stress-Deformation Behavior of Expansive Soils-Preface to Set of Papers', Proc. 3rd International Conference Expansive Soils (Haifa, Israel), Volume 2, pp. 79-82.
- Anderson, M.G. and Richards, K.S. (1987), 'Modeling slope stability: the complimentary nature of geotechnical and geomorphological approaches', Slope Stability, John Wiley & Sons, Inc., pp. 1-9.
- Biot, M.A. (1941), 'General Theory of Three-Dimensional Consolidation', Journal of Applied Physics, Volume 12, No. 2, pp. 155-164.
- Bishop, A.W. (1959), 'The Principle of Effective Stress', Lecture delivered in Oslo, Norway, 1955, published in Teknisk Ukeblad, Volume 106, No. 39, pp. 859-863.
- Chau, K.T. and Wong, R.C.K. (2003), 'A non-linear slider-block model for modelling landslides', International Workshop on Prediction and Simulation Methods in Geomechanics, Athens, Greece, 14-15, October, 2003.
- Dorsey, N.E. (1940), 'Properties of Ordinary Water-Substances', American Chemical Society, Mono. Series, New York: Reinhold, p.673.
- Escario, V. and Sáez, J. (1986), 'The Shear Strength of Partly Saturated Soils', Geotechnique, Volume 36, No. 3, pp. 453-456.
- Fredlund, D.G., (1996), 'Microcomputers and Saturated/Unsaturated Continuum Modelling in Geotechnical Engineering', Symposium on Computers in Geotechnical Engineering, INFOGEO 96, Sao Paulo, Brazil, August 28-30, Volume 2, pp. 29-50.
- Fredlund, D.G. and Morgenstern, N.R. (1977), 'Stress State Variables For Unsaturated Soils', Journal of the Geotechnical Engineering Division, Volume 103, May 1977, pp. 447-466.
- Fredlund, D.G. and Rahardjo, H. (1993), 'Soil Mechanics For Unsaturated Soils', John Wiley & Sons, Inc., pp. 14, 15, 38-49, 64-70, 227-229.

- Fredlund, M.D., Fredlund, D.G., and Wilson, G.W. (1997), 'Prediction of the Soil-Water Characteristic Curve from Grain-Size Distribution and Volume-Mass Properties', 3rd Brazilian Symposium on Unsaturated Soils, Rio de Janeiro, Brazil, April 22-25, 1997, pp. 1-12.
- Gan, J.K.M. (1986), 'Direct Shear Strength Testing of Unsaturated Soils', M.Sc. thesis, Department of Civil Engineering, University of Saskatchewan, Saskatoon, Sask., Canada, p. 587.
- Hardy, R.M. (1963), 'Final Report - Stabilization of Sunnyside Hill, Calgary, Alberta', Report submitted to the City of Calgary by R.M. Hardy & Associates Ltd., December 1963.
- Hardy, R.M., Clark, J.I., and Stepanek, M. (1980), 'A Summary of Case Histories Spanning 30 Years of Slope Stabilization in Calgary, Alberta', Special Conference on Slope Stability Problems in Urban Areas, Canadian Geotechnical Society, National Research Council, Toronto, Ontario.
- Holtz, R.D. and Kovacs W.D. (1981), 'An Introduction to Geotechnical Engineering', Prentice Hall, pp. 463-465.
- Iverson, R.M. (1986), 'Dynamics of slow landslides: a theory for time-dependent behavior', Hillslope Processes. Abrahams, A. (ed.), George Allen & Unwin, London, pp. 297-317.
- Janbu, N. (1963), 'Soil Compressibility as Determined by Oedometer and Triaxial Tests', European Conference on Soil Mechanics & Foundations Engineering, Wiesbaden, Germany, Volume 1, 1963, pp.19-25.
- Mahmoud, M. and Burwash, W.J. (1997), 'Stability of Sunnyside Hill in Calgary, Alberta.', Report submitted to the City of Calgary by Golder Associates Ltd., pp. 1-5.
- Mahmoud, M. and Burwash, W.J. (1998), 'Assessment of Stability of Sunnyside Hill in N.W. Calgary, Alberta.' Geology and Engineering Geology in Southern Alberta Calgary Geotechnical Society Seminar, Calgary, Canada, 1998, pp. 1-7.
- Material Testing Laboratories Ltd. (1964), 'Instability – West Sunnyside Hill.', Report submitted to the City of Calgary by Material Testing Laboratories Ltd., pp. 1-5.

- Meyboom (1961), 'Groundwater Resources of the City of Calgary and Vicinity.' Research Council of Alberta, Bulletin No. 8.
- Moran, S.R. (1986), 'Surficial Geology of the Calgary Urban Area.' Alberta Research Council Bulletin no. 53.
- R.M. Hardy & Associates Ltd. (1974), 'Sunnyside Hill Slide, Landscaping and Irrigation, Calgary, Alberta.', Report submitted to the City of Calgary by R.M. Hardy & Associates Ltd., 1974.
- Terzaghi, K. (1936), 'The Shear Resistance of Saturated Soils', in Proc. 1st International Conference Soil Mechanics for Foundation Engineering (Cambridge, MA), Volume 1, pp. 54-56.
- Yam, E. (2005), 'Numerical modelling of movement in shallow landslides due to suction loss and softening', MEng thesis, in preparation, Department of Civil Engineering, The University of Calgary, Calgary, Alberta.

Appendix A: Soil compaction curves results

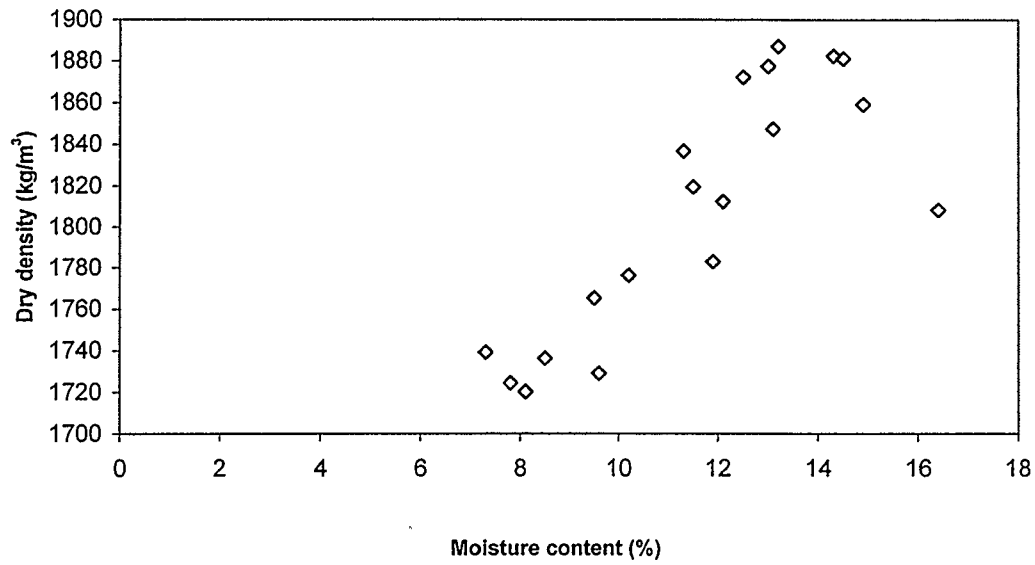


Figure A-1: Density curve of Discovery Ridge soil sample

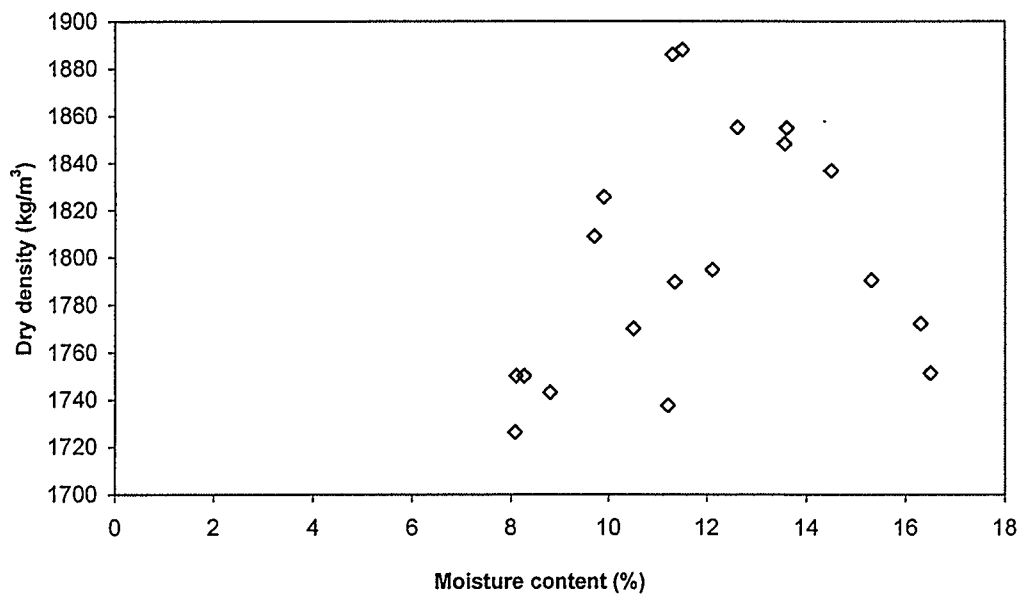


Figure A-2: Density curve of Sunnyside Hill soil sample

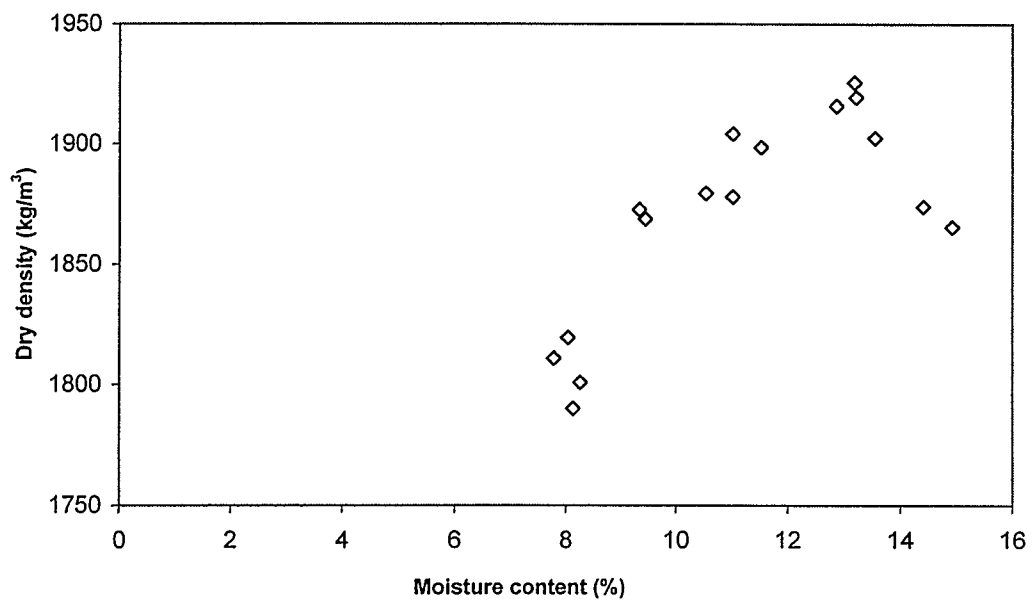


Figure A-3: Density curve of UC Site soil sample

Appendix B: Raw data of direct shear box tests

Summary of Data from Shear Box Tests

Normal stresses	Discovery Ridge				Sunnyside Hill				UC site			
	100kPa	50kPa	30kPa	10kPa	100kPa	50kPa	30kPa	10kPa	100kPa	50kPa	30kPa	10kPa
Initial tangent loading slope (kPa/mm)												
Test 1	416.7	270	333.3	242.9	350	93.3	225	166.2	192.9	129.5	111.9	106.3
Test 2	214.3	405	222.2	377.8	175	224	144	166.2	135	98.3	90.4	30.9
Test 3	250	192.9	222.2	136	155.6	52.5	55.4	20.8	51.9	21	39.2	17.9
Test 4	187.5	71.1	50	54.4	82.4	11.4	6.2	7.4	17.3	12	5.9	12.1
Test 5	111.1	.	45.5	27.2	12.7	6.6	3.5	2.9	8.1	1.7	3.8	5.3
Stress ratio (peak)												
Test 1	1.609	2.53	3.243	10.17	1.581	1.738	3.233	7.05	1.525	2.266	3.77	13.44
Test 2	1.625	2.852	4.643	11.42	1.43	1.71	2.47	8.42	1.938	2.226	4.16	6.4
Test 3	1.422	2.53	4.347	11.83	1.477	2.056	2.813	5.32	1.25	1.466	2.46	4.16
Test 4	1.313	1.588	1.667	6.17	1.163	0.994	0.987	3.37	0.625	1.12	0.676	3.12
Test 5	1.156	.	1.727	6	0.616	0.428	0.667	1.37	0.313	0.52	0.276	1.68
Stress ratio (residual)												
Test 1	1.313	1.764	2.023	3.08	1.209	1.394	2.05	4.21	1.437	1.814	2.323	5.44
Test 2	1.391	1.676	2.827	3.08	1.291	1.668	1.68	3.53	1.8	1.706	2.53	.
Test 3	1.125	1.676	3.72	4.75	1.36	2	1.68	2.95	.	1.346	.	.
Test 4	1.023	.	.	2.53
Test 5
Saturation												
Test 1	0.478	0.662	0.507	0.483	0.321	0.417	0.443	0.365	0.565	0.484	0.474	0.732
Test 2	0.595	0.895	0.611	0.612	0.674	0.626	0.668	0.586	0.787	0.752	0.725	0.925
Test 3	0.785	0.941	0.867	0.754	0.789	0.847	0.81	0.818	0.935	0.925	0.939	0.928
Test 4	0.934	0.464	0.946	0.938	0.854	0.859	0.855	0.86	0.896	0.921	0.85	0.828
Test 5	0.947	.	0.907	0.94	0.844	0.824	0.821	0.824	0.83	0.822	0.803	0.825
Void ratio												
Test 1	0.51	0.456	0.501	0.51	0.587	0.527	0.514	0.559	0.436	0.46	0.464	0.398
Test 2	0.472	0.406	0.468	0.468	0.421	0.436	0.425	0.452	0.387	0.395	0.398	0.384
Test 3	0.429	0.456	0.425	0.432	0.413	0.444	0.406	0.421	0.391	0.384	0.398	0.429
Test 4	0.406	0.514	0.448	0.421	0.456	0.485	0.48	0.48	0.464	0.44	0.514	0.563
Test 5	0.436	.	0.514	0.406	0.527	0.573	0.568	0.573	0.559	0.554	0.621	0.559
Suction (kPa)												
Test 1	19	20	19	24	34	32	30	38	30	37	48	43
Test 2	8	2	10	13	28	26	20	28	20	32	28	25
Test 3	3	6	11	.	23	21	19	20	14	27	26	18
Test 4	5	6	7	8	15	11	11	10	8	15	3	4
Test 5	3	.	4	5	11	6	4	5	2	3	2	3

**Appendix C: Plots of shear stress versus horizontal displacement for
three soil samples**

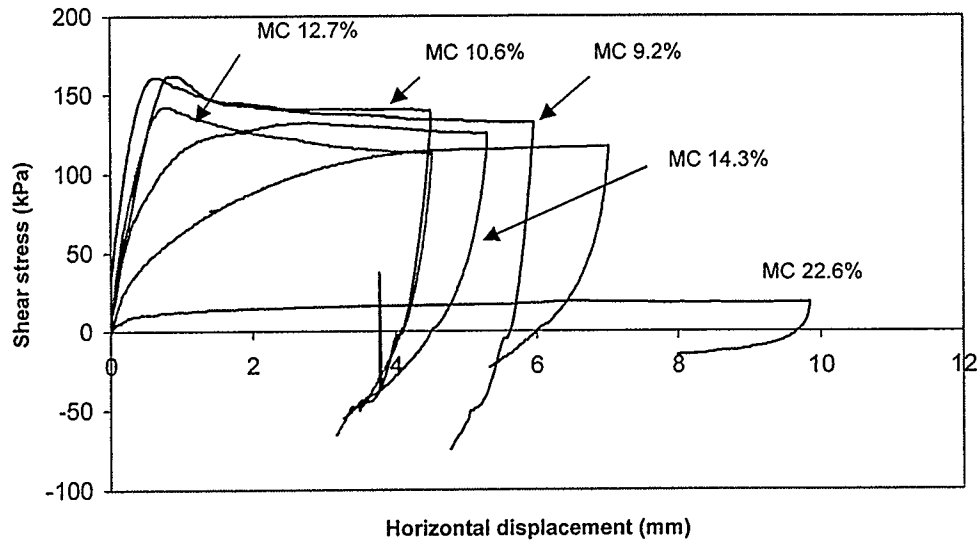


Figure C-1: Shear stress versus horizontal displacement
(Soil sample: Discovery Ridge, Normal stress 100 kPa)

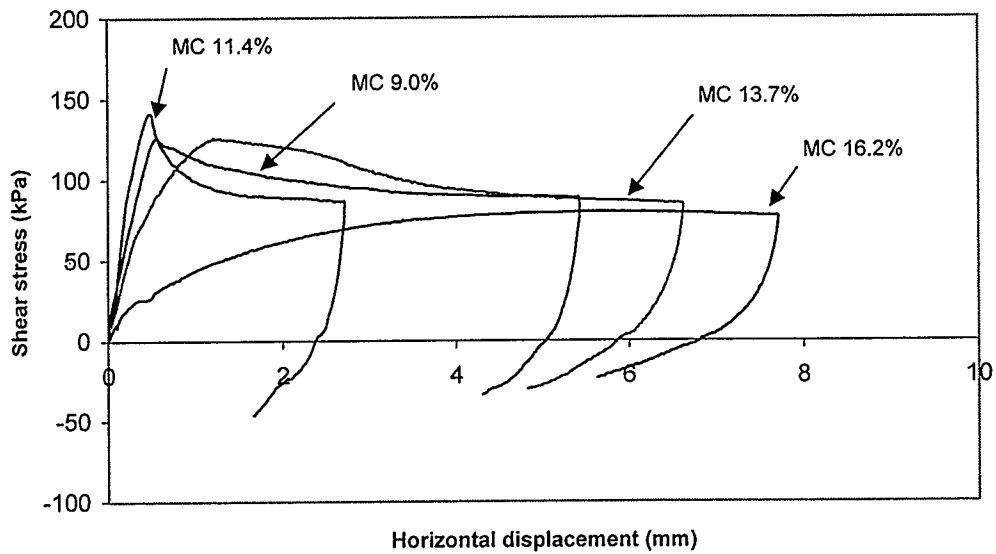


Figure C-2: Shear stress versus horizontal displacement
(Soil sample: Discovery Ridge, Normal stress 50 kPa)

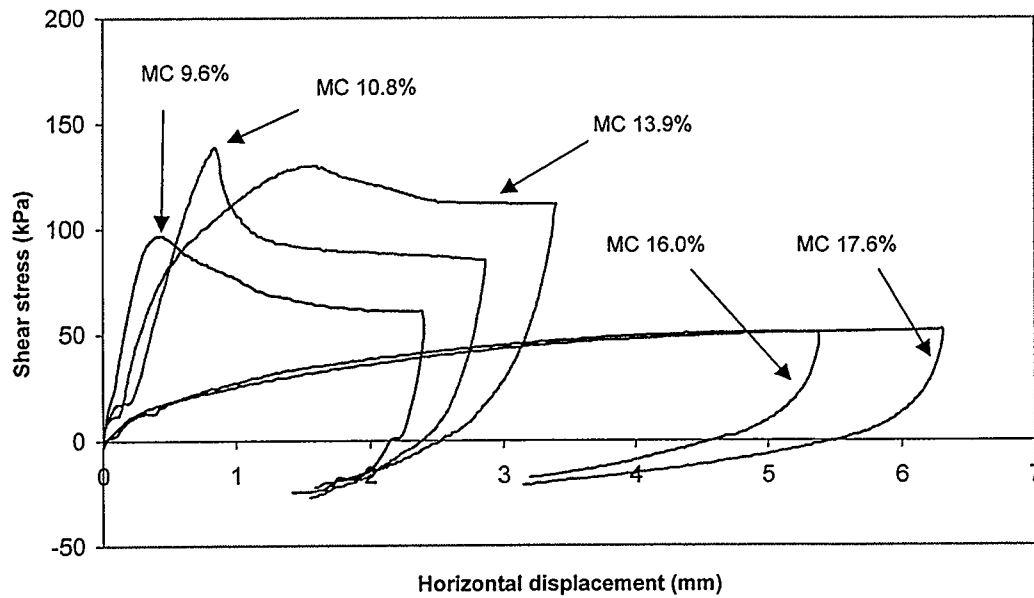


Figure C-3: Shear stress versus horizontal displacement
(Soil sample: Discovery Ridge, Normal stress 30 kPa)

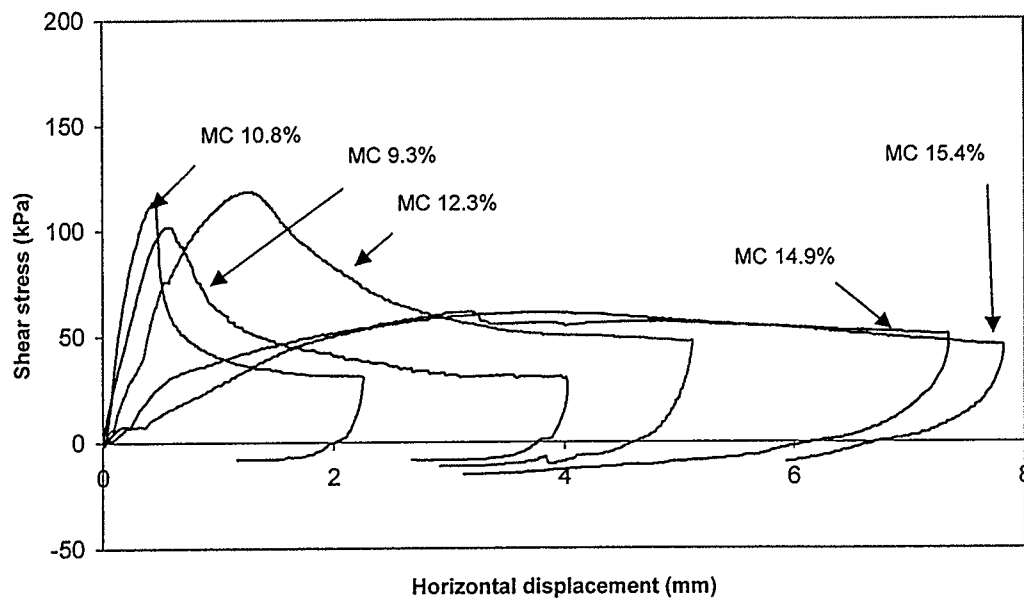


Figure C-4: Shear stress versus horizontal displacement
(Soil sample: Discovery Ridge, Normal stress 10 kPa)

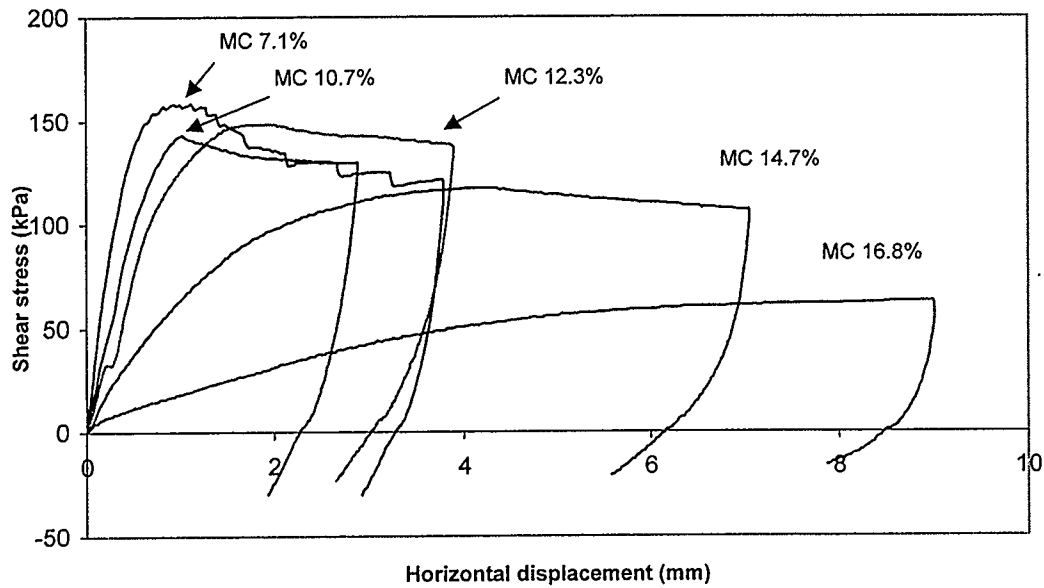


Figure C-5: Shear stress versus horizontal displacement
(Soil sample: Sunnyside Hill, Normal stress 100 kPa)

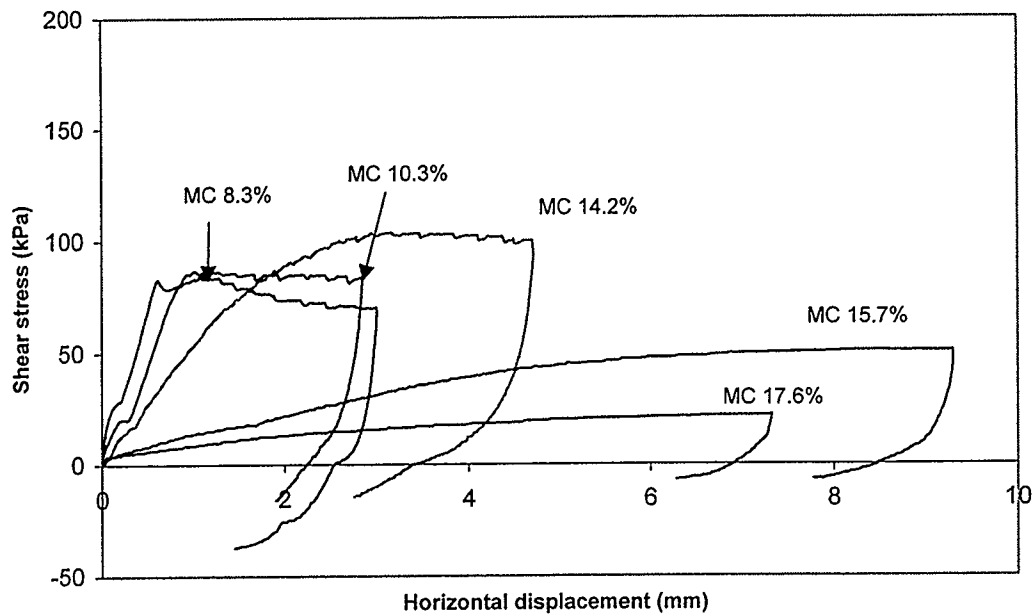


Figure C-6: Shear stress versus horizontal displacement
(Soil sample: Sunnyside Hill, Normal stress 50 kPa)

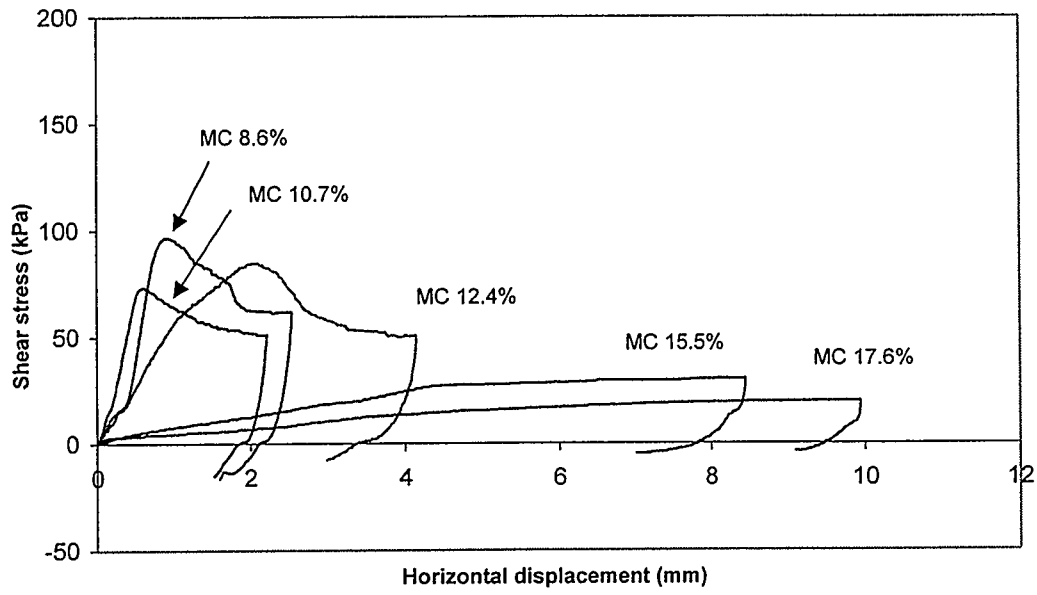


Figure C-7: Shear stress versus horizontal displacement
(Soil sample: Sunnyside Hill, Normal stress 30 kPa)

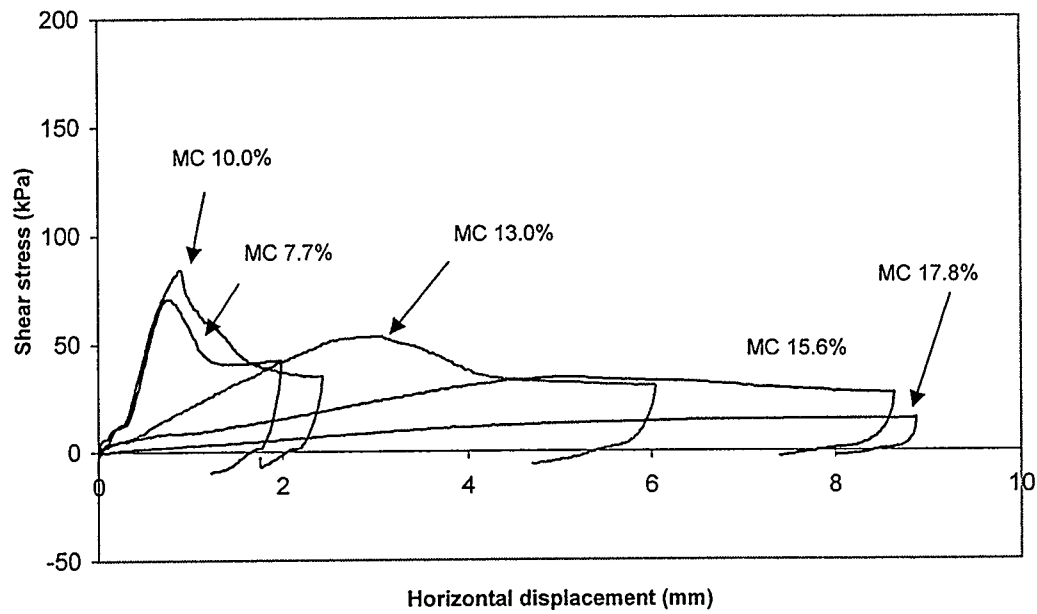


Figure C-8: Shear stress versus horizontal displacement
(Soil sample: Sunnyside Hill, Normal stress 10 kPa)

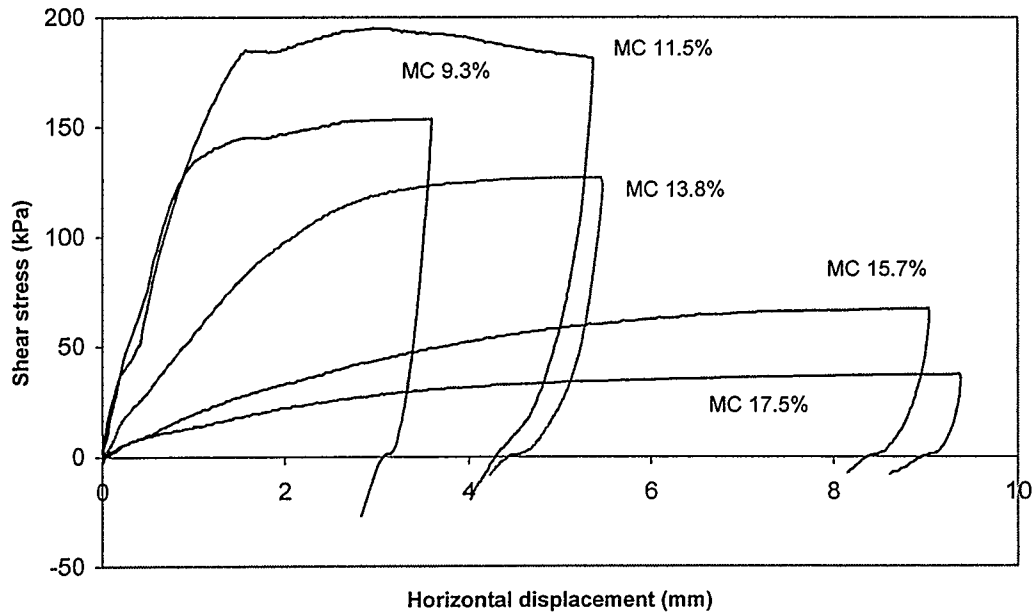


Figure C-9: Shear stress versus horizontal displacement
(Soil sample: UC Site, Normal stress 100 kPa)

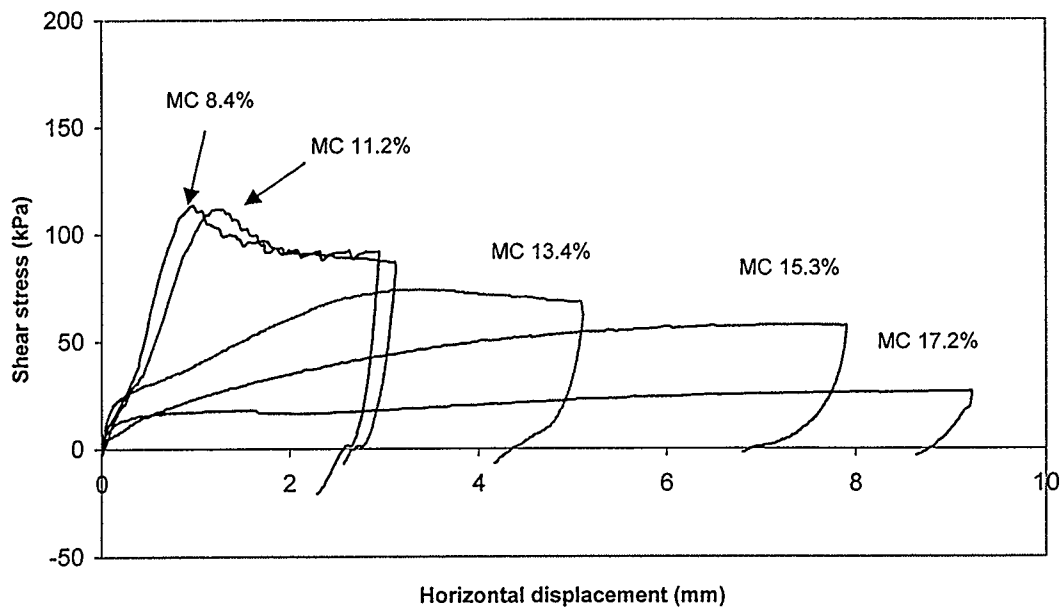


Figure C-10: Shear stress versus horizontal displacement
(Soil sample: UC Site, Normal stress 50 kPa)

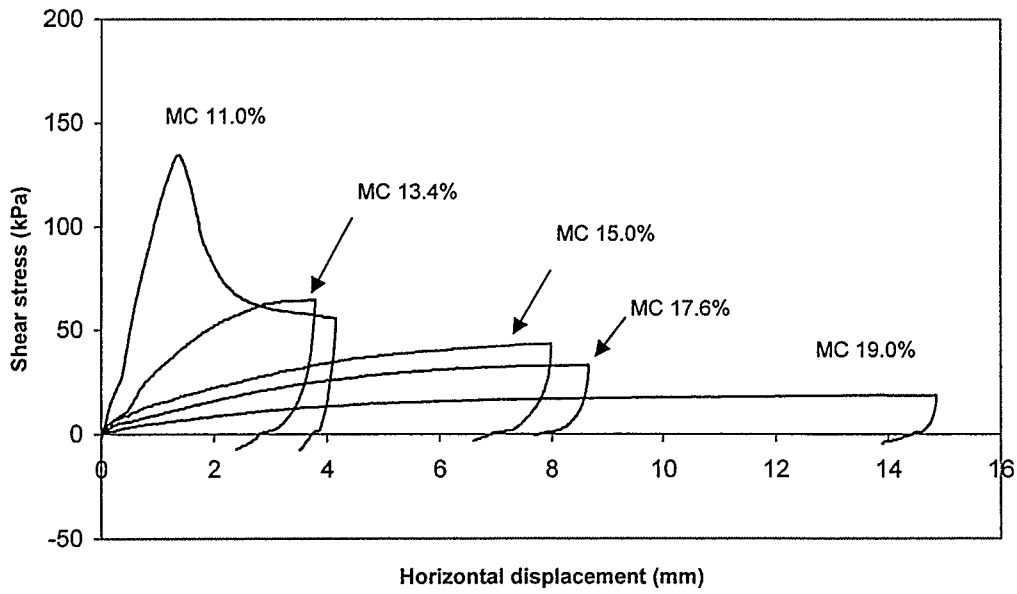


Figure C-11: Shear stress versus horizontal displacement
(Soil sample: UC Site, Normal stress 30 kPa)

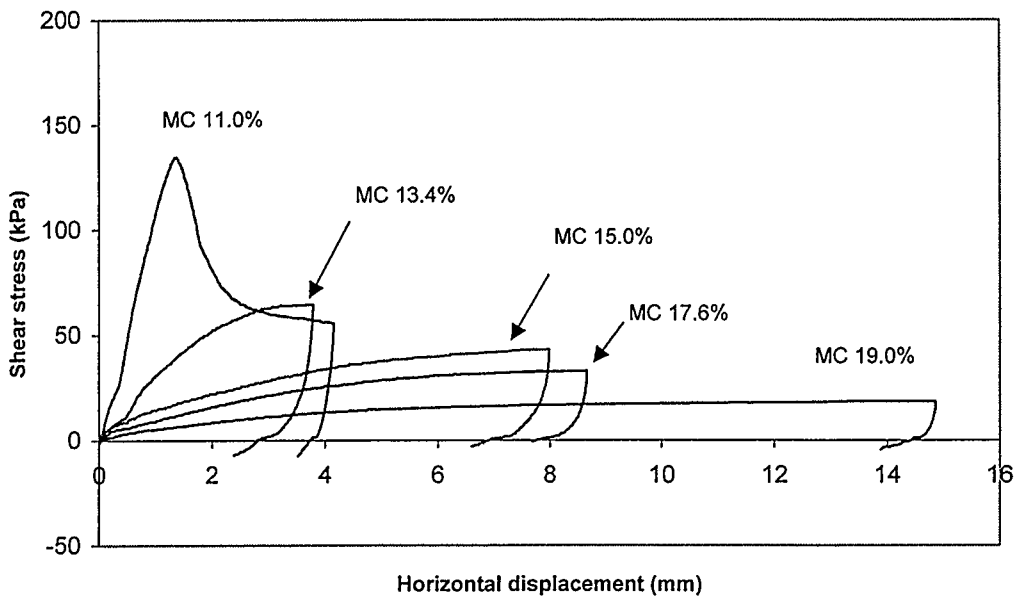


Figure C-12: Shear stress versus horizontal displacement
(Soil sample: UC Site, Normal stress 10 kPa)

Appendix D: Plots of vertical displacement versus horizontal displacement for three soil samples

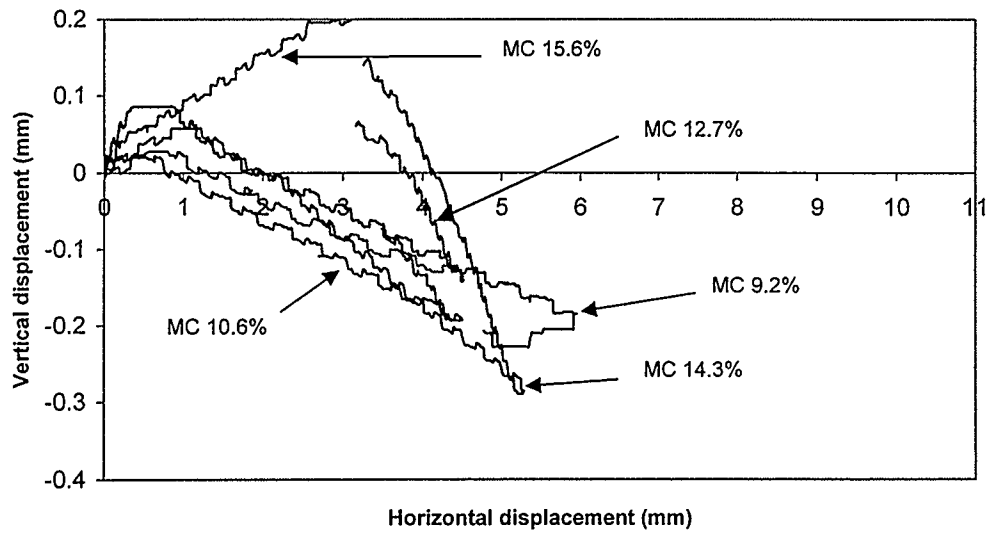


Figure D-1: Vertical versus horizontal displacement
(Soil: Discovery Ridge, Normal stress 100 kPa)

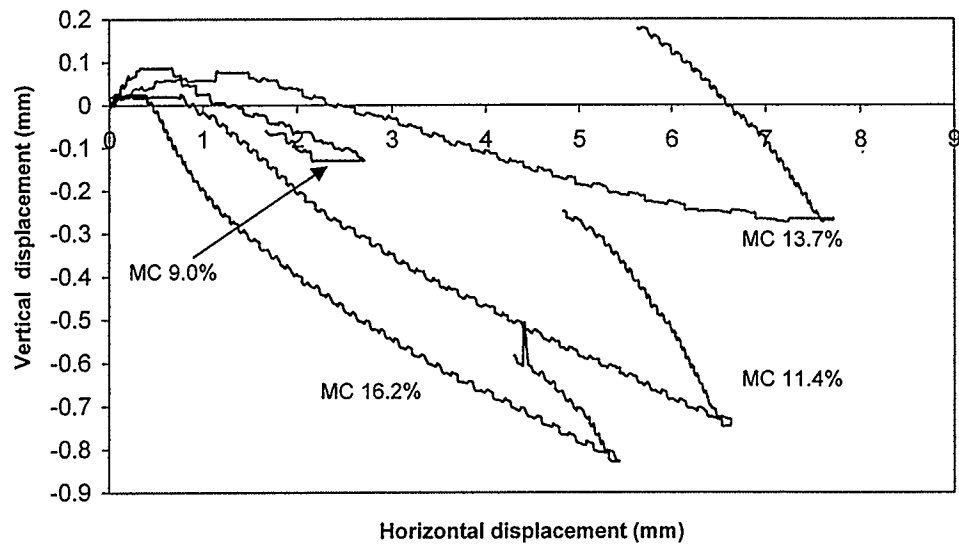


Figure D-2: Vertical versus horizontal displacement
(Soil: Discovery Ridge, Normal stress 50 kPa)

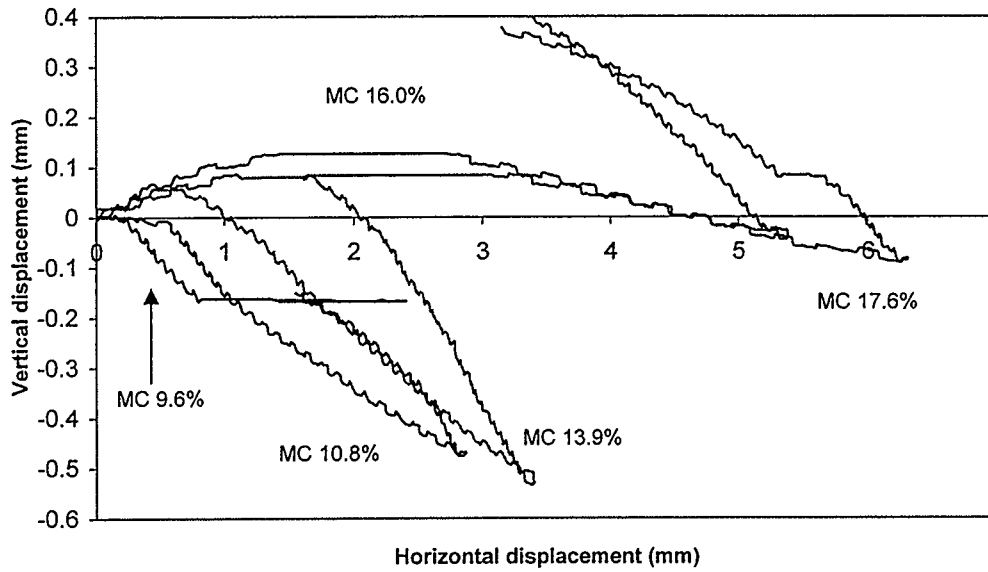


Figure D-3: Vertical versus horizontal displacement
(Soil: Discovery Ridge, Normal stress 30 kPa)

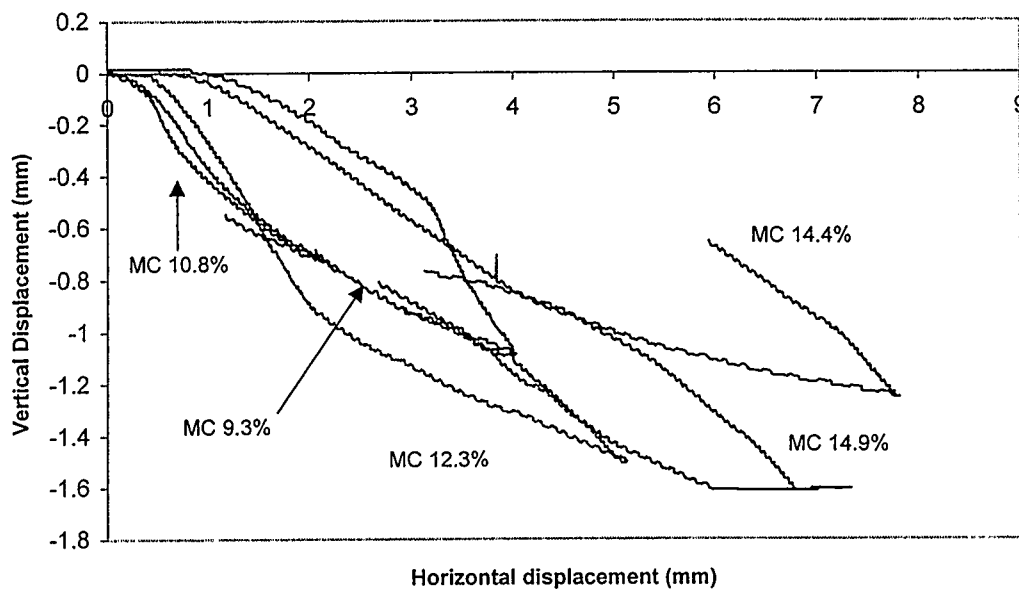


Figure D-4: Vertical versus horizontal displacement
(Soil: Discovery Ridge, Normal stress 10 kPa)

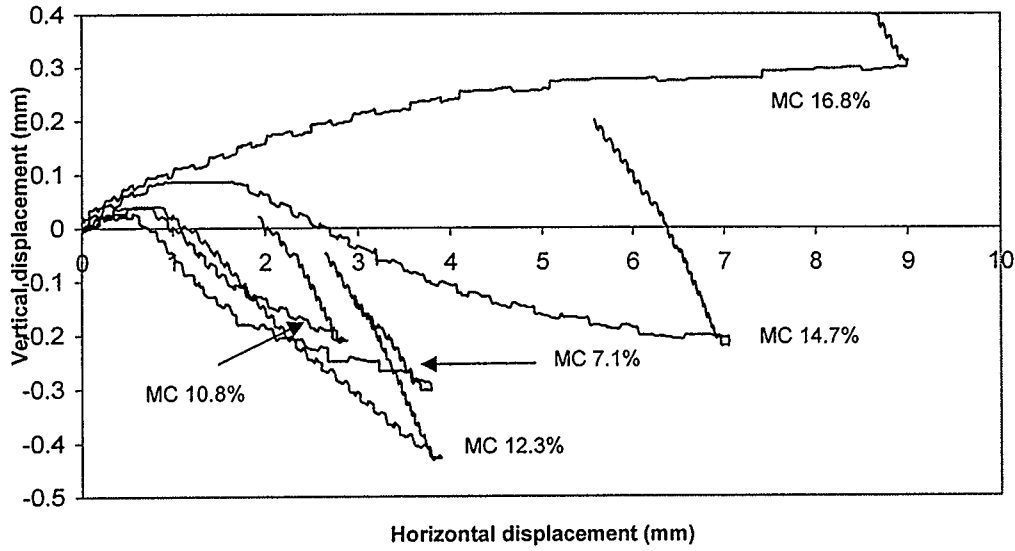


Figure D-5: Vertical versus horizontal displacement
(Soil: Sunnyside Hill, Normal stress 100 kPa)

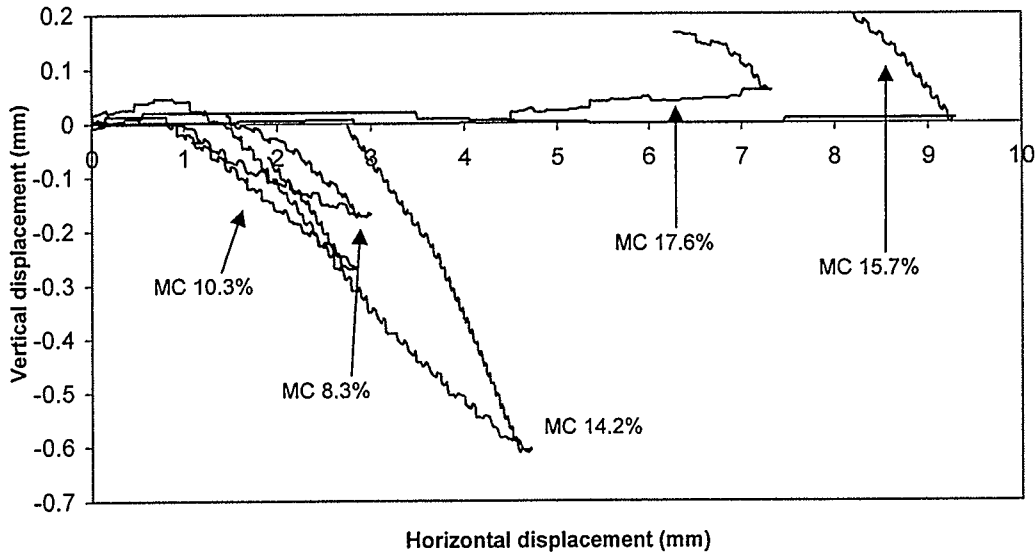


Figure D-6: Vertical versus horizontal displacement
(Soil: Sunnyside Hill, Normal stress 50 kPa)

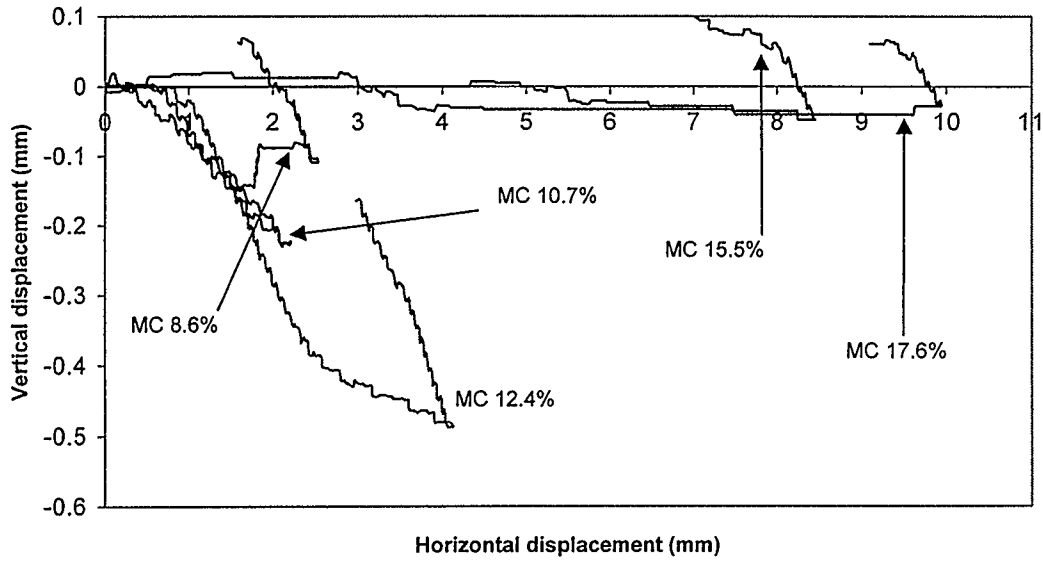


Figure D-7: Vertical versus horizontal displacement
(Soil: Sunnyside Hill, Normal stress 30 kPa)

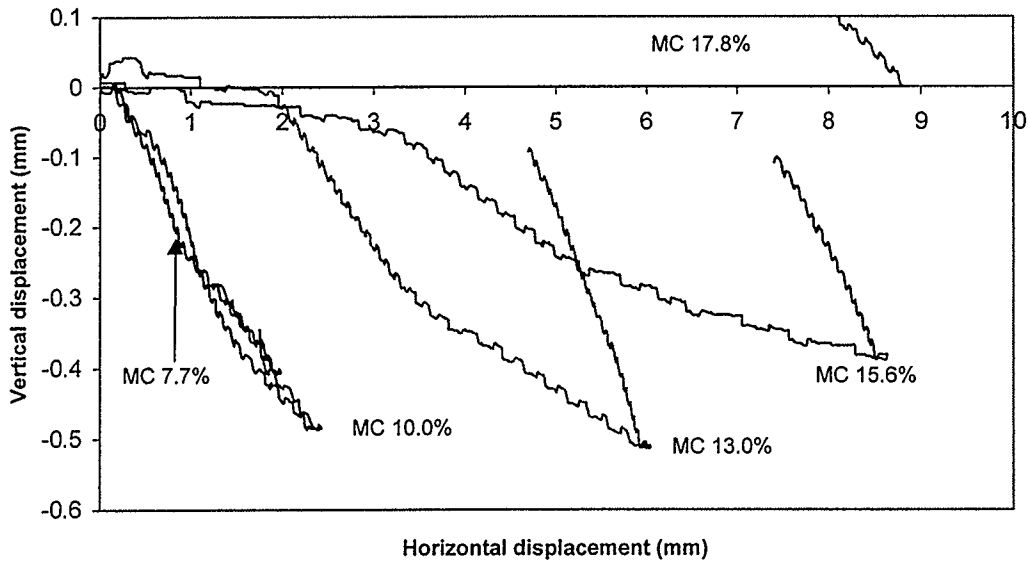


Figure D-8: Vertical versus horizontal displacement
(Soil: Sunnyside Hill, Normal stress 10 kPa)

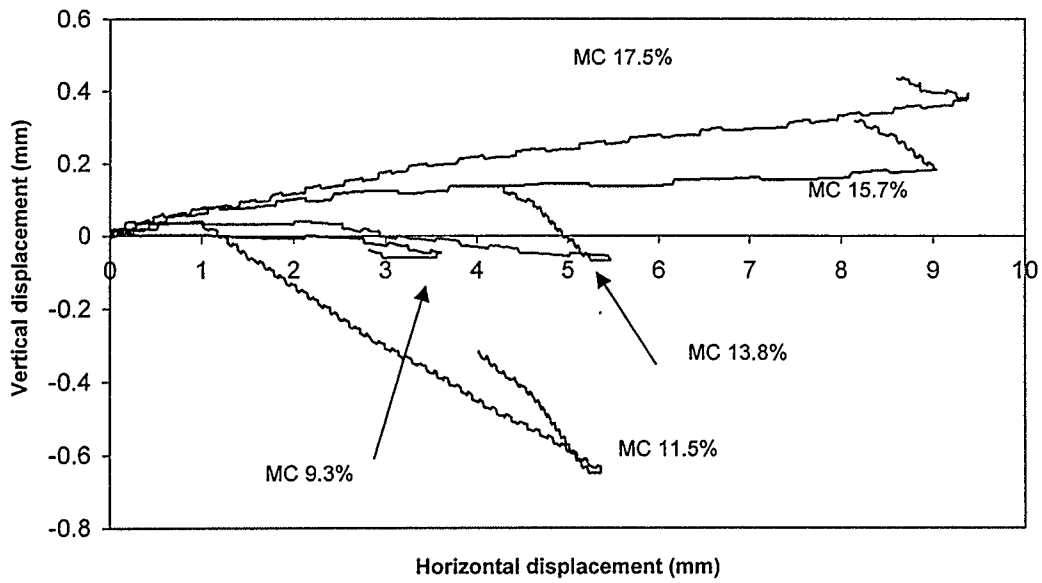


Figure D-9: Vertical versus horizontal displacement
(Soil: UC Site, Normal stress 100 kPa)

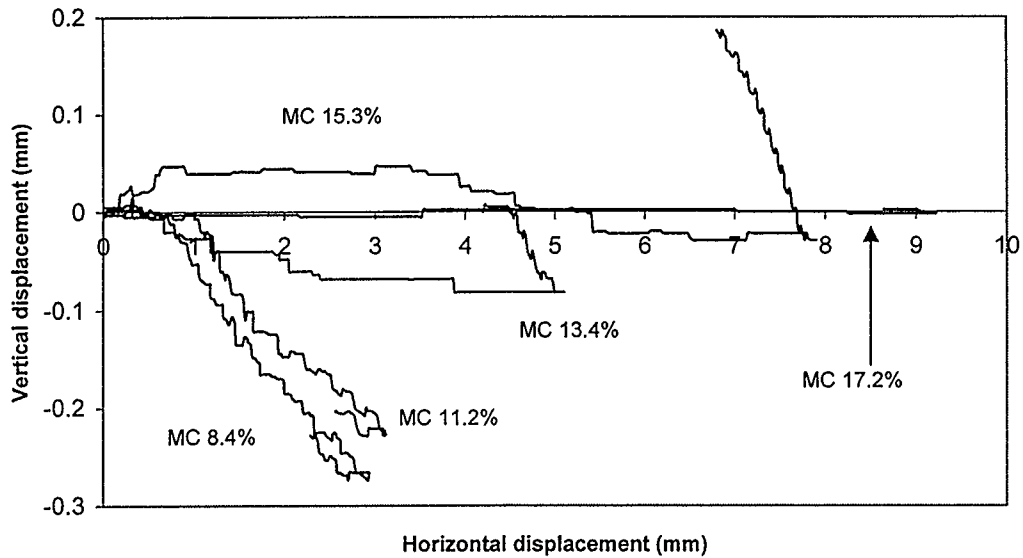


Figure D-10: Vertical versus horizontal displacement
(Soil: UC Site, Normal stress 50 kPa)

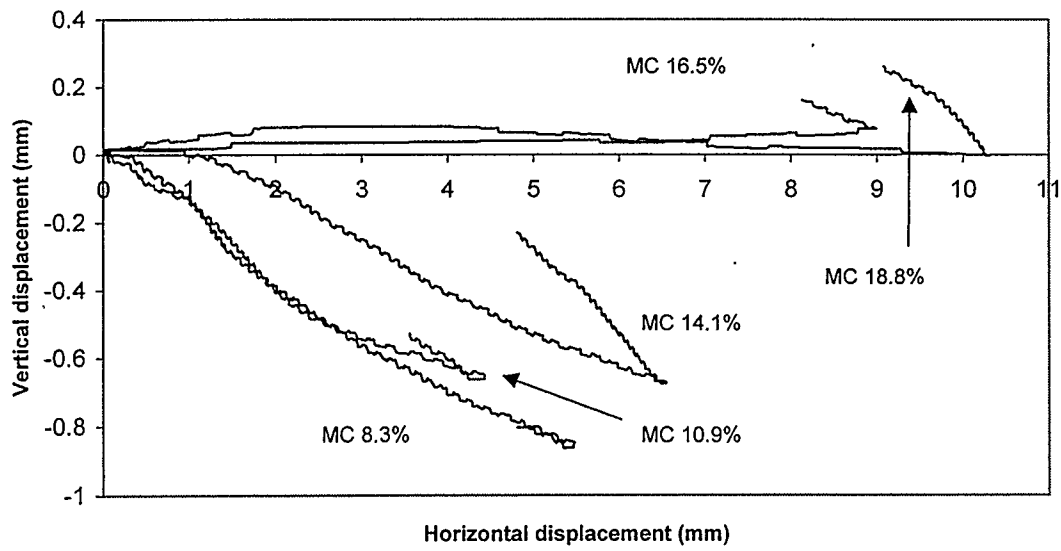


Figure D-11: Vertical versus horizontal displacement
(Soil: UC Site, Normal stress 30 kPa)

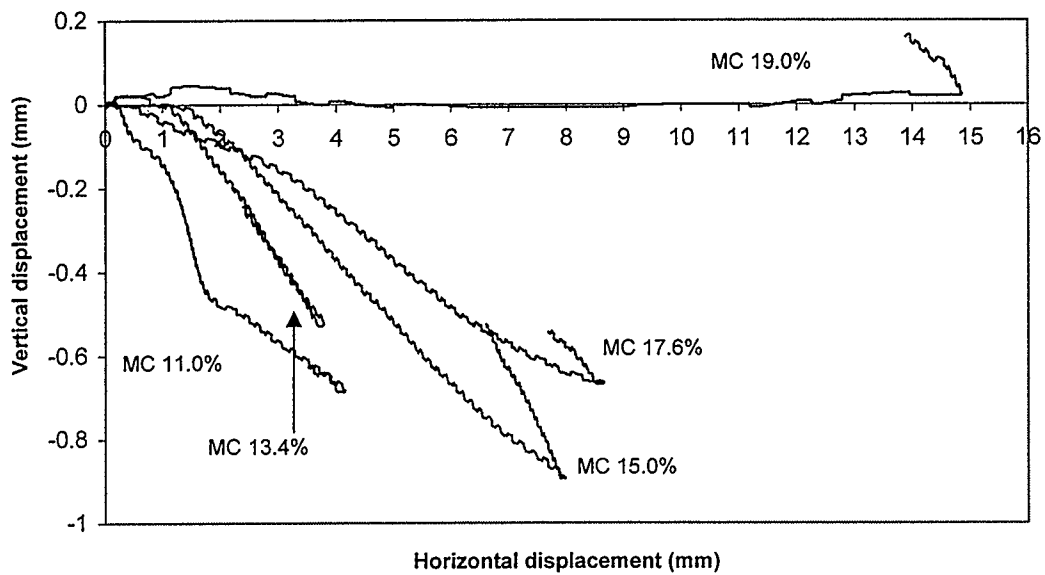


Figure D-12: Vertical versus horizontal displacement
(Soil: UC Site, Normal stress 10 kPa)

Appendix E: Raw data of triaxial compression tests

Summary of Data from Triaxial Test

Net confining Stresses	Discovery Ridge				Sunnyside Hill				UC site			
	100kPa	50kPa	30kPa	10kPa	100kPa	50kPa	30kPa	10kPa	100kPa	50kPa	30kPa	10kPa
Initial tangent loading slope (kPa/mm)												
Test 1	259.3	208.3	178.6	116.7	333.3	285.7	238.1	200	266.7	333.3	238.1	250
Test 2	250	185.2	192.3	181.8	250	193.5	131.6	178.6	181.8	263.2	200	151.2
Test 3	156.3	151.2	294.1	125	125	58.8	38	131.4	46.9	100	46.2	63.6
Test 4	93.8	34.5	47.6	100	11.7	9.7	19.2	100	6.9	13.8	20	25.8
Test 5	43.5	8.5	19.4	13.8	3.75	2	6.7	30	1.6	6.2	7.5	7.3
Stress ratio (peak)												
Test 1	4.35	7	10.3	19	4.4	7.7	10.8	26.5	4.3	8	10.8	35
Test 2	3.83	6.9	12.2	26.3	3.65	6	8.7	26.7	3.15	7.6	10	27.7
Test 3	2.92	5.4	12.8	25.7	3	4.2	5.9	22.6	1.55	5.1	5.1	16
Test 4	1.78	3.4	4.3	16.6	1.15	2	4.5	21.2	0.65	2.2	3.8	13.8
Test 5	1.12	1.6	2.4	8.2	0.55	0.7	2.3	13.5	0.35	1	1.6	6.3
Unloading slope (kPa/mm)												
Test 1	555.6	555.6	487.8	200	566	500	461.5	151.5	454.5	500	555.5	215.1
Test 2	555.6	526.3	454.5	285.7	566	500	394.9	238.1	454.5	500	555.5	416.7
Test 3	480.8	444.4	588.2	296.3	333.3	500	394.9	200	373.1	400	300	250
Test 4	347.2	363.6	312.5	242.4	312.5	322.6	394.9	236.2	219.6	333.3	300	317.5
Test 5	373.1	300	222.2	222.2	333.3	500	235.3	238.1	333.3	400	300	285.7
Saturation												
Test 1	0.427	0.4	0.349	0.379	0.465	0.397	0.417	0.397	0.543	0.445	0.455	0.427
Test 2	0.553	0.584	0.507	0.498	0.554	0.58	0.731	0.649	0.724	0.565	0.725	0.576
Test 3	0.657	0.674	0.716	0.728	0.744	0.731	0.807	0.725	0.922	0.732	0.787	0.85
Test 4	0.846	0.826	0.84	0.773	0.833	0.85	0.833	0.783	0.954	0.92	0.92	0.908
Test 5	0.947	0.934	0.945	0.946	0.854	0.85	0.859	0.808	0.93	0.94	0.93	0.934
Void ratio												
Test 1	0.527	0.536	0.554	0.545	0.501	0.541	0.527	0.541	0.459	0.476	0.472	0.485
Test 2	0.489	0.476	0.501	0.506	0.464	0.452	0.41	0.429	0.41	0.436	0.398	0.432
Test 3	0.456	0.452	0.44	0.44	0.406	0.41	0.417	0.41	0.379	0.398	0.387	0.38
Test 4	0.413	0.417	0.413	0.429	0.432	0.452	0.432	0.41	0.386	0.38	0.38	0.377
Test 5	0.406	0.406	0.46	0.417	0.506	0.514	0.472	0.413	0.427	0.406	0.425	0.406
Suction (kPa)												
Test 1	32	35	42	37	29	33	32	33	30	49	43	52
Test 2	11	8	16	16	25	26	22	29	24	30	30	31
Test 3	5	7	9	10	24	24	18	23	26	25	22	18
Test 4	7	5	5	7	17	15	16	20	18	22	22	20
Test 5	5	4	2	2	10	9	12	17	9	15	11	10

**Appendix F: Plots of deviator stress versus vertical displacement of
three soil samples**

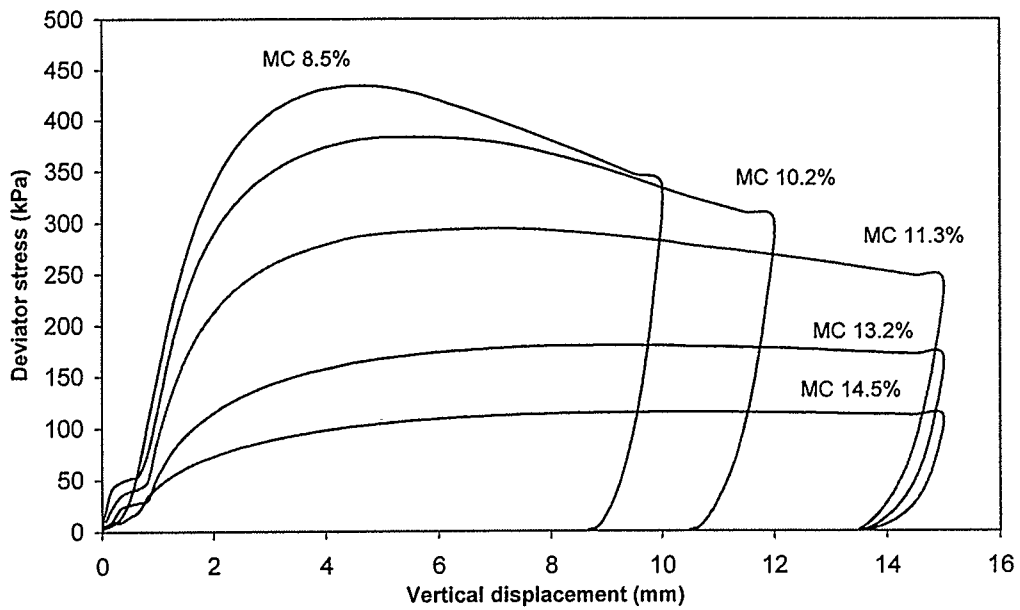


Figure F-1: Deviator stress versus vertical displacement
(Soil sample: Discovery Ridge, Net confining stress 100 kPa)

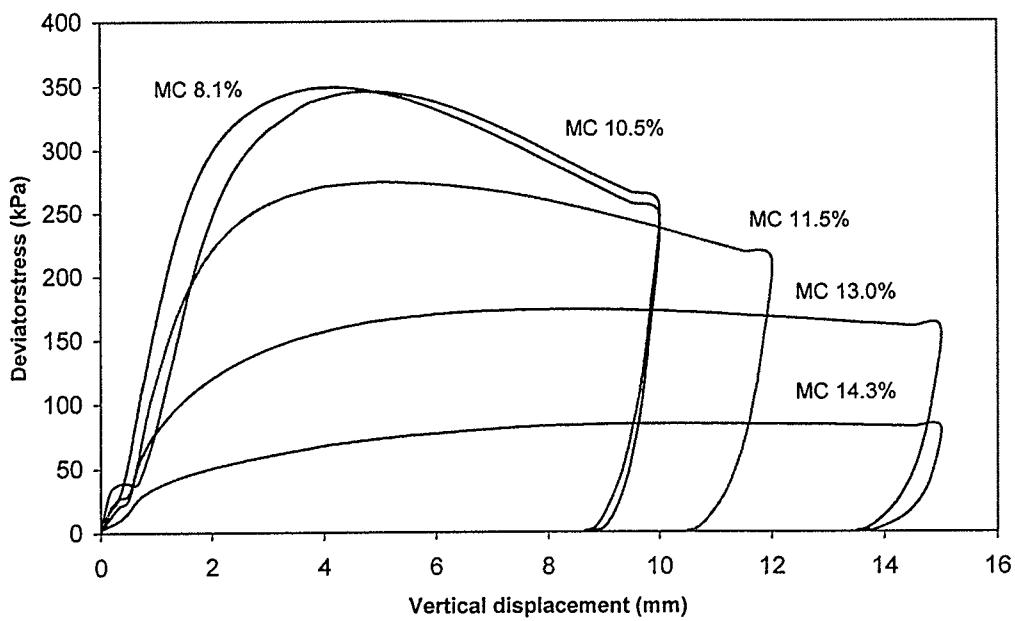


Figure F-2: Deviator stress versus vertical displacement
(Soil sample: Discovery Ridge, Net confining stress 50 kPa)

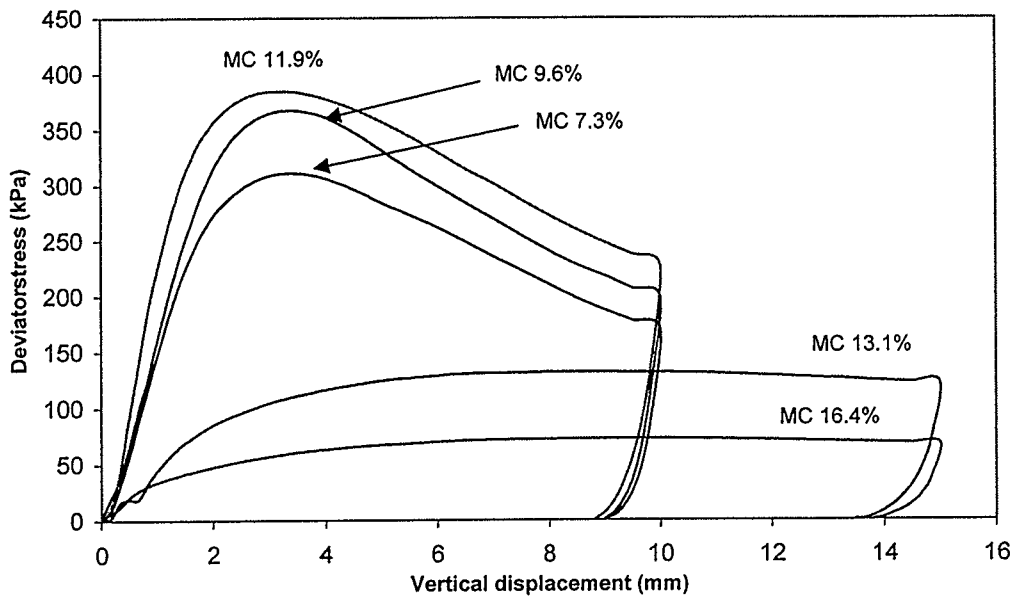


Figure F-3: Deviator stress versus vertical displacement
(Soil sample: Discovery Ridge, Net confining stress 30 kPa)

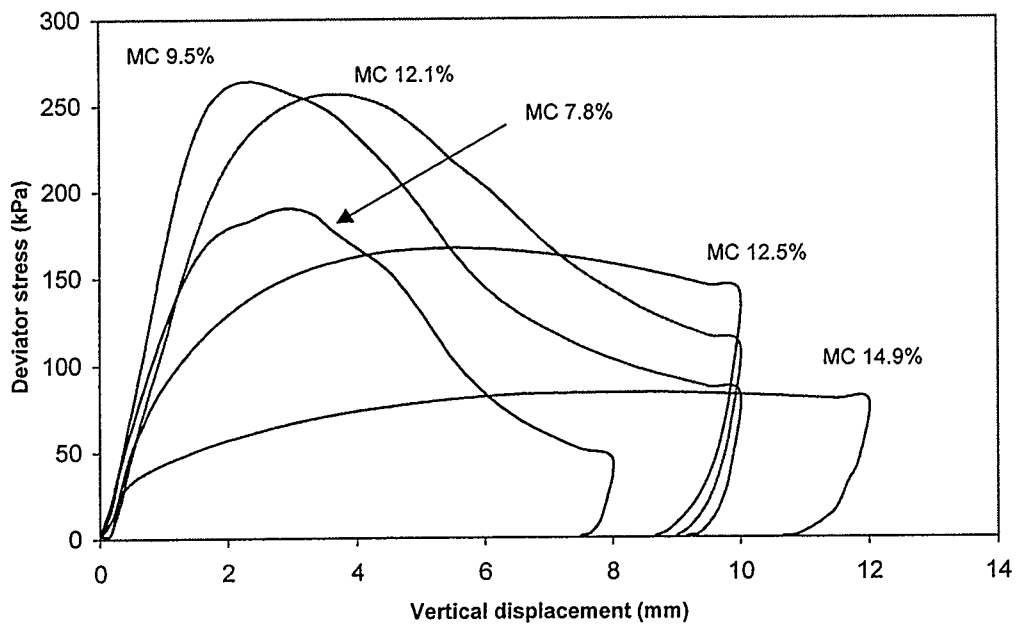


Figure F-4: Deviator stress versus vertical displacement
(Soil sample: Discovery Ridge, Net confining stress 10 kPa)

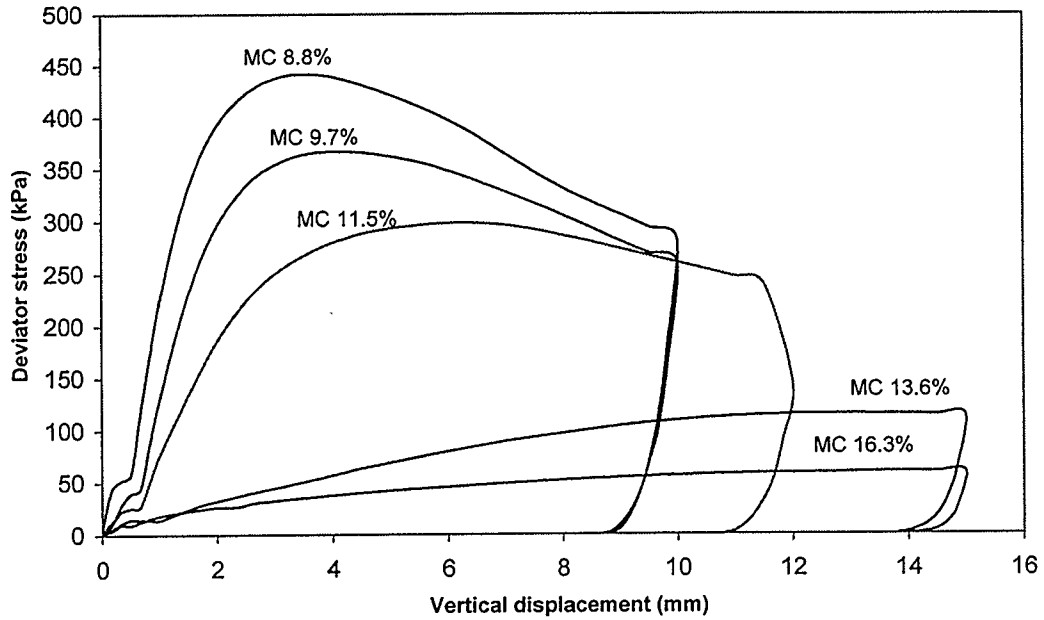


Figure F-5: Deviator stress versus vertical displacement
(Soil sample: Sunnyside Hill, Net confining stress 100 kPa)

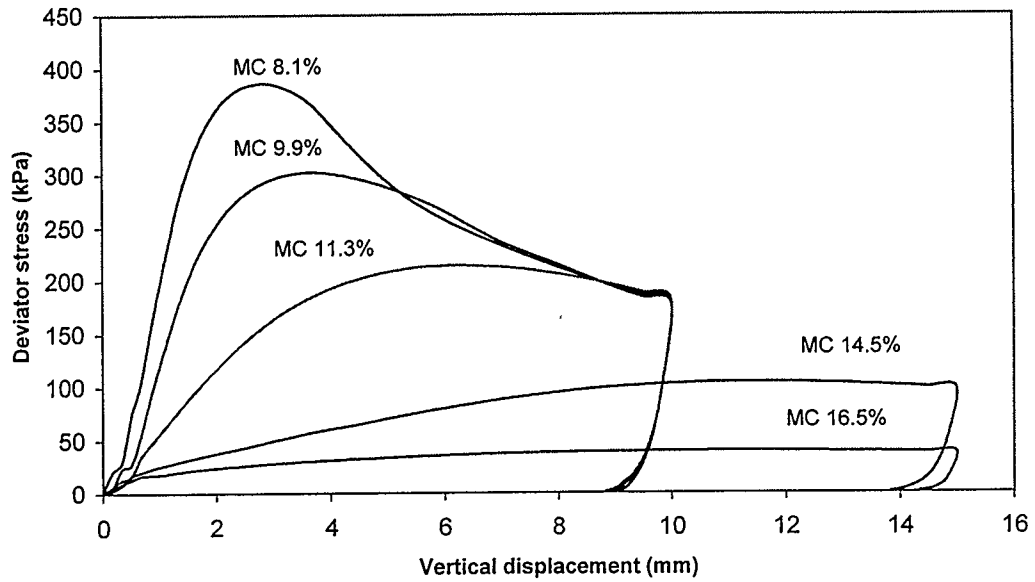


Figure F-6: Deviator stress versus vertical displacement
(Soil sample: Sunnyside Hill, Net confining stress 50 kPa)

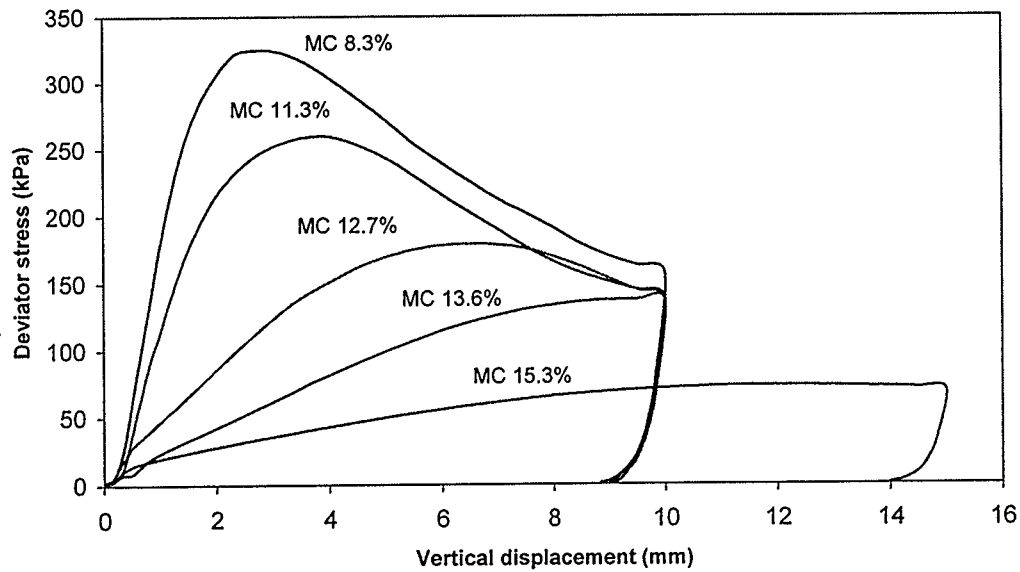


Figure F-7: Deviator stress versus vertical displacement
(Soil sample: Sunnyside Hill, Net confining stress 30 kPa)

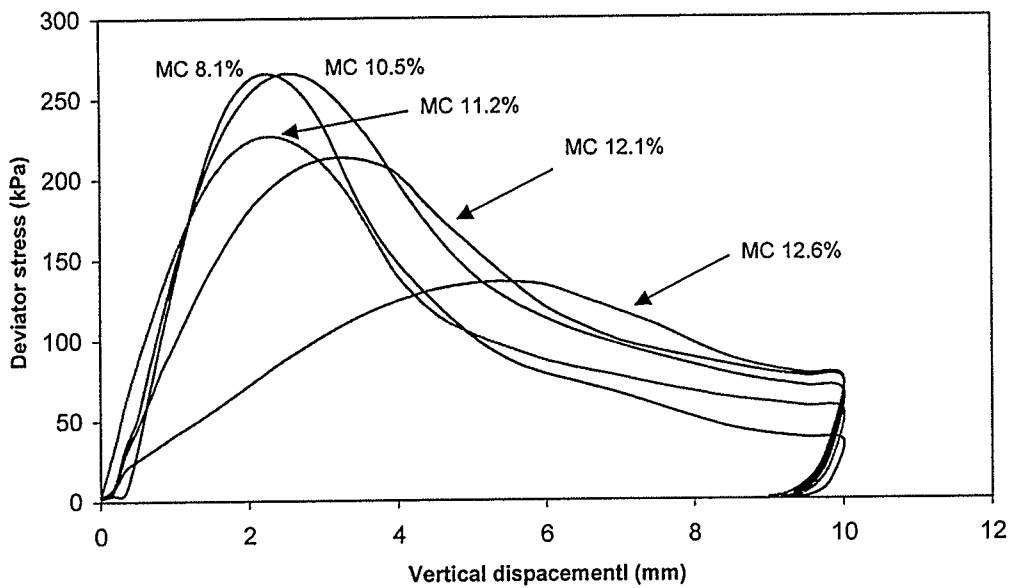


Figure F-8: Deviator stress versus vertical displacement
(Soil sample: Sunnyside Hill, Net confining stress 10 kPa)

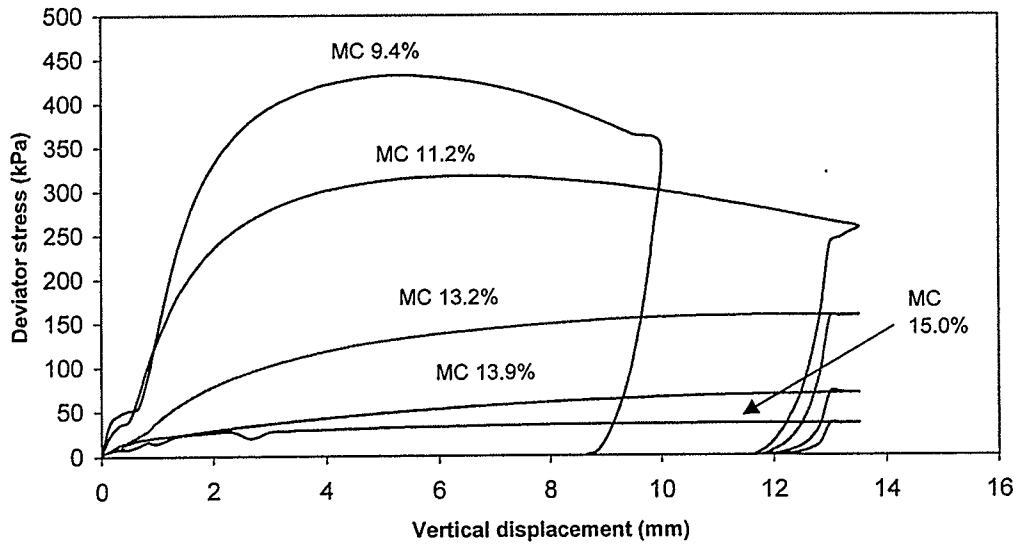


Figure F-9: Deviator stress versus vertical displacement
(Soil sample: UC Site, Net confining stress 100 kPa)

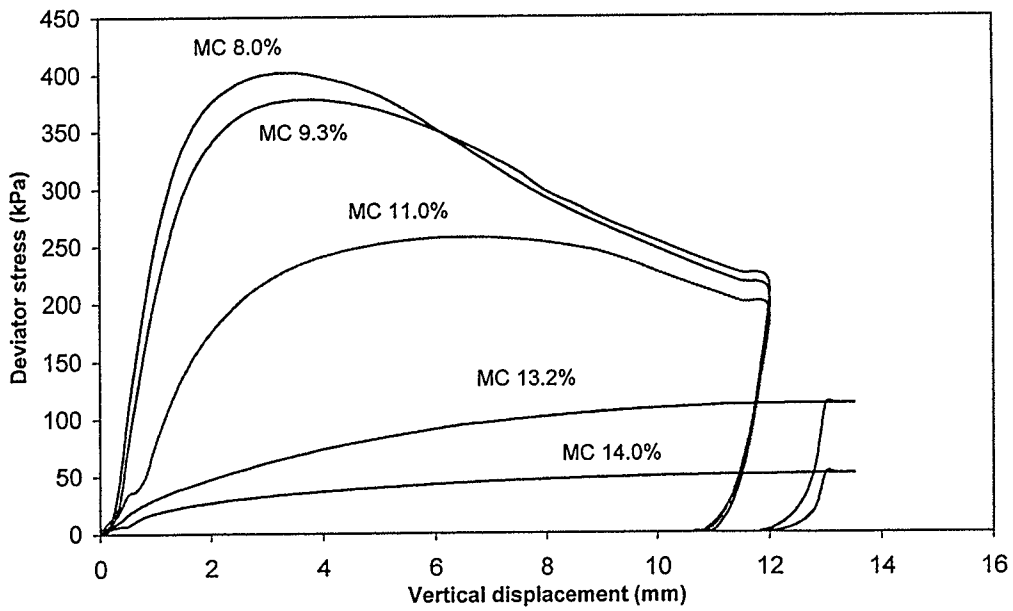


Figure F-10: Deviator stress versus vertical displacement
(Soil sample: UC Site, Net confining stress 50 kPa)

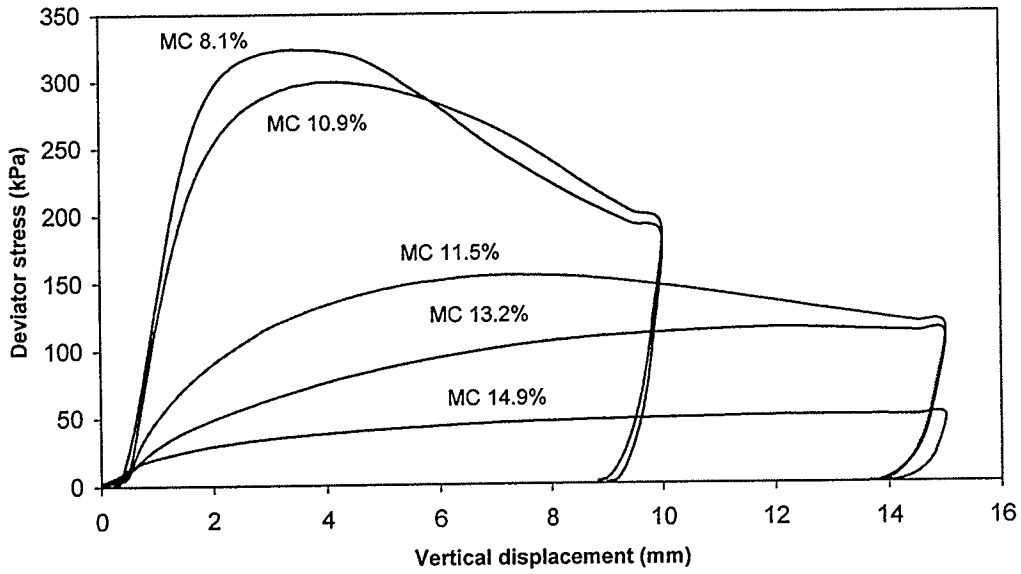


Figure F-11: Shear stress versus vertical displacement
(Soil sample: UC Site, Net confining stress 30 kPa)

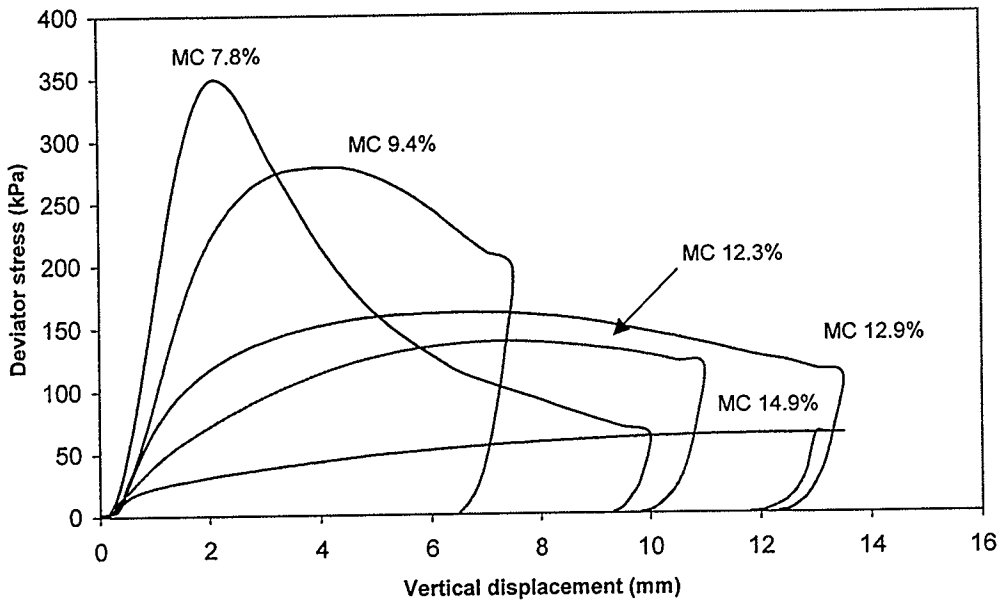


Figure F-12: Deviator stress versus vertical displacement
(Soil sample: UC Site, Net confining stress 10 kPa)

Appendix G: Field testing in Sunnyside Hill

Locations	2001													
	May		June		July		August		September		October		November	
	Moisture content (%)	Soil suction (kPa)												
S1	27.5	10	23.8	9	30.4	9	26	10	27.3	13	29.1	2	18.8	10.1
S2	16.9	20	14.2	18	15.7	24	10.8	49	8	51	11	25	8.5	31
S3	6.7	56	3.5	39	9	39	6.7	38	6	41	12.3	21	13.5	24
S4	20.5	24	12.9	23	26.7	20	12.1	46	11.7	47	17.2	29	12.2	33
S5	16.7	22	12.4	21	10.6	35	15.8	45	5.6	39	29.6	15	13.3	28
S6	9.3	44	9.8	20	16.7	16	10.9	50	7.1	40	18.1	24	16.7	18
S7	17.3	2	13.2	12	17.5	12	15.7	45	11.8	25	12	12	15.2	22
S8	23.8	18	16.7	8	13.3	16	12.4	25	9.5	22	11.1	20	9.3	38
S9	23.4	16	10.3	30	15.3	15	8.7	51	6.6	31	9.1	17	15.2	11
S10	20.5	15	5	28	17.2	10	2.9	55	2.1	40	13.2	18	15	14

Table G-1: Soil suction measurements and the corresponding moisture contents for 2001

Locations	2002			
	May		June	
	Moisture content (%)	Soil suction (kPa)	Moisture content (%)	Soil suction (kPa)
S1	26.7	3	27.5	3
S2	19.4	29	16.8	21
S3	10	27	9.8	29
S4	27.4	12	18.8	18
S5	15.3	19	11.4	13
S6	12.8	13	10	22
S7	19.1	10	17.7	15
S8	22.6	8	15.1	9
S9	24.7	5	19.7	7
S10	18.7	15	12.4	21

Table G-2: Soil suction measurements and the corresponding moisture contents for 2002

Locations	Dry density (kg/m ³)
S1	1755
S2	1802
S3	1800
S4	1830
S5	1702
S6	1722
S7	1756
S8	1785
S9	1745
S10	1752

Table G-3: Dry density